UNIVERSIDAD DE CHILE
FACULTAD DE CIENCIAS FÍSICAS Y MATEMÁTICAS
DEPARTAMENTO DE INGENIERÍA ELÉCTRICA

ENERGETICS, DYNAMICS AND STRUCTURE OF SPIKING NEURAL NETWORKS UNDER METABOLIC CONSTRAINTS

TESIS PARA OPTAR AL GRADO DE DOCTOR EN INGENIERÍA ELÉCTRICA

ISMAEL SEBASTIÁN JARAS CASTAÑOS

PROFESOR GUÍA:
MARCOS ORCHARD CONCHA

PROFESORES CO-GUÍA:
PEDRO MALDONADO ARBOGAST
RODRIGO VERGARA ORTÚZAR

MIEMBROS DE LA COMISIÓN:
MATÍAS ZAÑARTU SALAS
PABLO ESTEVEZ VALENCIA
PATRICIO ORIO ALVAREZ

SANTIAGO DE CHILE
2023

RESUMEN DE LA TESIS PARA OPTAR AL
GRADO DE DOCTOR EN INGENIERÍA ELÉCTRICA
POR: ISMAEL SEBASTIÁN JARAS CASTAÑOS
FECHA: 2023
PROF. GUÍA: MARCOS ORCHARD CONCHA
PROF. CO-GUÍA: PEDRO MALDONADO ARBOGAST,
RODRIGO VERGARA ORTÚZAR

ENERGÍA, DINÁMICA Y ESTRUCTURA DE REDES NEURONALES DE IMPULSO BAJO RESTRICCIONES METABÓLICAS

Todo tejido biológico o sistema físico está sometido a restricciones físicas que acotan su funcionamiento. Específicamente en redes neuronales, restricciones energéticas determinan estados físicamente factibles en los que estas pueden evolucionar. Sin embargo, este concepto fundamental de energía ha sido mayormente omitido al modelar y simular las dinámicas de redes neuronales.

Esta tesis busca formalizar, estudiar y simular la dinámica y estructura emergente en las redes neuronales de impulso cuando hay restricciones metabólicas locales que afectan el comportamiento a nivel neuronal y sináptico. Mediante la creación de un modelo de neurona individual dependiente de la energía y una regla de plasticidad dependiente de la energía, se analiza el impacto de diferentes tipos e intensidades de restricciones energéticas en la conectividad y actividad en una red excitatoria-inhibitoria , tanto de manera analítica como mediante simulación. La sensibilidad de las neuronas y sinapsis a los desequilibrios energéticos da lugar a puntos fijos metabólicamente estables a nivel de la red, descritos matemáticamente y validados en simulaciones.

El marco desarrollado permite el estudio de redes neuronales bajo condiciones metabólicas alteradas, y podría resultar valioso para profundizar en la comprensión de la relación entre enfermedades neurodegenerativas y alteraciones metabólicas a nivel neuronal, sináptico y de red.

RESUMEN DE LA TESIS PARA OPTAR AL
GRADO DE DOCTOR EN INGENIERÍA ELÉCTRICA
POR: ISMAEL SEBASTIÁN JARAS CASTAÑOS
FECHA: 2023
PROF. GUÍA: MARCOS ORCHARD CONCHA
PROF. CO-GUÍA: PEDRO MALDONADO ARBOGAST,
RODRIGO VERGARA ORTÚZAR

ENERGETICS, DYNAMICS AND STRUCTURE OF SPIKING NEURAL NETWORKS UNDER METABOLIC CONSTRAINTS

Every biological tissue or physical system is subject to physical restrictions that limit its functioning. Specifically in neural networks, energy constraints determine physically feasible states in which they can evolve. However, this fundamental concept of energy has been largely overlooked when modeling and simulating the dynamics of neural networks.

This thesis aims to formalize, study and simulate the dynamics and structure that emerges in spiking neural networks when there are local metabolic restrictions that affect behavior at the neuronal and synaptic level. In particular, through the creation of an energy dependent single-neuron model and an energy dependent plasticity rule, the impact generated by different types and intensities of energy constraints on connectivity and activity in an excitatory-inhibitory balanced network is studied both analytically and through simulation. When neurons and synapses are sensitive to energy imbalances, metabolic stable fixed points appear at the network level, which are mathematically described and validated through simulations.

The developed framework allows the study of neural networks under impaired metabolic conditions. Therefore, the proposed theoretical and simulation framework introduced in this work could be valuable to deepen the knowledge about the relationship between neurodegenerative diseases and metabolic impairments at the neuronal, synaptic, and network levels.

There is no excellence without integrity,
there is no integrity without equilibrium,
and there is no equilibrium without adaptation,
there where change is the only constant; life

Acknowledgements

I would like to thank all the professors who were part of this thesis work. A special mention to Marcos Orchard, Pedro Maldonado, and Rodrigo Vergara for supervising and guiding me, and for all the lessons taught during this process. Also, I would like to thank all the colleagues and friends from the Neurosistemas lab, you make this experience much more enriching and fun.

I would like to thank my family and friends for being constant support throughout this process and making it much more enjoyable and fun. A very special thank you to my grandfather, who, without knowing, has been close to me all these years, and who sowed all the love for science and the curiosity which have been driving and inspiring me, I miss you a lot. I also would like to thank, of course, my friends and colleagues from Solsticio with whom I have had the great honor of working and playing in cool and challenging projects and adventures during these years. You make this process much more fun and full of learning.

The author wants to thank ANID for funding this work under ANID-PFCHA/Doctorado Nacional/2019-21190330 grant. And for funding a very productive, enriching, and fun internship at the Neuro-inspired theory, modeling and application lab. The time expended in Bern as well as Heidelberg was an inspiring and full of learning stage of this doctorate and allowed and pushed me to improve as a scientist and as a person. *Vielen Dank* to all the colleagues and friends from the NeuroTMA group.

Powered@NLHPC: This research was partially supported by the supercomputing infrastructure of the NLHPC (ECM-02). We also want to thank the National Center for Artificial Intelligence CENIA FB210017, Basal ANID.

Table of Content

List of Tables

List of Figures

Chapter 1

Introduction

The ultimate goal of technological development is to facilitate the adaptation of human beings to their environment and satisfy their needs and aspirations. One of the greatest ambitions in the face of this challenge is the ability to build autonomous systems that relieve humans of dangerous or strenuous tasks. Artificial intelligence is the field of study that tries to meet these objectives by building *intelligent* agents, that is, devices that can mimic cognitive functions such as learning or problem solving, with the aim that they can perceive their environment and manage to make decisions that maximize their chances of succeeding in performing a task. The inherent capacity that living systems have to achieve this autonomy positions them as a reference when thinking about and building algorithms that try to replicate this capacity. Among the living beings, the human being stands out for his ability to solve problems and learn, with the brain being the main organ involved in this task. This observation has opened the dialogue between mathematics and biology and has been a source of inspiration for the construction of bio-inspired algorithms, such as artificial neural networks, starting from the single-layer perceptron and its subsequent extensions, which gave rise to a whole branch of studies within machine learning; the *Deep Learning*. This suggests that understanding the mechanisms and phenomena that occur in the brain is essential for the development of bio-inspired algorithms that can better mimic the cognitive processes of intelligent beings.

From a neuroscientific perspective, one of the most ambitious challenges in this area is to understand how neurons interact with each other, enabling neural activity that gives rise to behavior [1]. To understand the magnitude of this challenge, it is necessary to consider that it is estimated that an adult brain has 8.6×10^{10} neurons [2], where each of them typically has tens of thousands connections with other neurons. There are 55 classes of neurons [3] and, despite the morphological differences, they all have particular structures that allow them to maintain operational relationships with others. Specifically, each neuron has a collecting surface made up of dendrites and another effector called an axon. Through the collecting surface one neuron can receive the afferent influence that another produces on its effector surface. These structures enable electrochemical interactions between neurons, giving rise to synapses. But what are the mechanisms that give rise to changes in the synapses and in the individual behavior of each neuron? Or, more generally, what are the organizing principles that drive the emergent behavior observed in neural networks?

Given the complexity of the system under study and the enormous number of constantly changing variables that give rise to new organizational states, no single theory or experiment has been capable of answering these questions. This stimulates the search for general organizational principles and the development of strategies that allow exploring how the elements of the system interact with each other. In this task, mathematical models and computational simulations have been essential to deepen our knowledge about the functioning of the brain, providing clear directions on new experiments to develop and pointing out critical aspects that are omitted in purely theoretical developments.

Energy consumption in the brain

The brain consumes an amount of energy disproportionate to its mass; in humans, the energy used by this organ amounts to 20% of all the oxygen consumed by a body at rest, while its mass only represents 2% of the total body mass [4, 5]. Furthermore, the energy consumption of neurons is high relative to other cells [6]. Considering these challenging demands, neurons have specialized structures for energy supply; externally, astrocytes are the main cellular structure that provides energy, while internally -and in the same way as for all eukaryotic cells- the mitochondria fulfill the function of producing energy.

For the brain to function properly, it is essential that the energy supply can compensate for the energy expenditure incurred by the neurons [7]. Under the idea that there is a close relationship between neuronal energy management and general organizational principles, it has been proposed that the energy in the brain imposes restrictions on the processing power [8, 9] or that the organization responds to a compromise between minimizing the energetic cost and allow the emergence of anatomically and functionally adaptable topological patterns in the connectivity between neuronal populations [10]. On the other hand, analyzing brain organization from a Bayesian and information theory perspective, it has been proposed that self-organization in the brain is driven by the *Free Energy Principle* [11]. Which proposes that the operations within the brain respond to minimize the *surprise* -or free energy- that it perceives with respect to the predictions it generates about its environment. This approach requires assuming that the brain works predictively, specifically, that it tries to determine the causes of its sensory inputs through inferential processes which are supported by the idea that the brain minimizes the *predictive error* between what is perceived and the prediction associated with that perception. In this work we will avoid assuming this symbolic informational approach and we will focus on the organizational rules that give rise to the complexity of behavior observed in biological neural networks.

Regarding the relevance of energy administration in the brain, several lines of evidence suggest that dysfunctions in the mitochondria and, therefore, in the neuronal energy supply, are a common cause of various neurodegenerative diseases, such as amyotrophic lateral sclerosis (ALS), Leigh, Alzheimer's and Parkinson's disease [12, 13, 14, 15, 16, 17]. However, there is a great lack of knowledge about how energy restrictions affect the operation of the network under normal conditions. As a result of this lack of knowledge, the need emerges to build a theoretical framework that allows (through neural models and describing synaptic transmission processes taking into account the effects that energy restrictions have on them) simulating neural networks and understanding in greater depth the relationship between energy, organization and emergent behavior within the brain.

Neuron: behavior and energy

A good strategy to understand in greater detail the connection between energy consumption and behavior in the brain is to study how this relationship occurs in the simplest functional element of the network: the cells of the nervous system.

The neuron, like any other cell, needs energy to carry out its daily tasks. In general, neuron activities can be classified as signaling and non-signaling [18]. Within non-signaling activities, the cell uses energy to carry out maintenance processes (such as organelle traffic and the synthesis of proteins and molecules) and to maintain the membrane potential during rest. This corresponds to the electrical potential in equilibrium generated as a consequence of the different ionic concentrations inside and outside the cell, together with the existence of a cell membrane selectively permeable to those ions, which gives rise to electrochemical potentials. Signaling activities are activities present only during the communication period, such as the generation of electrical pulses -called action potentials- or synaptic transmission processes, which refer, mainly, to the energy expenditure present in the postsynaptic neuron product of a presynaptic neuron that sends electrochemical messages, thus generating a disturbance -called postsynaptic potential- in the ionic concentration of the receiving neuron and that it must reverse. In the nerve cell, the energy expenditure associated with maintaining the membrane potential at resting values and the signaling activities have been widely studied and their values can be known with precision [6, 19, 18]. In contrast, and despite various studies and estimates, there is no quantitative consensus on the energy expenditure associated with maintenance activities [9].

The energy supply within each neuron changes dynamically according to activity and there are several mechanisms that allow this precise coupling [20]. An example of the above is that the mitochondria is able to increase its energy production (increases the synthesis of ATP, which is the main source of energy that cells can use to carry out their activities) in response to an increase in synaptic stimulation [17]. However, the energy reserves are small, which is why there is a narrow margin between the energy that can be generated and that required to reach maximum activity. This suggests that the energy supply must impose a limit on the activity that the neuron can perform under normal conditions [20]. It has also been suggested that energy consumption should contribute to limiting the cognitive abilities of the brain, since the total energy that it consumes restricts the temporal rate at which information can be encoded and processed at the neuronal level [21]. In particular, energetic constraints on the neuron can determine the average frequency at which action potentials occur [9].

Even though the relationship between energy administration and neuronal activity is known, the vast majority of mathematical and computational models that allow simulating neuronal activity have omitted this relationship. Despite the above, there are models that account for the tight relationship between available energy and electrophysiological activity [22, 23, 24, 25]. These results support the idea that the energy available in each neuron has a significant impact on its activity. However, the computational complexity that they present, makes it practically impossible to study the impact that energy has on networks made up of thousands of neurons.

Synaptic transmission and energy constraints

The basic functional unit of the neural network is the nerve cell and the formation of connections that allow the transmission of electrochemical signals between them is called synapses. Every time a neuron experiences an electrical pulse, it releases chemical substances -neurotransmitters- housed in organelles called vesicles. During synapsis, neurons make use of specialized structures that allow them to modify their behavior depending on the neurotransmitters they receive. The number of these specialized structures and how they change over time, along with the different types of neurotransmitters, give rise to different ways that neurons can interact. This explains, to a great extent, the wealth of possible behaviors in a brain.

In general terms, the ability of neurons to modify their connections is known as synaptic plasticity. This flexibility is a fundamental property of the brain, since it allows its connectivity to be modified in response to experience. Thus, it is thought as a condition for cognitive processes such as learning, the ability to remember patterns, or to predict the outcome of some event and obtain rewards [26]. For several decades, understanding the mechanisms behind synaptic plasticity has been a challenge for the neuroscientific community. The first studies on plasticity date back to the work carried out by the neurophysiologist Donal O. Hebb [27] and the basic idea of his proposal can be summarized by the following phenomenological description "cells that fire together, wire together" [28]. One way to understand the previous sentence is to think that when neurons fire simultaneously there is a common cause. Furthermore, if one neuron consistently fires just before the firing of another, then a causal relationship between the firing of the first and second cells can be inferred. This causal relationship gives rise to an increase in the intensity of the connection, that is, it generates synaptic plasticity [29].

Regarding energy administration, the mitochondria, being responsible for meeting the ATP demands required by the synapses, has a fundamental and regulatory role in synaptic plasticity processes. Indeed, the literature supports the idea that alterations in the functioning of the mitochondria lead to a dysfunction in the synapse; that is, in the mechanisms that facilitate communication between neurons [30, 23, 31, 17, 32]. Moreover, it is estimated that problems in the functioning of the mitochondria are responsible for abnormalities in brain plasticity processes and also in the neuronal degeneration present in diseases such as Alzheimer's, Parkinson's, or psychiatric disorders [33]. In this regard, the brain has mechanisms to adapt the synaptic function to the energy supply. One of the most obvious examples of this is the effect on synaptic plasticity when homeostasis is challenged by stress: in the presence of chronically high levels of glucocorticoids (also called stress hormones), mitochondrial function, synaptic growth, cell formation, and neurotransmission are inhibited [34]. In the same sense, studies carried out in rats show the increase in the number and volume of mitochondria in presynaptic neurons in response to high firing rates in the auditory system [35]. It has also been suggested that brain energy use determines key parameters such as the size of synaptic contacts and the probability of vesicle release [9, 31]. In particular, vesicle cycling, specifically the rate of vesicle replenishment by endocytosis, is an energetically dependent process [17, 32, 16]. However, the construction of rules of interaction between neurons, through the mathematical abstraction of these phenomena, has largely omitted the close relationship between energy management, mitochondria, and synaptic plasticity.

Consequently, there is no clear consensus on how to extend synaptic plasticity rules to include energy dependencies in the interaction, nor how to define a mathematical conceptual framework that accounts for the relationship between energy and synaptic transmission.

From neuron to neural network

Neurons are the basic element that makes up a neural network and synapses are the biological structures through which these elements can interact with each other. Together, neurons and synapses are essential for functional neural circuits to exist. Furthermore, and considering the enormous number of factors and structures interacting in the brain, the challenge of finding general principles to explain the complex phenomena that occur in it is particularly difficult. The idea that the organization of neural networks responds to energy homeostatic constraints imposed on each neuron has been proposed as one of those general principles: The Energy Homeostasis Principle [36]. Under this scheme, the behavior of the neural network as a whole is presented as the consequence of each neuron seeking to maintain a homeostatic energy level.

Specifically, from the perspective of the *Energy Homeostasis Principle*, the brain is an organ that has a high energy demand and, for each of the constitutive elements that compose it -neurons- to function properly, the existence of synchronization between energy supply and consumption is essential, thus indicating the relevance of the administration and energy restrictions in its operation. Given this relationship, the energy budget of each neuron and how it manages it has an impact on its behavior. Moreover, since there are synaptic connections, the individual behavior of a presynaptic neuron has consequences on the postsynaptic neurons connected to it and thus the interaction imposes an energy consumption on the postsynaptic neurons, displacing them from their energy balance. In this way, the postsynaptic neuron will also modify its behavior successively affecting other neurons. The foregoing shows how a local energy administration rule can generate a population modularity effect, through a recursive mechanism. In this manner, the global behavior observed in neural networks emerges, mainly, as a consequence of the energy administration of each neuron. That is, the dynamics and structure of the neural network can be understood as the projection of a local energy rule on the functioning of the network as a whole.

Finally, regarding the relationship between neural networks, *Energy Homeostasis Principle* and artificial intelligence, it is important to mention the possible impact of these studies on the development of algorithms for learning in Spiking Neural Networks (SNNs). SNNs correspond to a type of artificial neural networks (ANNs) that, unlike classical ANNs, respect some mechanisms that are typical of the functioning of biological neural networks, such as the inclusion of certain types of synaptic plasticity (Spike-Timing Dependent Plasticity) and the communication of binary signals asynchronously, analogous to the existence of action potentials in the brain. This makes them interesting candidates for the efficient implementation of deep neural networks and, simultaneously, allows efficient mapping to hardware [37]. In this sense, SNNs are a meeting point between artificial intelligence and biological neural networks that allow, in principle, to study the extension of neuronal and synaptic plasticity models considering local homeostatic energy constraints, enabling the opportunity to propose improvements and modifications to these networks and their learning rules through biologically plausible mechanisms.

1.1 Hypothesis

This thesis considered the following hypothesis:

Local homeostatic energy constraints modulate network structure in biological neural networks. Specifically, we anticipate that the network actively avoids states where energy consumption surpasses the capacity for on-demand energy production.

1.2 Objectives

1.2.1 General objectives

This research aims to build a theoretical framework that allows mathematically formalizing and studying the dynamics described by individual neurons and networks composed of them, in terms of their energy dependence.

1.2.2 Specific objectives

1. To develop and verify an energy-dependent single neuron model.
2. To define a conceptual framework and mathematically formalize synaptic plasticity rules that include dependence on the available neuronal energy.
3. To mathematically analyze and computationally simulate a biological neural network, including local homeostatic energy constraints.

1.3 Contributions of the thesis

The contributions of this thesis to the state-of-the-art are described hereby accordingly with each of the next chapters; from Chapter 3 to Chapter 5:

- **Chapter 3**: Build on the leaky integrate-and-fire model, this chapter introduces a new simple neuronal model that includes energy-dependencies affecting the neuron dynamics. The results shown in this chapter were published in [38].
- **Chapter 4**: Build on previous spike-timing-dependent plasticity models, this chapter introduces an energy-dependent spike-timing-dependent plasticity, where drops in postsynaptic energy levels suppress synaptic potentiation. In addition, we derived analytical expression predicting the postsynaptic energy level at the synaptic plasticity fixed point.
- **Chapter 5**: Leveraging on the developed energy-dependent single-neuron and plasticity models, in this chapter the effect of local metabolic constraints in spiking neural networks is studied. Analytical expression for the network's fixed points are derived, predicting the metabolic constraints effects on network's structure and activity. In addition, motivated by the relation between neurodegenerative diseases and metabolic im-

pairments, through an Excitatory-Inhibitory balanced network, we simulate a metabolic impairment at neuron level to study its effects in network's structure and activity.

1.4 Thesis outline

This thesis is organized as follows: In Chapter 2 the basic biological background, as well as classical computational neuroscience models, are introduced. In Chapter 3 the Leaky Integrate-and-Fire model is extended to account for metabolic dependencies affecting neuronal behavior, giving rise to the energy-dependent Leaky Integrate-and-Fire model. In Chapter 4, based on previous plasticity models, a new energy-dependent plasticity rule is introduced: the energy-dependent spike-timing-dependent plasticity model. Additionally, plasticity fixed points are analytically studied and their existence is proven through *in silico* experiments. Based on both, the energy-dependent neuronal model as well as the energy-dependent plasticity rule, in Chapter 5 the impact of different metabolic constraints at the neuronal and synaptic level in the network structure and activity is studied. The evolution of the network towards attractor states is mathematically studied and theoretical predictions are tested against computational simulations. Finally, in Chapter 6 the main conclusions of this thesis as well as potential future work are described.

Chapter 2

Background and theoretical framework

2.1 Neurons

In order to build a theoretical framework that makes it possible to study the dynamics of a neural network and the effect of energy management on it, a strategy is to fragment this problem into smaller problems. The neuron is the cellkind which has been pointed as essential for neural processing, which is why it constitutes the morphological and functional unit of the nervous system. To build a neural model in which there is a relationship between behavior and energy management, it is essential to understand how science has approached the challenge of modeling neurons. The essentials of neural modeling are introduced for the unfamiliar reader.

Neurons have a cell membrane that spatially separates them from the external environment, and the existence of mitochondria that provides them with energy. In the neuron, the soma extends generating branched structures called neurites, as can be seen in Figure 2.1a. Neurites can be classified into dendrites: a substructure that allows receiving signals sent by another neuron, and axons: a protruding branch that gives the neuron the ability to send electrochemical signals to others. As for the cell membrane, this is a selective permeable barrier that isolates the cell from its exterior. The permeability of the cell membrane to certain ions is possible through the presence of specific proteins embedded in the cell membrane called ion channels (Figure 2.1b), these generate pores allowing the entry and exit of specific ions. Commonly, the ions involved in neuronal processes are sodium (Na^+), potassium (K^+), calcium (Ca^{2+}) and chlorine (Cl^-). The presence of these ions both inside and outside the neuron, together with the existence of ion channels, gives rise to electrochemical gradients between the outside and inside of the cell, producing an electrical potential called membrane potential. Depending on the opening or closing of ion channels, the membrane potential changes over time. Sometimes, if the neuron is out of electrochemical equilibrium, it is necessary to move ions against their concentration gradient, a process that requires energy. The sodium potassium pump allows to perform this task; extrude three sodium ions (Na^+) and inject two potassium ions (K^+) into the neuron at the expense of consuming one

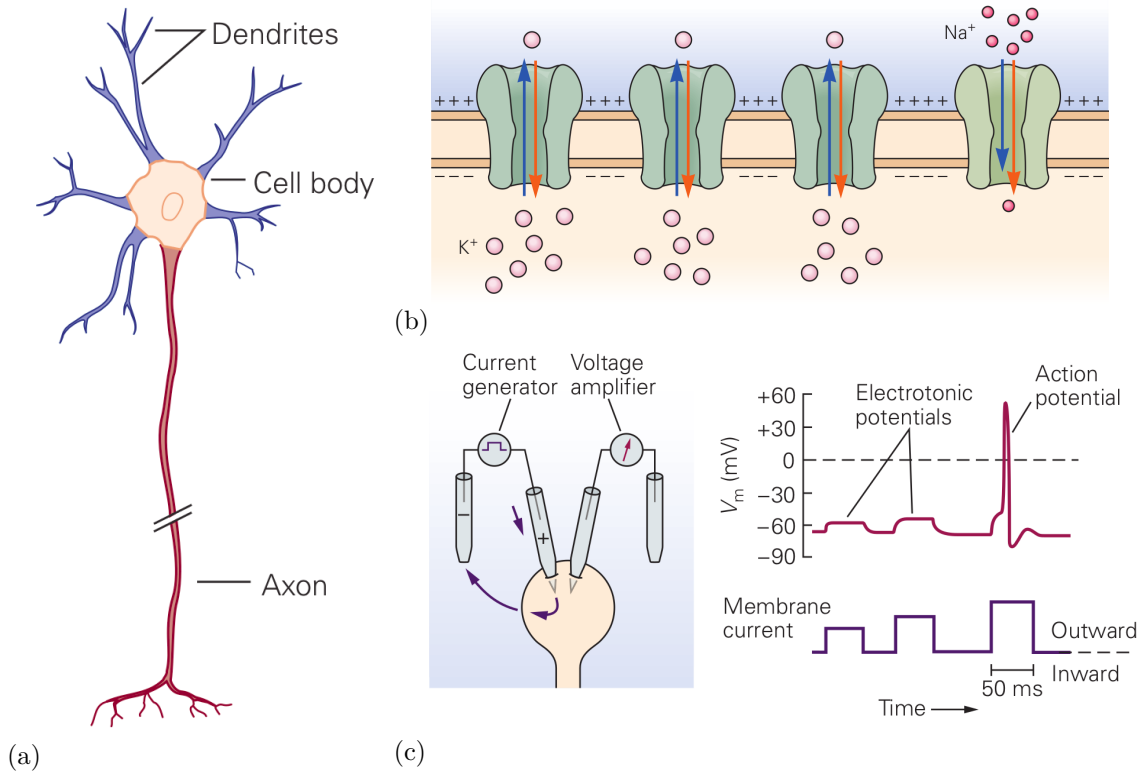

Figure 2.1: **The neuron.**
a) Structure and parts of a neuron. b) Cell membrane with the presence of ion channels permeable to K^+ and Na^+ c) Measurement of cell membrane potential as a function of external excitation. Adapted from [39].

ATP molecule.

From a functional point of view, the cell membrane, by isolating the neuron from its exterior and presenting ionic channels that allow the selective passage of certain ions that produce potential differences, can be represented as an object with electrical properties. Considering those electrical properties, the study of neuronal behavior -specifically the dynamics associated with the membrane potential according to the entry or exit of ions, or as a consequence of the excitation or inhibition that a neuron experiences- has historically been approached from a circuital point of view by means of constructing equivalent electrical circuits. Let us now briefly describe the neuron from a circuital point of view, by starting with the well known Hodgkin-Huxley neuron model.

2.1.1 Hodgkin-Huxley model

The Hodgkin-Huxley (HH) circuit model [40] is one of the most detailed and its construction was the reason why its authors won the Nobel Prize in Physiology in 1963. In the circuit analogue of the neuron according to the HH model (Figure 2.2 and Equation (2.1)) the current injected into the neuron is $I_{inj}(t)$, the cell membrane potential is represented by $v(t)$, while C_m conceptualizes the capacitive characteristic of the cell membrane by acting as an electrical insulator between the extracellular environment and the interior of the neuron.

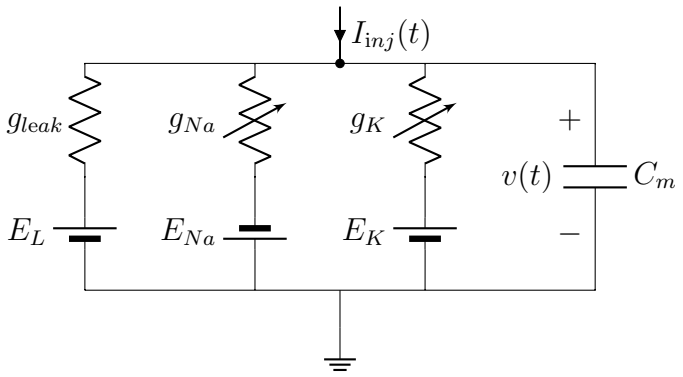

Figure 2.2: **Hodgkin-Huxley model.**
Circuit analogue of the Hodgkin-Huxley neural model. The circuit represents the cell membrane and its electrical properties.

Each ionic channel is represented by a variable conductance that depends on the membrane voltage (voltage-gated channel), g_K and g_{Na} correspond to the conductances of the sodium and potassium channels respectively (with $\bar{g}_K$ and $\bar{g}_{Na}$ maximum conductance values), while g_L is associated with current leakage, since the cell membrane is an imperfect capacitor as it has ionic channels that allow the escape of ions. Regarding the electrochemical gradients between the inside and outside of the neuron, E_K, E_{Na} and E_L represent the electrochemical equilibrium value -for each type of ions- that a neuron has at rest. The chemical force produced by the ionic concentration gradient is represented by a battery, where the value of the associated electromotive force can be calculated by thermodynamic principles (Nernst potential), as follows:

$$C_m \frac{\mathrm{d}v(t)}{\mathrm{d}t} = -\bar{g}_K n^4 (v(t) - E_K) - \bar{g}_{Na} m^3 h (v(t) - E_{Na}) - g_L (v(t) - E_L) + I_{inj}(t), \tag{2.1}$$

where the dynamics of $x = (n, m, h)$ is described by the Equation (2.2):

$$\frac{\mathrm{d}x(t)}{\mathrm{d}t} = \alpha_x(v)(1 - x) - \beta_x(v)x, \tag{2.2}$$

where $\alpha_x(v)$ and $\beta_x(v)$:

$$\begin{aligned} \alpha_x(v) &= \frac{x_\infty(v)}{\tau_x}, \\ \beta_x(v) &= \frac{1 - x_\infty(v)}{\tau_x}. \end{aligned} \tag{2.3}$$

$x_\infty(v)$ and $(1 - x_\infty(v))$ are the steady state activation and inactivation values for each ion channel respectively.

The HH model describes in detail the dynamics of ion channels and allows to accurately simulate the temporal evolution of the membrane potential. However, the specificity of the model entails such a complexity that its computational cost prevents the use of thousands of these neurons to simulate networks [41]. In contrast, there are other types of neural models that capture some fundamental properties of the neuron, making it possible to describe the membrane potential in a simpler manner and avoiding high computational costs by omitting, mainly, certain details about the operation of ion channels, as explained below.

2.1.2 Integrate-and-Fire models

Despite the relevance of the Hodgkin-Huxley model from a biological point of view, there are much simpler neuronal models that are tremendously useful for simulating and studying spiking neural networks. In 1907, long before the creation of the Hodgkin-Huxley neuronal model, Lapicque introduced a simple neuronal model that represent the neuron as an electric circuit consisting of a parallel capacitor and resistor: the integrate-and fire model [42]. Because the aforementioned circuit cannot generate action potentials, Lapicque postulate that when the membrane capacitor reach a certain threshold potential, an action potential would be generated and the capacitor would be discharge, resetting the membrane potential. Based on Lapicque's idea, there has been a great development of integrate-and-fire models. In a general nonlinear integrate-and-fire model, the membrane potential v evolves according to:

$$\tau_m \frac{\mathrm{d}v(t)}{\mathrm{d}t} = f(v(t)) + R(v(t))I(t), \tag{2.4}$$

where τ_m is the neuron time constant, $R(v(t))$ is the voltage-dependent input resistance, and $I(t)$ the incoming current to the neuron. Different choices of the function $f(\cdot)$ allows to obtain different integrate-and-fire models, such as the quadratic integrate-and-fire [43], the adaptive exponential integrate-and-fire [44], or the leaky integrate-and-fire (LIF) model. In particular, in the leaky integrate-and-fire model the function $f(\cdot)$ defines a linear voltage dependence, which simplifies the analytical study of the neuron as well as the mathematical analysis of large-scale neural networks. Therefore, we focus on the leaky integrate-and-fire model. However, for more details about the general nonlinear integrate-and-fire model and specific models not covered here, the reader is refered to [43].

2.1.2.1 Leaky Integrate-and-Fire model

The LIF neuron model is a single compartment model that describes the membrane potential in terms of the synaptic inputs and the current that it receives. An action potential is generated when the membrane potential reaches a fixed threshold (v_{th}) [45]. The model is described by the dynamic of the neurons membrane potential $v(t)$ as follows:

$$C_m \frac{\mathrm{d}v(t)}{\mathrm{d}t} = -g_{leak}(v(t) - v_{rest}) + I(t), \tag{2.5}$$

where C_m is the membrane capacitance, v_{rest} is the equilibrium potential of leak channel from the resting state, $g_{leak} = R^{-1}$ is the conductance associated with the current leakage through the cellular membrane and the passive membrane time constant is $\tau_m = (g_{leak}/C_m)^{-1}$. Whereas $I(t)$ describes the incoming current to the neuron; it accounts for the effect of synaptic input and the current stimuli presented by an external device.

If the membrane potential crosses the threshold v_{th} from below at time t^s, a spike is emitted at t^s (Eqn. (2.6)) and the neuron's potential is immediately reset ($\lim_{\delta\to 0;\delta>0} v(t^s+\delta) = v_{reset}$) to a new value $v_{reset} < v_{th}$ for a period of time called the refractory period, and denoted by τ_{ref}:

$$t^s = \{t | v(t) = v_{th}\}. \tag{2.6}$$

This straightforward conceptualization of the neuron is the root of a wide variety of model extensions that aim to improve the original LIF models characterization of real neuronal

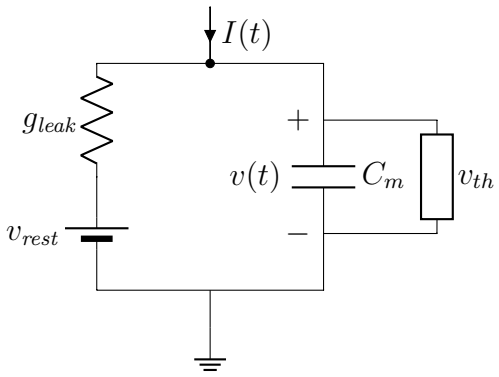

Figure 2.3: **Leaky Integrate-and-Fire model.**
Circuit representation of the leaky integrate-and-fire model. $g_{leak} = R^{-1}$ is the conductance associated with current leakage, C_m is the membrane capacitance, v_{rest} the resting voltage of the cell, v_{th} is the threshold which determines the occurrence of an action potential, and $I(t)$ is the incoming current to the cell.

behavior [41]. Figure 2.3 shows a circuital representation of the leaky integrate-and-fire model. The incoming current $I(t)$ to the neuron in Eqn. (2.5) could be split in two terms:

$$I(t) = I_{ex}(t) + I_{syn}(t), \tag{2.7}$$

where $I_{ex}(t)$ is the injected current to the neuron from an external source, and $I_{syn}(t)$ is the current coming from connected presynaptic neurons. A more detailed explanation and analysis of the effect of $I_{syn}(t)$ in the LIF will be given in sections 2.2.

Subthreshold dynamics

To gain some intuition about the integrate-and-fire model, let us study the neuron dynamics omitting the threshold effect and synaptic currents. To do so, we can set the firing threshold to infinity ($v_{th} = \infty$) and calculate the response of the system (2.5) to a pulse current at time $t = 0$ injecting q total charge (*i.e.* $\int_{-\infty}^{\infty} I(t)\mathrm{d}t = q\delta(t)$). If the initial condition for the membrane voltage is $v(0) = v_0$, then the membrane voltage evolves as follows:

$$v(t) = v_{rest} + [v_0 - v_{rest}]\mathrm{e}^{-t/\tau_m} + \frac{q}{C_m}\mathrm{e}^{-t/\tau_m} \quad \text{for } t \geq 0. \tag{2.8}$$

Thus, using the superposition principle and the impulse response from Eqn. (2.8), we can calculate how Eqn. (2.5) evolves when an arbitrary time-dependent input current $I(t)$ is injected:

$$v(t) = v_{rest} + [v_0 - v_{rest}]\mathrm{e}^{-t/\tau_m} + \frac{R}{\tau_m}\int_0^t \mathrm{e}^{-(t-t')/\tau_m} I(t')\mathrm{d}t', \tag{2.9}$$

which is the convolution between the impulse response of the system and the current $I(t)$.

Threshold and spikes

Now we are prepared to include the threshold v_{th} and study the neuron dynamics. We denote the firing times of the neuron i by $t_i^{(f)}$, where f is the spike label. Formally, the spike train

S of the neuron i is denoted by a sequence of firing times:

$$S_i(t) = \sum_f \delta(t - t_i^{(f)}). \tag{2.10}$$

It will be shown how the LIF model response if a constant supra-threshold current $I_{ex} > (v_{th} - v_{rest})/R$ is injected to the cell when $v(0) = v_{rest}$. Using Eqn. (2.5) the voltage dynamic before reaching the threshold can be derived:

$$v(t) = v_{rest} + I_{ex}R[1 - \mathrm{e}^{-t/\tau_m}]. \tag{2.11}$$

Using Eqn. (2.11) and imposing $v(t^*) \stackrel{!}{=} v_{th}$[1] it is possible to calculate the time t^* at which an action potential occurs:

$$\begin{aligned} t^* &= \tau_m \ln\Big(\frac{I_{ex}R}{I_{ex}R - (v_{th} - v_{rest})}\Big) \\ &= \tau_m \ln\Big(\frac{v_\infty - v_{reset}}{v_\infty - v_{th}}\Big), \end{aligned}$$

where $v_\infty = I_{ex}R + v_{reset}$. After each action potential the neuron will be in the refractory period clamped to v_{reset} (without integrating any current) for τ_{ref} ms. Then, the period between action potentials (also called the interspike interval) for a constant supra-threshold current I_{ex} is described as follows:

$$T_n = \tau_{ref} + \tau_m \ln\Big(\frac{v_\infty - v_{reset}}{v_\infty - v_{th}}\Big). \tag{2.12}$$

Consequently, the neuron firing rate will be T_n^{-1} kHz, and for high excitatory currents ($I_{ex} \to \infty$) the firing rate is $\nu \approx \tau_{ref}^{-1}$ KHz. In section 2.2, it will be shown how this analysis could be extended when synaptic currents are included.

2.2 Synapses

Synapses enable electrical signals transmission between neurons. Let us briefly described how synapses allows signal transmission from a biological point of view, and then explain how this object can be abstracted and mathematically modeled.

When an action potential reaches the axon terminal of the neuron producing it, neurotransmitter release occurs. These neurotransmitters are coupled to receptors on the postsynaptic neuron (see Figure 2.4). The most common excitatory neurotransmitter is glutamate and, after being released by the presynaptic neuron, it is coupled to AMPA and NMDA receptors, stimulating their opening and generating a small depolarization in the receiving neuron. This depolarization is called an excitatory postsynaptic potential (EPSP). If the neuron that transmits the action potential is inhibitory, then an analogous process occurs, but instead of producing depolarization in the receiving neuron, it produces hyperpolarization, in this case the induced voltage variation it is called an inhibitory postsynaptic potential (IPSP).

[1] In this thesis, the $a \stackrel{!}{=} b$ notation is used to express that *a has to be equal to b*.

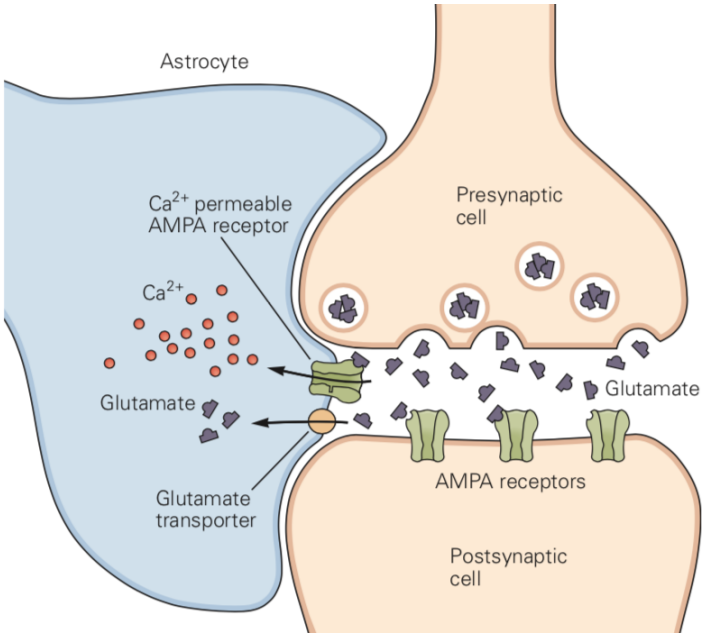

Figure 2.4: **Neurotransmitter release.**
The presynaptic neuron releases neurotransmitters (glutamate) activating specific receptors on the postsynaptic neuron, causing it to depolarize. Figure taken from [39].

2.2.1 Abstract synapses

From a phenomenological perspective, we are interested in describing how the aforementioned postsynaptic potential (PSP) can be produced by the effect of incoming synapses to the neuron. Therefore, let's focus on how I_{syn} (Eqn. (2.7)) can be mathematically described and the effect that it produces in the membrane potential of the postsynaptic neuron. In general, synaptic interactions are modeled by stereotypical functions of time called interaction kernels ε, and the impact of all incoming synapses to a neuron can be described as follows:

$$f^{syn}(t) = \sum_{synapses} \sum_{k\ spike\ s} w_k \varepsilon_k (t - t_s), \tag{2.13}$$

where w_k is the weight or strength of the kth synapses. In most models, the shape of the interaction kernel ε it is constrained by the biophysics of the synaptic interaction. Some widely used interaction kernels are: α-function ($\varepsilon(t) = \Theta(t) t \mathrm{e}^{-t/\tau_{syn}}$) and the exponential kernel ($\varepsilon(t) = \Theta(t) \mathrm{e}^{-t/\tau_{syn}}$), where $\Theta(\cdot)$ denotes the Heaviside step function. For the upcoming analysis, we will focus on the synaptic interaction under the exponential kernel.

In principle, there are two main approaches to model synapses: conductance-based and current-based synapses. Particularly, because of the chemical nature of synapses transmission, synapses can be modeled as a change in the conductance of the neuron's membrane towards the reversal potential of the ion type. In contrast, the membrane potential of the soma changes because it receives a current that is passively propagated towards it. Therefore, if we model the neuron as a point and assume that this point represents the soma of the neuron, then is natural to model the synapses as a current (for a more detailed discussion about the subject, the reader is refered to [46, 47]).

2.2.1.1 Conductance-based synaptic interaction

As previously mentioned, modeling the synaptic interaction as a dynamic conductance related to a specific reversal potential associated with a particular ion type it is coherent with chemical synapses interactions. In principle, different ion types have different reversal potentials. In this case, the conductance of the kth synapses g_k with ε interaction kernel can be written:

$$g_k(t) = \sum_{spike\ s} \Theta(t - t_s) w_k \varepsilon_k(t - t_s), \tag{2.14}$$

allowing to express f^{syn} as:

$$f^{syn}(t) = \sum_{synapses\ k} \sum_{spike\ s} \Theta(t - t_s) w_k \varepsilon_k(t - t_s)(E_k^{rev} - v), \tag{2.15}$$

where E_k^{rev} is the reversal potential of the kth synapses. Then f^{syn} is the synaptic injected current to the neuron ($f^{syn} = I_{syn}$), and we can plug it in the LIF Eqn. (2.5), obtaining:

$$C_m \frac{\mathrm{d}v}{\mathrm{d}t} = -g(v - v_{rest}) + I_{ex} + \sum_{synapses\ k} \underbrace{\sum_{spike\ s} \Theta(t - t_s) w_k \varepsilon_k(t - t_s)}_{g_k(t)} (E_k^{rev} - v). \tag{2.16}$$

Using the exponential kernel for the conductance's dynamic we obtain:

$$C_m \frac{\mathrm{d}v}{\mathrm{d}t} = -g(v - v_{rest}) + I_{ex} + \sum_{synapses\ k} \sum_{spike\ s} \Theta(t - t_s) w_k \mathrm{e}^{-(t-t_s)/\tau_{syn}} (E_k^{rev} - v). \tag{2.17}$$

Please note that using the conductance-based approach, the PSP depends on the distance between the membrane voltage and the reversal potential. Therefore, the summation of PSP is nonlinear. Thus, finding closed-form expressions for the membrane voltage of the neuron under the conductance-based approach is more difficult than using the current-based synaptic interaction approach, as we will explain in the following subsection.

2.2.1.2 Current-based synaptic interaction

As previously mentioned, an action potential of a presynaptic neuron generates a signal that is propagated through the synapse generating a current that is passively propagated to the soma of the postsynaptice neuron, modifying the membrane voltage of the soma. Therefore, from a point-neuron perspective (assuming the model is representing the soma) it is possible to describe the synaptic interaction as a current-based process. In this scenario, instead of modifying the conductance of the synapse as in Eqns. (2.14) and (2.15), the kernel is used to describe the current shape directly. Consequently, the synaptic current generated by the kth presynaptic neuron, when an exponential kernel is used, is described by:

$$I_{syn}^k(t) = \sum_{spike\ s} \Theta(t - t_s) w_k \mathrm{e}^{(t-t_s)/\tau_{syn}}. \tag{2.18}$$

Plugging Eqn. (2.18) into Eqn. (2.5) we obtain:

$$C_m \frac{\mathrm{d}v}{\mathrm{d}t} = -g(v - v_{rest}) + I_{ex} + \sum_{synapses} \underbrace{\sum_{k\ spike\ s} \Theta(t - t_s) w_k \mathrm{e}^{-(t-t_s)/\tau_{syn}}}_{I^k_{syn}(t)}, \tag{2.19}$$

which allows to linearly sum up PSP, simplifying the search of closed-form expressions for the membrane potential. Accordingly, in this work we will focus on current-based synapses and now we will show some analytical expression for the membrane potential when a current-based I_{syn} is received.

Synapses and membrane potential dynamic

The simplest case is when there is no external current (*i.e* $I_{ex} = 0$), $v(0) = v_{rest}$, and the neuron receives only one spike at time t^f with shape:

$$I_{syn}(t) = \Theta(t - t^f) w \mathrm{e}^{-(t-t^f)/\tau_{syn}}. \tag{2.20}$$

For this case, the membrane potential of the neuron evolves as follows:

$$v(t) = v_{rest} + \frac{Rw\tau_{syn}}{(\tau_{syn} - \tau_m)} [\mathrm{e}^{-(t-t^f)/\tau_{syn}} - \mathrm{e}^{-(t-t^f)/\tau_m}]. \tag{2.21}$$

Because the effect of current-based synapses can be linearly summed up for different spikes and synapses, it is possible to use Eqn. (2.21) to find a general expression describing the membrane potential dynamic for a postsynaptic neuron connected with several presynaptic neurons, as follows:

$$v(t) = v_{rest} + \sum_{synapse} \sum_{k\ spike\ f} \frac{Rw_k\tau^k_{syn}}{(\tau^k_{syn} - \tau_m)} [\mathrm{e}^{-(t-t^f)/\tau^k_{syn}} - \mathrm{e}^{-(t-t^f)/\tau_m}]. \tag{2.22}$$

In the previous analysis we have assumed that synaptic connections are static, but in our brains the strength of the connection between neurons are constantly changing. In section 2.3 some of the mechanisms behind the change between neuronal connections explained.

2.3 Plasticity in the brain

The connections between neurons that allow the transmission of electrochemical messages change over time according to experience and allow structural modifications in the brain. The concept of synaptic plasticity refers to the flexibility that these connections enjoy. Without synaptic plasticity, the brain would not be able to modify the strength of connections between neurons. It is currently thought that these structural changes are the mechanisms behind

cognitive processes such as learning and memory, so synaptic plasticity would be essential to accomplish our daily tasks and develop new skills.

Synaptic plasticity occurs at different time scales [48], short-term plasticity [49], for example, is only maintained on time scales of less than one second. In contrast, long-term plasticity considers persistent changes in the synaptic response that can be generated in the order of miliseconds and last for hours [50, 51], such potentiation and depression phenomena are called long-term potentiation (LTP) and long-term depression (LTD), respectively. There are also slower stabilization processes, such as homeostatic plasticity (or synaptic scaling) that occurs on the order of minutes to hours [52]. In this work we will mainly study long-term synaptic plasticity. Particularly, the long-term plasticity described by Spike-Timing-Dependent-Plasticity (STDP).

2.3.1 Spike-Timing-Dependent Plasticity

Spike-Timing-Dependent-Plasticity (STDP) roots can be tracked back to Hebb's ideas about plasticity [27]. For Hebb, long-term plasticity phenomena can be summarized as follows: 'Cells that fire together, wire together'. Formalization of Hebb's ideas in their simplest form can be achieved using the equation:

$$\dot{w} = F(w, \nu_{pre}, \nu_{post}), \tag{2.23}$$

where $\dot{w}$ described the rate of change of the weight w, $F(\cdot)$ is an arbitrary function, and ν_{pre} and ν_{post} are the pre- and postsynapic firing rate, respectively. However, although relaying on firing rate, Eqn. (2.23) neglects the relevance of precise timing between spikes, which is in opposition with several experiments which demonstrate the relevance of spike timing on synaptic weight evolution [51, 50].

STDP is a temporal asymmetric form of Hebbian learning induced by tight temporal correlations between the spikes of pre- and postsynaptic neurons [53, 51, 50]. There are different protocols for measuring how the spike times affect synapse modification, however, one of the most recognized results are the measurement made in [50] (see Fig. 2.5), where the effect of different pre- and postsynaptic spike-time on synaptic strength can be clearly recognized.

Mathematically, general STDP can be described as follows:

$$\dot{w} = H(S_{pre}, S_{post}), \tag{2.24}$$

where $\dot{w}$ describes the rate of change of the weight w and H is some arbitrary function of the pre- (S_{pre}) and postsynaptic (S_{post}) spike trains.

There are several ways in which $H(\cdot)$ can be described to fit the data in Fig. 2.5, but for now we will focus on one of the most accepted formalization of STDP across the computational neuroscience field, the one introduced in [54]. In this formalization, a single pair of presynaptic and postsynaptic action potential with time difference $\Delta t = t_{post} - t_{pre}$ induces a change in synaptic efficacy Δw as follows:

$$\Delta w = \begin{cases} \lambda f_+(w) K(\Delta t), & \text{if } \Delta t > 0. \\ -\lambda f_-(w) K(\Delta t), & \text{if } \Delta t \leq 0. \end{cases} \tag{2.25}$$

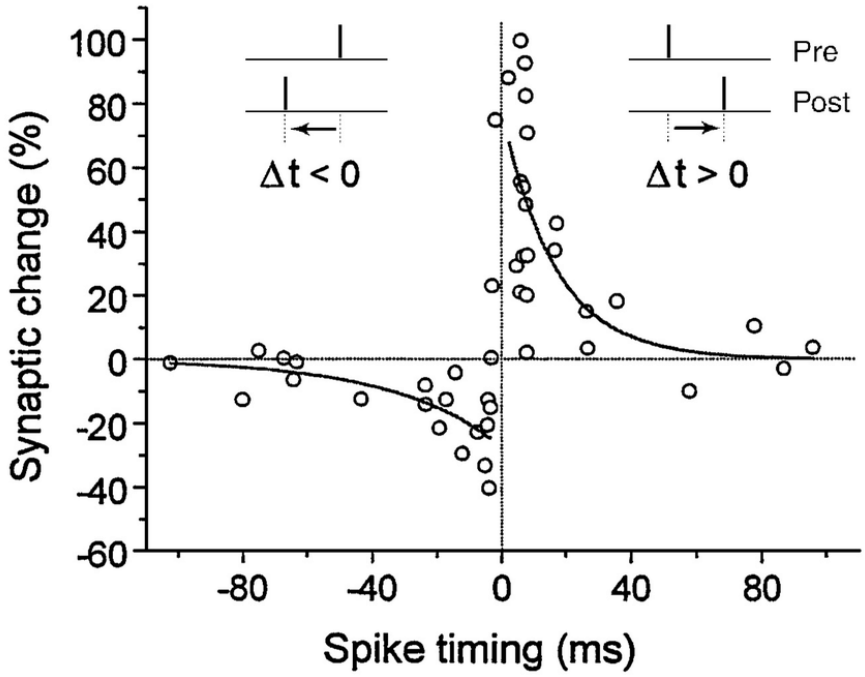

Figure 2.5: **Experimental in-vitro measurement of STDP for an excitatory synapse.** Spike timing refers to the difference in spike-time between the pre and the postsynaptic cell ($\Delta t = t_{post} - t_{pre}$). Dark circles represent the percentage in synaptic change for different spike-times. If the postsynaptic cell fires after the presynaptic cell, then the synapses experience potentiation. If the postsynaptic cell fires before the presynaptic cell, then the synapses is depressed. Higher potentiation and depression occurs when there is a small spike-timing difference, while for bigger spike-timing difference between cell, potentiation and depression are weaker. Figure taken from [50].

Where the synaptic efficacy w is normalized to $[0, 1]$. The learning rate λ $(0 < \lambda \leq 0)$ scales the magnitude of the individual weight change, and $K(\cdot)$ is a temporal filter $K(x) = \mathrm{e}^{-\|x\|/\tau_{stdp}}$.

In principle, potentiation and depression has their own τ_{stdp} time constant. They will be denoted by τ_+ for potentiation, and τ_- for depression. Finally, the updating functions $f_+(w), f_-(w) \geq 0$ scale the synaptic changes taking into account the current weight value, and has the form of a power law with non-negative exponent μ_+ for potentiation, and μ_- for depression (see Fig. 2.6):

$$f_+(w) = (1 - w)^{\mu_+} \text{ and } f_-(w) = \alpha w^{\mu_-}, \tag{2.26}$$

with $\alpha > 0$ accounting for the asymmetry between the scales of potentiation and depression, as can be seen in Fig. 2.5, where the maximum magnitude of depression is smaller than the maximum magnitude of potentiation. Note that modifying μ_+ and μ_- in Eqn. (2.26), allows to recover previous STDP rules such as the ones introduced in [55, 56, 57], unifying previous rules in a single framework. Thus, Eqn. (2.25) gives a general rule as a starting point for creating an energy-dependent STDP rule, and is the one that we will use later in section 4 as a starting point for energy-dependent STDP.

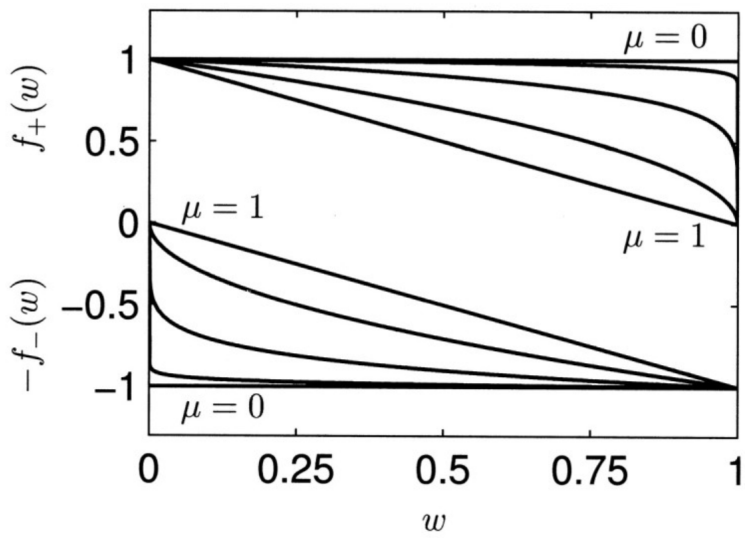

Figure 2.6: **Non-linear temporal asymmetric Hebbian plasticity**
Effect of the parameter μ on the updating functions $f_+(w)$ (top half) and $f_-(w)$ (bottom half) for $\mu = 0, 0.02, 0.15, 0.5, 1$ ($\alpha = 1$). When $\mu = 0$ there is no dependence of the weight value in the updating rule (additive rule), while for $\mu > 0$ the updating rule depends on the current weight value (multiplicative rule). Figure taken from [54].

Spike-timing and neuromodulators

Classical Hebbian learning rule, as STDP, puts the emphasis on joint pre- and postsynaptic firing times, but neglects the potential role of neuromodulators. Three-factor learning rules [58], extends STDP rules for accounting the effect from neuromodulators in plasticity. In general, any three-factor synaptic plasticity rule can by written as:

$$\dot{w} = F(M, S_{pre}, S_{post}), \tag{2.27}$$

where S_{pre} and S_{post} are the pre- and postsynaptic spike trains, respectively and M is the modulator signal. Since three-factor rules are a modern generalization of the original concept of Hebb, they are also called neo-Hebbian. Particularly, the function $F(\cdot)$ is sometimes assumed to consist of a Hebb-like term $H(S_{pre}, S_{post})$,multiplied by a modulator function $G(M)$, hence:

$$\dot{w} = F(M, S_{pre}, S_{post}) = G(M)H(S_{pre}, S_{post}). \tag{2.28}$$

Under the energy homeostasis principle, available energy in the neuron can be thought as a neuromodulator affecting classical STDP rules, as we will explore in more detail in section 4.

Chapter 3

Energy-dependent Leaky Integrate-and-Fire

The content of this chapter has been published in the European journal of Neuroscience[1]. We thank Taiki Harada for helping throughout the project, mainly with the code and the writing, and Rodrigo Vergara, Pedro Maldonado, and Marcos Orchard for supervising and guiding the work.

It is widely accepted that the brain, like any other physical system, is subjected to physical constraints that restrict its operation. The brain's metabolic demands are particularly critical for proper neuronal function, but the impact of these constraints continues to remain poorly understood. Detailed single-neuron models are recently integrating metabolic constraints, but these models' computational resources make it challenging to explore the dynamics of extended neural networks, which are governed by such constraints. Thus, there is a need for a simplified neuron model that incorporates metabolic activity and allows us to explore the dynamics of neural networks. This chapter introduces an energy-dependent leaky integrate-and-fire (EDLIF) neuronal model extension to account for the effects of metabolic constraints on the single-neuron behavior. This simple, energy-dependent model could describe the relationship between the average firing rate and the Adenosine triphosphate (ATP) cost as well as replicate a neuron's behavior under a clinical setting such as amyotrophic lateral sclerosis (ALS). Additionally, EDLIF model showed better performance in predicting real spikes trains -in the sense of *spike coincidence* measure- than the classical leaky integrate-and-fire (LIF) model. The simplicity of the energy-dependent model presented here makes it computationally efficient and, thus, suitable for studying the dynamics of large neural networks.

During the last decade, some of the classical single-neuron models have been extended to include the relationship between available energy and electrophysiological activity [22, 23, 25]. For example, the study conducted by Chander & Chakravarthy (2012) [22] illustrated how different initial ATP levels affect the neuron's behavior, leading to different types of activities. In the study by Le Masson et al. (2014) [23] the Hodgkin-Huxley model was

[1]Link to the article: 10.1111/ejn.15326

extended to include behavioral dependencies on the neuronal metabolic dynamics in order to study the effects of energetic neuronal dysfunction. These results support the idea that the neuron's available energy generates a significant impact on its activity. However, these multi-compartment and highly detailed Hodgkin-Huxley models demand increasing computational resources. This high computational cost makes them impractical for studying the effect of energetic dynamics on large neuronal population networks (for a further review of biological plausibility and computational resources trade-off of different neuronal models, see [41]).

As an alternative, the leaky integrate-and-fire (LIF) model is a popular and widely used single-neuron model. It is characterized by its simplicity, and at the same time, it is sufficiently complex; this enables it to capture many of the essential features of neural dynamics [45]. These attributes make the LIF model a suitable tool for the study of sizable neuronal population dynamics simulations. Despite the popularity and simplicity of the LIF model, it is not clear how we can use it to study large neuronal populations under a metabolic perspective. The main advantage of the LIF model is the balance between its simplicity and capacity to capture essential features of neuronal behavior. Despite these attributes, as mentioned previously, the model and its consecutive extensions neglect metabolic dependence in their dynamic. The main reasons for this omission are the following: (1) The model assumes that the neuron has unlimited access to energy resources. (2) the available energy is restored instantaneously. (3) Under normal conditions, the metabolic effect on neuronal behavior is negligible.

Notwithstanding such omission, a metabolic imbalance could have a meaningful impact on neuronal behavior and the development of neurodegenerative diseases. Therefore, given the relevance of the metabolic dynamics for the brain's proper function, it is beneficial to have a simple single-neuron model that can account for the relationship between the metabolic dynamic and neuronal behavior. The aforementioned model allows us to reinterpret the single-neuron behavior under metabolic constraint. In this chapter, we develop a simple single-neuron model that incorporates metabolic rules. Considering that single-neuron models are essential building blocks of *in silico* extensive neuronal population simulations, this constituted the first step required to explore neural network dynamics that are constrained by metabolic demands. Concretely, we extend the LIF model to account for metabolic dependencies. Therefore, we grant it the simplicity and computational inexpensiveness but allow it to describe metabolic dynamics and dependencies. We focus on evaluating three relevant aspects of this single-neuron extended model: (1) comparing its performance against the classical LIF model using spike recording from real neurons, (2) evaluating its biological plausibility in relation with in vitro empirical data, and (3) assessing whether metabolic predictions of more elaborate models can be replicated.

3.1 EDLIF formalization and dynamics

We used the LIF model's structure and extended it to account for the relationship between energetic dynamics and neuronal activity. We termed this new model the energy-dependent leaky integrate-and-fire model (EDLIF). Specifically, we used an incomplete repolarization mechanism [59] and made it ATP-sensitive, thereby making the post-reset membrane potential ATP-dependent. We examined how LIF model can be extended through an ATP-sensitive

incomplete repolarization mechanism. While developing these concepts, we also analyzed the cost and dynamic of energy consumption in the neuron.

The extension of the LIF model through the inclusion of adaptation terms has led to a major improvement in the models predictive capabilities. There are several explanations for the inclusion of adaptation terms; however, ultimately, the functioning of the neuron rests on its ability to produce energy. Specifically, the sodium-potassium pump relies on available ATP so that proper function can restore the resting potential. Consequently, neuronal behavior depends on energy production. Therefore, an energetic imbalance should affect several adaptation processes in the neuron, but it is not clear how previous extended LIF models made their adaptation process metabolic-dependent or how they could be used to explore the neuronal dynamics while accounting for metabolism. EDLIF model addresses this question by making the adaptation process explicitly dependent on the available neuronal energy through the energy-dependent partial repolarization mechanism.

3.1.1 Energy Dependent Leaky Integrate-and-Fire model

Our proposed model is, as its name suggests, an energy-dependent neuronal model inspired by the LIF. The model's main objective was to include energy dependence in the neuronal dynamics while maintaining the LIF model's simplicity, so it requires low computational resources and is suitable for the simulation and study of the networks of thousands of neurons from an energy-dependent perspective. In this regard, the dynamic of neurons' membrane potential is to be described in the same way as done in Eqn. (2.5). However, the repolarization mechanism induces an energy-dependent relationship, and it will affect the neuron's temporal evolution if an energy imbalance is present. In the EDLIF model, the neuron's energy dynamic is described by the intracellular ATP concentration dynamics.

3.1.1.1 ATP dynamics

In our model, the ATP dynamics are characterized while considering two collections of processes: those that supply ATP to the neuron ($A_s(t)$ (mM/ms)), and those that consume ATP ($A_c(t)$ (mM/ms)). The ATP dynamic concentration ($A(t)$ (mM)) can be formalized as follows [36]:

$$\frac{\partial A(t)}{\partial t} = A_s(t) - A_c(t), \tag{3.1}$$

where both terms $A_s(t)$ and $A_c(t)$ are divided per volume unit.

The observation that the neuron has relatively constant ATP can be interpreted as a reflection of homeostatic feedback. Thus, the neuron's homeostatic mechanisms keep ATP levels close to the homeostatic ATP level (A_H). In this work, the homeostatic feedback is introduced explicitly in the ATP production dynamics, which fixis mathematically formalized by Equation (3.2). Thus, ATP production depends on two terms: the actual ATP level with respect to a homeostatic one ($K(A_H - A(t))$) and a basal production term (A_B) accounting for resting potential and housekeeping activities:

$$A_s(t) = K(A_H - A(t)) + A_B, \tag{3.2}$$

where the parameter K ($(1/ms)$ units) s the rate at which ATP is produced and its value is equal to 1 [23].

3.1.1.2 Energy consumption by neuron

The neuron, like any other cell, requires energy to carry out its activities, which can be classified as signaling and non-signaling [18]. Within the non-signaling activities, the neuron uses energy to carry out maintenance processes (such as organelle traffic and the synthesis of proteins and molecules) and conserve the membrane potential during rest. Signaling activities are present only during the communication periods, such as action and postsynaptic potentials and presynaptic activity associated with synaptic transmission.

Since we are working with a single-neuron model, our main concern is quantifying the energy expenditure related to general homeostasis maintenance (house-keeping: E_{HK}), conditions required for nonsignaling (maintaining resting potential: E_{RP}), and signaling (action potentials: E_{AP}). Consequently, the total energy consumption ($A_c(t)$) is derived by the sum of E_{HK}, E_{RP} and E_{AP}. These three energetic budget items have been already estimated as shown in Table 3.1. These specific values emerged from the combination of the anatomic and physiologic measurements and the theoretical calculation of bottom-up energy budget using biophysical properties in conjunction with electrophysiological and morphological data [60, 6]. The associated postsynaptic potential and presynaptic activity were beyond the scope of this study. Since the total amount of energy consumed per action potential is not instantly

Table 3.1: **Energy consumption.**
Energy consumption related to different processes in a rat excitatory neuron, using experimental data from [6].

Activity	Unit energy consumption
House-Keeping (E_{HK})	8.41×10^8 *ATP/(neuron · s)*
Resting potential (E_{RP})	3.42×10^8 *ATP/(neuron · s)*
Action Potential (E_{AP})	1.25×10^8 *ATP/(neuron · spike)*

expended, the consumption is described in a biologically plausible way through the inclusion of a time-varying function (see Equation (3.3)) [61].This smooth decay in time reflects the characteristic dynamic of the metabolic energy expenditure in an action potential in time.

$$A_{ap}(t) = \frac{(t - t^{'})}{\tau_{ap}^2} \cdot exp\Big(- \frac{(t - t^{'})}{\tau_{ap}} \Big), \quad \forall t \geq t^{'}, \tag{3.3}$$

where $t^{'}$ is the time in ms at which the action potential occurs and $\tau_{ap} = 3945.66$ ms.

To determine the parameter τ_{ap}, a detailed biophysical model of the brain's metabolic interactions is used. The model integrates three different approaches: the Buxton-Wang model of vascular dynamics, the Hodgkin-Huxley formulation of neuronal membrane excitability, and a biophysical model of metabolic pathways [25]. To reach equilibrium, the model is left without stimulation for more than 100 *seconds*. Then, the neuron is stimulated to only produce one spike (see Figure 3.1) and study the ATP dynamic imbalance that it produces (see Figure 3.2).

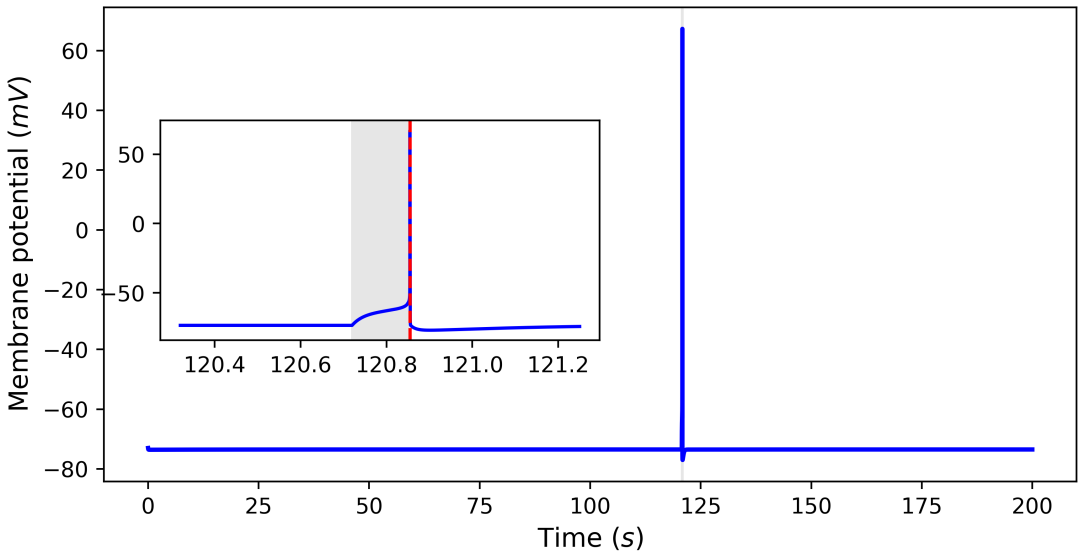

Figure 3.1: **Metabolic-dependent Hodgkin-Huxley membrane potential.** Membrane potential generated by a detailed Hodkin-Huxley model accounting for biophysical description of metabolic pathways [25].

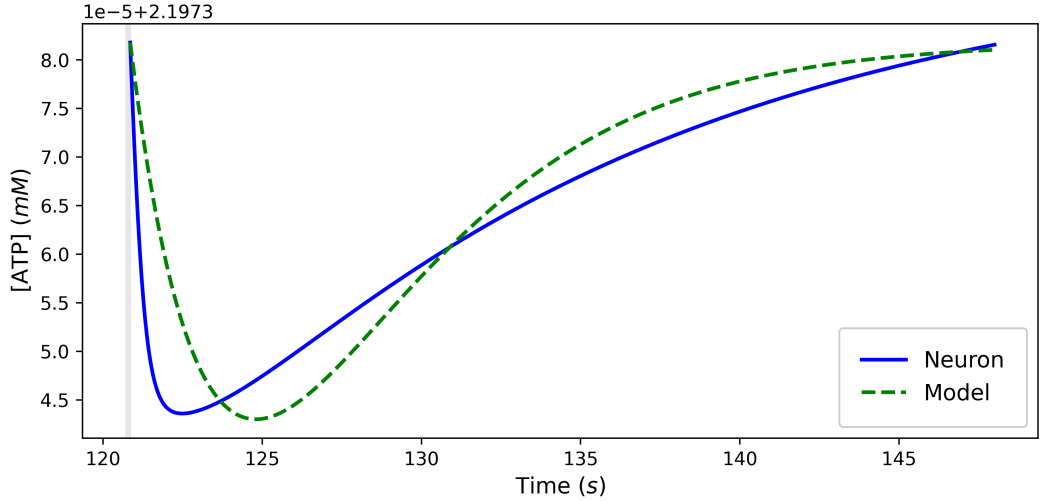

Figure 3.2: **Available ATP dynamic and spike occurrence.** The occurrence of one spike produces the ATP dynamic shown in the blue line, while the green line shows the curve obtained by fitting τ_{ap} in Eqn. (3.3) through least square minimization. For clarity, the y-axis ticks have been autoscale using the upper left number above the Figure. Therefore, every [ATP] value it is equivalent to the base number (2.1973, plus the offset 10^{-5}) times the tick-values.

3.1.1.3 Energy dependencies and incomplete repolarization

So far, we have introduced energy expenditure to EDLIF; however, we still need to factor in how energy availability may impact neuron physiology. ATP imbalance in the neuron is

known to alter the sodium-potassium pump. Specifically, a decrease in ATP concentration implies a partial restoration of the resting potential as can be inferred from the following equation: [23]:

$$\begin{aligned} pump \; + 3\,\mathrm{Na}_i^{+} + 2\,\mathrm{K}_e^{+} + \mathrm{ATP} \; &\underset{k_{\mathrm{p2}}}{\overset{k_{\mathrm{p1}}}{\rightleftharpoons}} \; pump_{active} \\ pump_{active} \; &\underset{k_{\mathrm{p4}}}{\overset{k_{\mathrm{p3}}}{\rightleftharpoons}} \; pump \; + 3\,\mathrm{Na}_e^{+} + 2\,\mathrm{K}_i^{+} + \mathrm{ADP} + \mathrm{P}, \end{aligned} \tag{3.4}$$

where ADP is adenosine diphosphate, '*pump*' and '$pump_{active}$' represent two possible states for the sodium-potassium pump; Na_i^+ and Na_e^+ are the intracellular and extracellular sodium concentrations, respectively K_e^+ and K_i^+ are the extracellular and intracellular potassium concentrations, respectively; ATP is the ATP concentration. This scheme shows that lower ATP concentration disables the functioning of the sodium-potassium pump, thereby reducing the rate at which sodium and potassium concentrations are restored. As such, the neuron is maintained above the resting potential. From Eqn. (3.4) it follows that when the occurring action potential and the neuron have ATP deficiency, the neuron remains slightly depolarized with respect to its resting potential, *i.e.* it experiences partial repolarization, making it more likely to produce a new action potential under stimulation.

One method that allows the modification of the membrane potential after the occurrence of an action potential is partial reset. Incomplete repolarization or partial reset is a simple and powerful tool for controlling the irregularity of spike trains fired by a leaky integrator neuron model, and it is a computationally simple way to reproduce the effects of more complex dynamical properties of the membrane. Previous works have shown that incorporating this mechanism into the LIF model produces highly irregular firing that is similar to the one observed in biological neurons [59]. The mechanism works by resetting the potential of the capacitor to $V(t) = \beta V_{th}$ after an action potential occurs where V_{th} is the firing threshold and β is called the reset parameter. In the EDLIF model, we use the reset parameter (β) to introduce variability in the firing of the neuron, but we made this beta term ATP-dependent in accordance with the interpretation of Eqn. (3.4). In our approach, we used sigmoidal relation to link the ATP level with resetting potential and optimize the slope of the sigmoid to find the sensitivity of the model to ATP level imbalance and its effect on resetting potential. Our model allows the construction of a soft and flexible function linking the available energy and its effect on neuronal behavior through reset potential. Nonetheless, it should be noted that other similar functions could be used for the same purpose.

Despite the highly irregular firing that can be observed in the LIF model through the inclusion of partial reset, the biological correlates that support this inclusion can not be clearly determined. In our model, we include and reinterpret the partial reset mechanism from a metabolic perspective. Specifically, we include the relationship between ATP level, sodium-potassium pump, and repolarization level formalized in Eqn. (3.4) by making the partial reset mechanism energy-dependent. Our model includes ATP dependencies explicitly in $\beta := \beta(A(t))$ and follows the rationale explained above through the following formalization exhibited:

$$\beta(A(t)) = 1 + \alpha\left(2 - \frac{2}{1 + \mathrm{e}^{-\frac{A_H - A(t)}{A_H}\gamma}}\right), \tag{3.5}$$

where $\alpha = E_L/V_{th} - 1$. Based on Eqn. (3.5), we assume that β dependencies on ATP

follow a sigmoidal relationship. This relationship represents the membrane repolarization voltage values after an action potential occurs as a function of the available ATP in the neuron. Given that the precise curve of the repolarization membrane voltage depending on ATP is unknown, we introduced a sensitivity parameter γ, to account for this uncertainty. This parameter provides the flexibility to adjust the intensity at which the repolarization membrane voltage value is affected by ATP level changes. To illustrate this relation, Fig. 3.3 presents how higher values of the sensitivity γ account for a repolarization membrane voltage that is extremely sensitive to ATP displacement from homeostatic ATP (ATP_H). Conversely, lower γ values represent a smoother $V_{reset}(A)$ transition as the ATP level changes. In other words, in the absence of stimuli, higher γ values will increase the difficulty of achieving the equilibrium potential E_L after an action potential occurs, keeping the neuron slightly depolarized with respect to the equilibrium potential for a longer time. In contrast, in the same scenario, E_L will be achieved faster with lower values of γ. The aforementioned

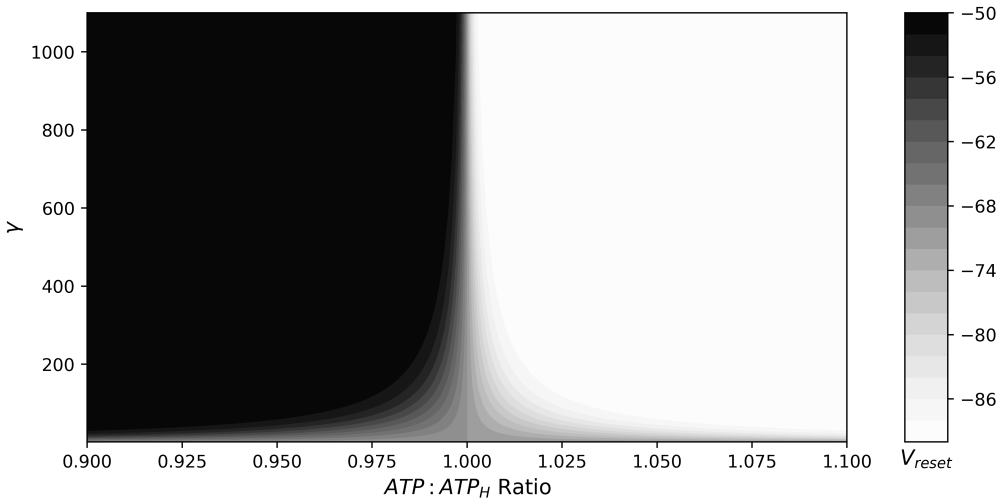

Figure 3.3: **Available ATP and repolarization.**
Relationship between available ATP ratio ($ATP : ATP_H$) and reset voltage V_{reset}, depending on the sensitivity parameter γ.

relationship between γ, neuronal ATP level and firing rate can be theoretically explored when a constant suprathreshold stimuli ($I_{inj} = I_0 > V_{th} g_{leak}$) is applied to the neurons model.

Given that the EDLIF model has an ATP-dependent reset potential $V_{reset}(A) = \beta(A)V_{th}$, using Equation (2.5) with initial condition $v_m(t = 0) = V_{reset}(A)$, gives the following trajectory for the membranes potential:

$$v_m(t) = v_\infty[1 - \mathrm{e}^{-t/\tau_m}] + V_{reset}(A)\mathrm{e}^{-t/\tau_m}, \tag{3.6}$$

where $v_\infty = (I_0/g_{leak} + E_L)$. The time it takes for a spike to be generated (*i.e.*, the interspike interval, s_0) is obtained imposing $v_m(s_0) = V_{th}$ [45]:

$$s_0(A) = \tau_m ln\big[\frac{v_\infty - V_{reset}(A)}{v_\infty - V_{th}}\big]. \tag{3.7}$$

Therefore, the corresponding ATP-dependent spiking-rate $\lambda(A)$ is described by the fol-

lowing equation (see Fig. 3.4):

$$\lambda(A) = (\tau_{ref} + s_0)^{-1}. \tag{3.8}$$

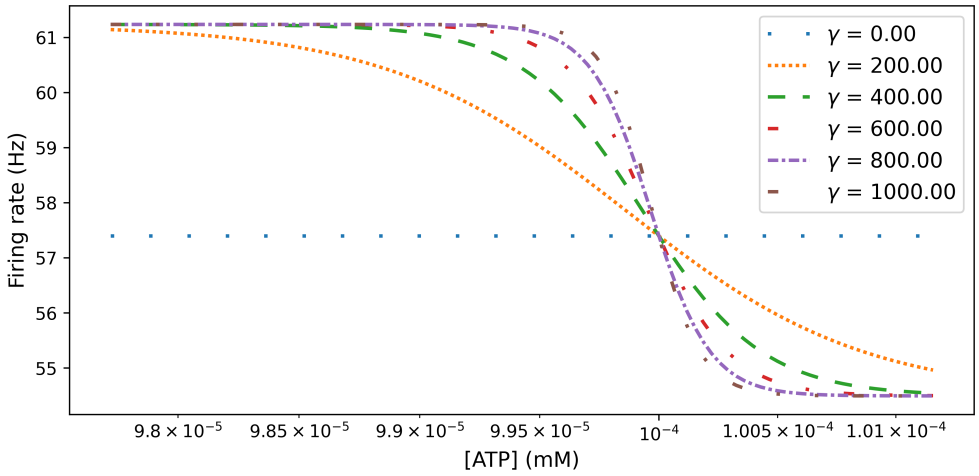

Figure 3.4: **Neuronal Firing rate and ATP.**
Neuronal theoretical firing rate for different γ values at distinct ATP level when a constant suprathreshold stimuli ($I_{inj} = I_0 > V_{th}$) is applied. $I_0 = 1000\ pA$.

As Fig. 3.4 shows, an ATP displacement from homeostatic ATP induces a different effect in the neuronal firing rate depending on the sensitivity parameter -γ- value. Higher values of γ imply an increasing sensitivity to slight ATP displacement from A_H. On contrary, with small values of $\gamma \sim 0$, the neuron is not affected by ATP displacement, as in the classic LIF or other GLIF models.

3.1.2 Parameter fitting

To fit our model to real spike trains and compare performances between EDLIF and LIF, we optimized both models using the dataset supplied by QSNMC ("Quantitative Single Neuron Modeling: Competition 2009") [62]. The QSNMC data comprise 13 voltage recordings of a layer five pyramidal neuron with the same stimulation for 39 *seconds*. Data were divided into training and test sets. First, we fitted the membrane conductance ($g_L = 32.9\ \mu\Omega^{-1}$), resting membrane potential ($V_{reset} = -67.54\ mV$), and equilibrium potential of the leak channel ($E_L = -67.54\ mV$) from the resting state. Specifically, we obtained them from the first five *seconds* of voltage recordings of the QSNMC dataset. The remaining 34 *seconds* of the recordings were divided as follows: the first 80% was used for fitting the remaining parameters and the last 20% for testing the model.

To fit the parameters of the model, we used the particle swarm optimization (PSO) algorithm, which was inspired by birds flocking behavior, where individuals share the best positions for getting food and finally converge to that point [63]. This algorithm seeks the best position of particles where the cost is minimum or the benefit is maximum. For the benefit function, we measured spike coincidence Γ (Eqn. (3.9)) between two spike trains

based on the competition method [64, 65]:

$$\Gamma = \frac{N_{coinc} - \langle N_{coinc} \rangle}{N_{data} + N_{model}} \frac{1}{N}, \tag{3.9}$$

where N_{data} is the number of spikes on real neuron recording, whereas N_{model} is the number of spikes given by the model; one spike coincidence is counted if the spike of the model exists within four *ms* (precision Δ) from that of reference. N_{coinc} is the total number of spike coincidences, and $\langle N_{coinc} \rangle = 2\nu\Delta N_{data}$ is the expected number of spike coincidences generated by an homogeneous Poisson process with the same frequency (ν) as the spike trains associated with N_{model}. Finally $N = 1 - 2\nu\Delta$ is a normalization term. To consider and measure spike trains reliability, we calculated the intrinsic reliability of the reference spike trains. For a detailed procedure of calculating intrinsic reliability and more information about spike coincidence, the reader is referred to the QSNMC articles [65, 62].

Finally, PSO seeks the best position around a bounded space, so we set the upper and lower bounds of each parameter. The bounds are presented in Table 3.2.

Table 3.2: **Upper and lower bounds of parameters**
Upper and lower bounds of parameters for optimization procedure. PSO algorithm fitted C_m, V_{th} and τ_r for LIF, and C_m, V_{th}, τ_r and γ for EDLIF.

	$C_m\ nF$	$V_{th}\ mV$	$\tau_r\ ms$	γ
Upper	400	-50	25	1000
Lower	200	-53	7	0

3.1.3 EDLIF evaluation

To test the EDLIF, we used three strategies:

- Performance contrast of EDLIF and LIF
- Evaluation of biological plausibility
- Evaluation of EDLIFs potential use in neurodegeneration

In order to evaluate the performance of EDLIF compared to LIF, we used publicly available data from *The quantitative single-neuron modeling competition* [62] and utilized the *spike-coincidence* (Γ) as a fitness function to measure the performance of each model, which allowed us to quantify the similarity between real spikes trains and the ones generated by each model. It is also possible to characterize the neurons spiking behavior through the *Inter-Spikes-Interval* (ISI) distribution. Fig 3.5 shows ISI distribution for the EDLIF and LIF model generated by a particular trial of neuronal recordings. To quantify the discrepancy between the real ISI distribution and the one generated by the model, the Jensen-Shannon metric [66] was used (the Jensen-Shannon metric is bounded between 0 and 1, and it is equal to 0 only if the two distributions under comparison are equal).

Biological plausibility was assessed by exploring the relationship between neuronal behavior and metabolism. Specifically, we wanted to explore two scenarios: (1) to evaluate the

on-demand ATP dynamics; (2) to study how the average firing rate impacts ATP consumption. For this purpose, we tested the model under stimulation conditions to trigger ATP productions *on-demand* similar to those reported in *in vitro* studies [17, 67]. This allowed us to evaluate if EDLIF presents on-demand ATP dynamics similar to those reported in vitro studies and to evaluate the impact of firing rate over ATP production.

To evaluate the potential of using EDLIF in neurodegeneration modeling, we used our model to explore neuronal behavior under a mitochondrial dysfunction scenario. One characteristic of the neurodegeneration firing rate dynamic in ALS is its increment under ATP deprivation, thereby leading to a higher firing rate, referred to as the deadly loop [23]. As such, we aimed to evaluate if EDLIF, which is a simple model, can mimic the deadly loop reported by the sophisticated model of Le Masson et al. (2014). To mimic a mitochondrial dysfunction, we simulated our model while considering different levels of reduced homeostatic ATP concentrations (A_H) where A_H can be interpreted as the severity of ALS, which is reflected in lower ATP availability. To evaluate the impact of A_H over firing rate in this scenario, we used a constant current (4 *seconds*), which was tuned such that the neuron fired at 15 Hz. Under this mitochondrial dysfunction scenario ($A_H < 10^{-4}$) , we expected an increment in the firing rate in relation to the A_H value. Therefore, our study indicated that the same stimulus should produce an increment in the neurons firing rate (> 15 Hz), following the rationale of the deadly loop [23]. In contrast, under homeostatic concentrations of ATP ($A_H = 10^{-4}$), the same stimulation should produce a constant firing rate (~ 15 Hz).

3.2 Results

In this chapter, we extended the LIF model to include ATP consumption and production in association with neuron physiology. As mentioned above, we evaluated the extended LIF model (EDLIF) by employing its ability to predict real data as well as predict a previously reported neurodegeneration pattern.

3.2.1 Models performance in predicting real spike trains

Table 3.3 shows, that the EDLIF model has a smaller average Jensen-Shannon metric (see column JS metric in Table 3.3) than the LIF model, implying that the EDLIF model is more akin to the real neuron ISI distribution than the one generated by the LIF model. Surprisingly, although the LIF model has a shorter refractory time compared to EDLIF (τ_r in Table 3.3), Figure 3.5 shows that for the EDLIF model, there exist ISI values within the range $(12.5, 25)$ *ms*, whereas interspike-intervals for the LIF model are always above 25 *ms*. This result can be explained through the energetic dependence introduced to the model through the incomplete repolarization mechanism.

Table 3.3 also presents the parameters (C_m, V_{th}, τ_r and γ) when executing the optimization algorithm in each model and the performance (Γ) that each one obtains.

These results showed that EDLIF exhibits better performance than the LIF model. It provides a better characterization of real neuron spikes trains under intracellular current

Table 3.3: **Model Parameters and Performance** Comparison of LIF and EDLIF model performance in test set in terms of *spike-coincidence* measure Γ (Mean ± SD). JS metric is the Jensen-Shannon (Mean ± SD) metric calculate between experimental ISI distribution and the one generate by the model. Results of the *Spike-coincidence* and Jensen-Shannon metric result are average across all trials of neuronal recording. Parameters are obtained by maximizing Γ in the training set through PSO optimization algorithm.

	C_m nF	V_{th} mV	τ_r ms	γ	Performance (Γ)	JS metric
LIF	279.94	-52.49	14.1		0.55 ± 0.0029	0.41 ± 0.018
EDLIF	202.43	-51.6	16.33	178.84	0.61 ± 0.0004	0.38 ± 0.02

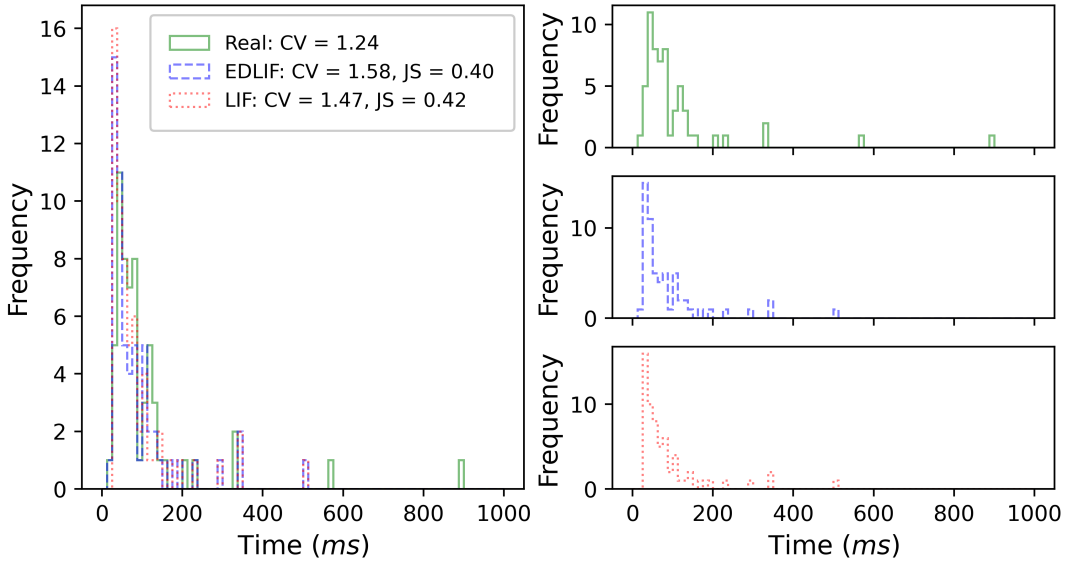

Figure 3.5: **Inter-spike-Interval distributions.**
Inter-spike-Interval distribution of LIF, EDLIF and real neuron recording. *CV* corresponds to the coefficient of variation, whereas *JS* is the Jensen-Shannon metric, which enables to contrast the discrepancy between the real ISI and the one given by each model. The distribution corresponds to an histogram with 80 bins.

stimulation either by considering the *spike-coincidence* measure (Γ) or by contrasting the similarity between the model and real ISI distribution using the Jenssen-Shannon metric.

3.2.2 Neurons energetics and behavior

To explore the biological plausibility by means of the relationship between energetics and neuronal behavior, we subjected the EDLIF model to different experiments. Figure 3.6 shows how stimulating the neuron affects ATP dynamics. When pulses of 600 pA amplitude and 10 seconds width were applied, the available ATP in the neuron started to drop. These stimuli generated a firing rate of approximately 36 Hz and caused a maximum of $\sim 0.4\%$ decrease in available ATP. Those minor ATP decreases mentioned earlier may be explained by the tight coupling between ATP consumption and production. Thus, ATP consumption was rapidly

supplied by ATP production, allowing the neuron to maintain a stable ATP concentration. These results are aligned with previous studies that showed the neuronal capacity to increase ATP production *on-demand* while consumption is increased [17, 67]. Regarding the rela-

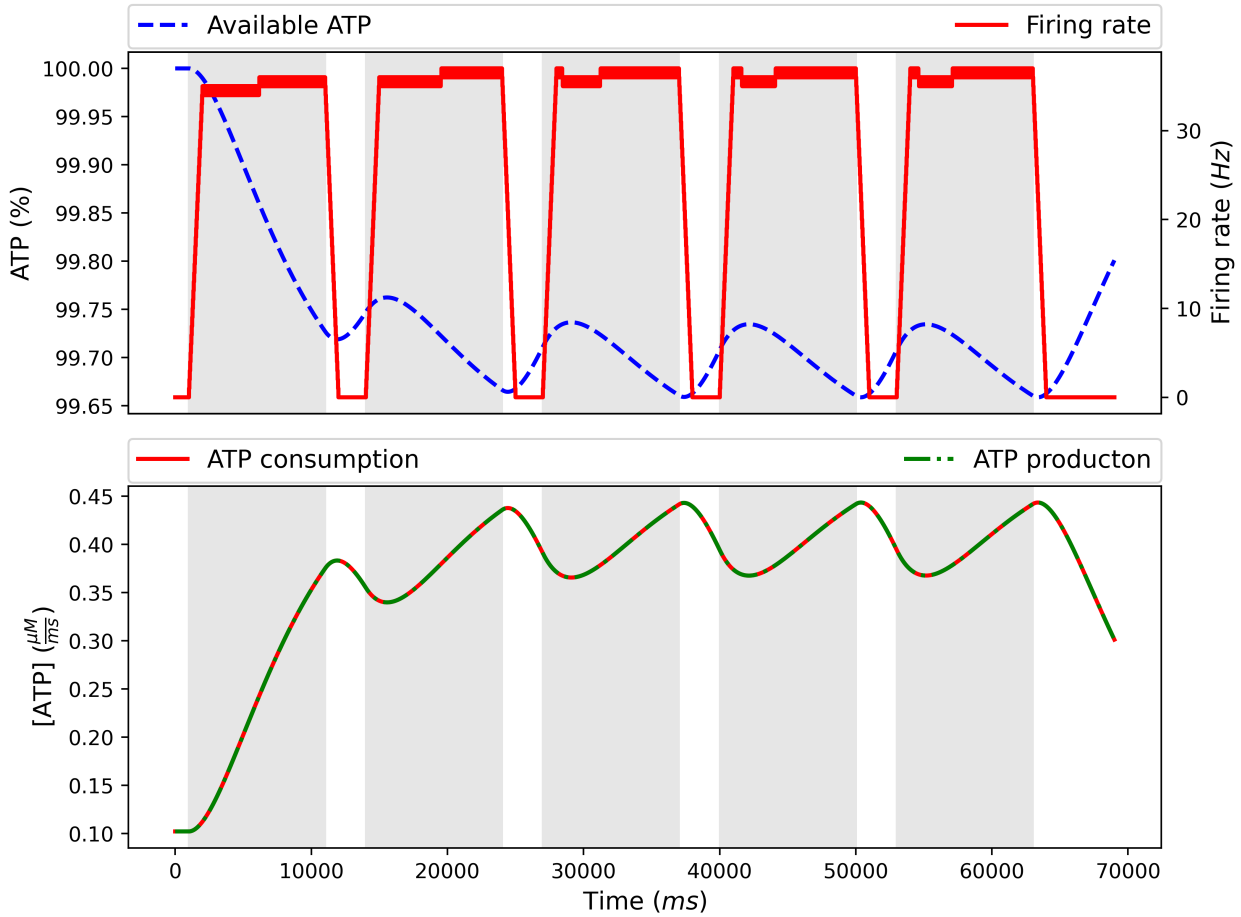

Figure 3.6: **Neuronal behavior and ATP dynamics.**
Neuronal behavior and ATP dynamics under 60 second stimuli: each pulse have an amplitude of 600 pA and 10 seconds width with a 3 sec 0 pA amplitud between each. Available ATP is measured in percentage with respect to homeostatic ATP level A_H (100% level means that available ATP is equal to A_H).

tionship between average firing rate and ATP consumption on the evaluation of biological plausibility, a thalamocortical biophysically-realistic model was used to show that the average firing rate, rather than temporal pattern, determined the ATP cost across firing patterns [68]. To study the relation between the average firing rate and ATP consumption, the EDLIF model was tested under different firing rates. Figure 3.7 shows that ATP demand increases linearly as a function of the firing rate in concordance with the study by Yi and Grill (2019). The increase in ATP consumption following an increase in firing rate could be explained by the depolarization phase of the action potential which generated abundant Na^+ entry, and this dominated the metabolic cost of neuronal activity. In summary, our model showed that there is a straightforward relation between ATP consumption and neuronal firing rate intensity, but because of the tight coupling between ATP consumption and production, the available ATP changes slightly.

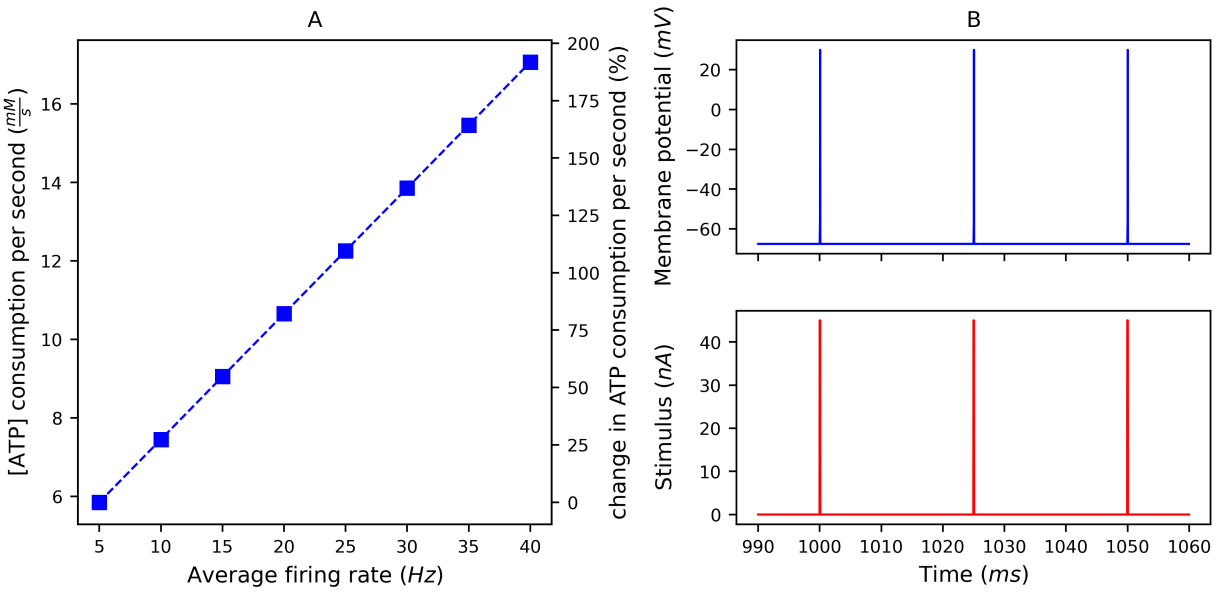

Figure 3.7: **Effect of average firing rate on estimated metabolic cost.**
(A) Total and relative (%) change in [ATP]/second consumption for different firing rates. (B) neuron's stimuli and corresponding membrane potential responds (mV). The stimuli consisted of 30 seconds of pulses of 0.1 ms width and 45 nA amplitude.

3.2.3 Neurodegeneration and energetics: amyotrophic lateral sclerosis

Because our model accounts for energy-dependencies affecting neuronal activity, it will be useful for studying neuronal behavior under a metabolic disorder. Specifically, to explore the link between bioenergetics and neuron degeneration, we used the EDLIF model and simulated neuronal behavior by stimulating the neuron with constant current (4 *seconds*) under mitochondrial dysfunction. As mentioned above, mitochondrial dysfunction was achieved by reduced homeostatic ATP concentration (A_H) by following Le Masson et al. (2014). As shown in Figure 3.8 , a more substantial mitochondrial dysfunction (lower A_H concentration) implies a higher firing rate response under the same stimuli. This shows how an energy depletion in the neuron affects sodium-pump activity and, consequently, the repolarization process. This entails a depolarization state, which increases the likelihood of an action potential, leading to a hyperexcitable state.

The inclusion of the sensitivity term (γ in Eqn. (3.5)) in the EDLIF model accounts for the different affection of energy imbalance in a particular neuron type; therefore, the model is suitable for describing energy-dependent sensitivity dynamics.

3.3 Discussion

This chapter introduced the EDLIF model, an energy-dependent extension of the classical LIF model. Our model aimed to integrate the effects of ATP imbalance levels in single-neuron dy-

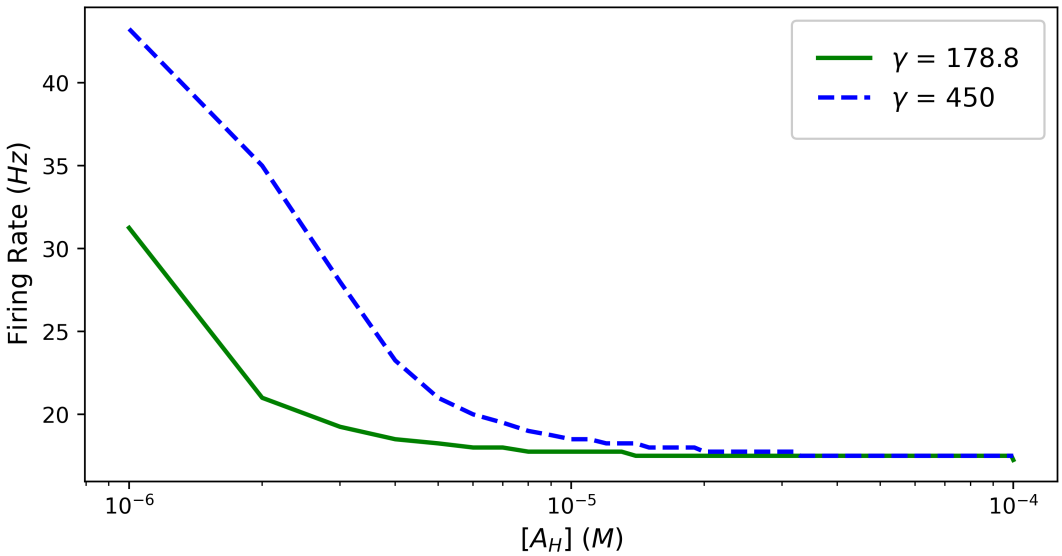

Figure 3.8: **Neuron behavior under ALS.**
Simulation of ALS disease by reduction of homeostatic ATP level (A_H). As ATP_H is reduced, neurons depolarize and their firing rate increases. When ATP_H is reduced, higher sensitivity values (γ) imply greater firing rate. These results are coherents with the effects of ALS in motor neurons described in [23].

namics through partial repolarization mechanisms. The biologically inspired inclusion of ATP dependence through partial reset mechanism allows the model to keep computational simplicity and improve predicting capabilities when representing real spike trains while considering both *spike coincidence* measure and the dissimilarity (*Jensen-Shannon metric*) between the real ISI distribution and the one generated by the models. Regarding predicting capabilities, we are aware of the predicting improvement associated with LIF with adaptation terms and, even thought the advances in this topic are valuable, our proposed neuronal model is strongly motivated for extending computational cheap neuronal models to account for metabolic dependencies. Therefore, in addition to the improvement in the models prediction capabilities concerning LIF, our model allows us to link energetics and neuronal behavior, keeping the simplicity of LIF and opening new possibilities to use simple-enough models to explore the neural activity and their link to energetics in the brain (*e.g.* Estimate ATP concentration dynamics). Additionally, EDLIF could be used to answer questions where LIF or LIF with adaptation are not suitable.

The EDLIF model can also emulate ALS neuronal behavior similar to the model introduced by Le Masson et al. (2014), but it uses a significantly more straightforward computation. In this sense, the EDLIF model seems suitable to study the effect of ALS *in silico* spiking neural networks with thousands of neurons. Naturally, EDLIF simplifications trade off with biological detailed description, such as avoiding specific modeling of channel kinetics in the neuron and the spatial dependencies stated in Le Massons (2014) model. Despite the limitations, the way in which the average firing rate affects ATP consumption was also quantified, indicating that the action potentials firing rate makes a significant contribution

to overall energy consumption. Quantifying the metabolic demand of neuronal activity influences the interpretation of functional brain imaging data through related metabolic mechanisms. Therefore, the EDLIF model prediction should be considered when interpreting findings of functional imaging studies that rely on estimates of neuronal metabolic demand, *e.g.*, functional magnetic resonance imaging [68].

Despite the advantages of the proposed model with respect to LIF and other more complex models, some limitations are worth mentioning. First, given that our goal was to develop a simple model that can simulate networks of thousands of neurons, the EDLIF model neglects calcium kinetics and morphological or spatial description, *i.e.* EDLIF is a single-compartment model. Evidence suggested that the sodium-potassium pump plays a significant role in neuronal activity by regulating membrane potentials and neuronal firing. Experiments showed that pharmacological blocking of sodium-potassium pumps increases the spontaneous firing rate and generates membrane depolarization [69]. It has also been shown that there is a membrane voltage depolarization of the neurons during hypoxia and ischemia. This increase is partly due to the inhibition of the Na-K pump due to lowered ATP levels [70]. These experiments emphasized the relevance of Na-K pumps in neuronal activity and their relationship with ATP levels. In this regard, the EDLIF model includes an ATP imbalance in the Na-K pump through incomplete repolarization mechanisms. Thus, the model is a suitable tool for studying the effect of ATP imbalance in neuronal behavior by accounting for the sodium-potassium pumps inhibition when the ATP level is low (as in the case of hypoxia) as well as its consequences on neural and network activity.

ALS results were coherent with other neurodegenerative conditions as the abnormal high-frequency burst firing in rapid-onset dystonia-parkinsonism, which suggested that partially blocking sodium-potassium pumps in the cerebellar cortex is sufficient to cause dystonia, as it increased the firing rate of cells and ultimately caused a conversion from tonic firing to high-frequency bursting activity [71]. Fremont et al., (2014) also showed the relationship between the sodium channel density and sensitivity to a partial block of the sodium-potassium pump. A lower sodium channel density implies less sensitivity to the partial blockade of sodium pumps. Thus, γ can be explained in biological terms associating it with the density of sodium channels and disclosing why different γ values better describe the behavior of different neuron types in the EDLIF model. Finally, considering the vast literature linking metabolic dysfunction and neurodegenerative disease [12, 13, 14, 15, 16, 17, 72], simple computational models as the one introduced in this thesis become relevant as an alternative to classical LIF extensions because of their capability to include energetic dependencies, which make them suitable for studying the effect of metabolic disorder using *in silico* networks.

Chapter 4

Energy-dependent Spike-Timing-Dependent Plasticity

Our goal is to study the impact of local energy constraints on the properties of the network and, to comply with that, although it is necessary to have an energy-dependent single-neuron model (Chapter 3), this is insufficient. The energy administration of the neuron is essential for its adequate operation, and considering the significant effect of these restrictions on synaptic activity [9, 31, 16, 17], then, before studying the relationship between energy management and organization in biological neural networks, the need to have synaptic transmission rules that depend on the energy management of the cell emerges naturally. Consequently, in this chapter we leverage on the EDLIF model as well as previously defined plasticity models to introduce an energy-dependent synaptic plasticity rule.

Synaptic plasticity occurs at different time scales [48]. For instance, short-term plasticity [49] is only maiintained on time scales of less than one second. In contrast, long-term plasticity considers persistent changes in the synaptic response that can be generated in the order of milliseconds and last for hours [50], such as long-term potentiation and depression (LTP and LTD, respectively). There are also slower stabilization processes, such as homeostatic plasticity (or synaptic scaling) that occurs on the order of minutes to days [52]. In this chapter we focus on the long-term synaptic plasticity mechanisms, specifically LTP and LTD.

Inspired by the experiments made by Bi and Poo [50], a very popular plasticity model in computational neuroscience is the spike-timing-dependent plasticity (STDP) model [54, 55, 56, 57]. However, to the best of our knowledge, non of those plasticity models include notions of energy dependencies or metabolic constraints, modifying plasticity as neuronal energy levels vary. Nevertheless, there are biological evidence showing the synaptic plasticity dependence on energy constraints [73]. Build on this observation, and in previously developed spike-timing-dependent plasticity models, now we proceed to mathematically define and numerically test an energy-dependent STDP model.

4.1 Synapses and energy consumption

In chapter 3, we studied single-neuron energy and voltage dynamics when energy constraints are imposed on the neuron. Previously, to study energy dynamics, detailed activity-related energy consumption values were used (see Chapter 3). However, in practice, it is very difficult to measure energy level in the neuron and it is not clear neither how to establish nor to measure the homeostatic energy level (A_H) in the neuron. To overcome this difficulty and to define a more general framework, from now on (Chapters 4 and 5) we will use percentage units to quantify available energy ($A(t)$), homeostatic energy ($A_H = 100\%$), and activity-related energy consumption such as action potential energy consumption (E_{AP}), house-keeping (E_{HK}), resting potential (E_{RP}), and postsynaptic energy consumption (E_{syn}).

To understand in detail the energy perturbations induced by presynaptic neurons in postsynaptic energy levels through synapses, let us analyze the neuron's energy dynamics when several presynaptic neurons are connected to it. In a network, each neuron's energy evolves as follow:

$$\frac{\mathrm{d}A(t)}{\mathrm{d}t} = A_s(t) - A_c(t), \tag{4.1}$$

where $A_s = K(A_H - A) + A_B$, and the energy consumption A_c can be divided into the following terms:

$$A_c(t) = A_B + A_{ap}(t) + A_{syn}(t), \tag{4.2}$$

where A_B is the basal consumption accounting for resting potential and housekeeping activities, A_{ap} is the energy consumption accounting for the neuron action potentials, and A_{syn} is the energy consumption related to receiving actions potential from other neurons through the synapses[1].

The solution to Eqn. (4.1) with an arbitrary energy consumption $A_c(t)$ is described by Eqn. (4.3):

$$A(t) = A_H - \int_0^t \mathrm{e}^{-(t-t')/\tau_A} A_c(t')\mathrm{d}t', \tag{4.3}$$

where $K = 1/\tau_A$ is the rate at which ATP can be produced in the neuron (see (3.2)). Eqn. (4.3) can be found using the impulse response of the system described by Eqn. (4.1), together with the superposition principle. Please realize that without considering each variable measurement unit, the energy dynamic in Eqn. (4.3) is analogous to the voltage dynamic in the LIF model under Eqn. (2.5), with the following modification $A(t) \to v(t)$, $I(t) \to -A_c(t)$, $v_{rest} \to A_H$, $g_{leak} \to K$, $C_m \to 1$.

In chapter 3 we explained how different activities change the available energy in the neuron. However, because we focused on the single-neuron dynamics, we excluded from the analysis the synaptic effect on energy dynamics. Now we will describe how presynaptic activity affects postsynaptic available energy levels. For one presynaptic action potential propagating through a synapse with strength w, the synaptic consumption on the postsynaptic neuron

[1] $A_{ap}(t)$ ($A_{syn}(t)$) is different than E_{AP} (E_{syn}). The former is the action potential (postsynaptic) energy consumption through time, and the latter is the total amount of energy related to that activity. Thus, A_{ap} (A_{syn}) is obtained using E_{AP} (E_{syn}) and a kernel function $\varepsilon(\cdot)$ which describes how the total energy consumption is expended through time.

can be described by:

$$A_{syn}(t) = E_{syn}\bar{w}\Theta(t - t_s)\varepsilon_{syn}(t - t_s), \tag{4.4}$$

where E_{syn} is the total energy expended for an incoming presynaptic action potential, $\bar{w}$ is the absolute value of the normalized synaptic strength ($\bar{w} = |w/w_{max}|$, where w_{max} is the maximum allowed weight strength) and $\varepsilon_{syn}(t)$ is a kernel describing how the synaptic energy expenditure is expended through time ($\int_0^\infty \Theta(t)\varepsilon_{syn}(t)\mathrm{d}t = 1$). If we choose a kernel that can be linearly summed up, then the synaptic energy expenditure in the postsynaptic neuron with several presynaptic cells and spike times is:

$$A_{syn}(t) = E_{syn} \sum_{synapse\ k} \sum_{spike\ s} \bar{w}_k \Theta(t - t_s)\varepsilon_{syn}(t - t_s). \tag{4.5}$$

Similarly, for each action potential in the postsynaptic neuron, the energy expenditure can be described by:

$$A_{ap}(t) = E_{ap}\Theta(t - t_s)\varepsilon_{ap}(t - t_s), \tag{4.6}$$

where E_{ap} is the energy expenditure related to one action potential and ε_{ap} is analogous to ε_{syn}, but for the postsynaptic action potentials ($\int_0^\infty \Theta(t)\varepsilon_{ap}(t)\mathrm{d}t = 1$). If ε_{ap} can be linearly summed up, then Eqn. (4.6) reads:

$$A_{ap} = E_{ap} \sum_{spike\ s} \Theta(t - t_s)\varepsilon_{ap}(t - t_s). \tag{4.7}$$

For finding closed-form expressions for the available energy in the postsynaptic neuron, it is possible to define ε_{ap} and ε_{syn} kernels and plugin Eqns. (4.5) and (4.7) into Eqn. (4.1). In particular, if exponential kernels are used for ε_{ap} and ε_{syn}, Eqn. (4.5) reads:

$$A_{syn}(t) = \sum_{synapse\ k} \sum_{spike\ s} \frac{\bar{w}_k E^k_{syn}}{\tau^{A,k}_{syn}} \Theta(t - t_s)\mathrm{e}^{-(t-t_s)/\tau^{A,k}_{syn}}, \tag{4.8}$$

where $\tau^{A,k}_{syn}$ is the energy time constant of the kth synapse and describes how *fast* is the change in the postsynaptic neuron's energy given the incoming action potential through the kth synapse. Note that if $w_k = w_{max}$ the total energy consumption in the postsynaptic neuron produced by the presynaptic neuron sending one action potential through synapse kth is E^k_{syn}. Thus, Eqn. (4.8) guarantees that for the maximum allowed synaptic weight, the total energy consumption perceived by the postsynaptic neuron is exactly E^k_{syn} and a fraction ($|w_k/w_{max}|$) of E^k_{syn} otherwise. Similarly, using an exponential kernel, Eqn. (4.7) can be expressed as:

$$A_{ap}(t) = \Theta(t - t_s)\frac{E_{ap}}{\tau_{ap}}\mathrm{e}^{-(t-t_s)/\tau_{ap}}, \tag{4.9}$$

where τ_{ap} is the time constant defining how *fast* is E_{ap} expended through time. Consequently with Eqn. (3.3), Eqn. (4.9) guaranties that the neuron will consume a total amount of E_{ap} for each action potential.

Therefore, plugin Eqns. (4.9) and (4.8) into Eqn. (4.3), we have a closed-form expression for the neuron's energy dynamics under exponential kernels (ε_{ap} and ε_{syn}) for energy

consumption:

$$A(t) = A_H - \overbrace{\frac{E_{ap}\tau_A}{\tau_A - \tau_{ap}} \sum_{spike\ s} \Theta(t - t_s)[\mathrm{e}^{-(t-t_s)/\tau_A} - \mathrm{e}^{-(t-t_s)/\tau_{ap}}]}^{A_{ap}(t)} - \underbrace{\sum_{synapse\ k} \sum_{spike\ f} \frac{E^k_{syn}\bar{w}_k\tau_A}{(\tau_A - \tau^{A,k}_{syn})}[\mathrm{e}^{-(t-t_f)/\tau_A} - \mathrm{e}^{-(t-t_f)/\tau^{A,k}_{syn}}]}_{A_{syn}(t)}. \tag{4.10}$$

Eqn. (4.10) describes the energy dynamics of a single neuron within a network, given all incoming synapses strengths and spike-times. Thus, it allows to precisely quantify and analyze the energy dynamics of each neuron within a network with arbitrary architecture.

4.2 Energy Dependent Spike-Timing-Dependent-Plasticity model

In section 4.1 closed-form expressions for available energy level in the cell were introduced. In Eqn. (4.10) the neuron's energy expenditure due to synaptic activities is pondered by the normalized synaptic strength $\bar{w}_k$, however, as explained in section 2.3, strength between neurons change over time (*i.e.* $w_k := w_k(t)$). Therefore, based on previous work, we introduced an energy-dependent plasticity rule for synaptic strength. We follow the formalization of STDP introduced in [54] (see section 2.3), and inspired our energy-dependent plasticity rule from the findings shown in [73]. We focus on the fact that plasticity, in particular Long-Term Potentiation (LTP), depends on metabolism. Specifically, when glycolysis is pharmacologically inhibited (thus ATP production from glucose is inhibited), then LTP is suppressed [73]. Consequently, our energy-dependent STDP rule should suppress LTP when there is a low energy level. Following this observation, we proceed to extend Eqn. (2.25) to account for energetics, while keeping in mind that this is a practical simplification of much more complex biological phenomena, but which allows deepening the understanding of metabolism and plasticity interactions, and its impact on neural network dynamics.

To account for energetics in STDP, it is possible to extend $f_+(w)$ in Eqn. (2.26) to include the energy level A of the postsynaptic neuron[2], obtaining $f_+(w, A)$. There are several ways to mathematically formalize the inclusion of postsynaptic energy level in $f_+(w)$, but we follow a similar rationale as the one used when formalizing the EDLIF neuron, namely, we want energy-dependent STDP to be *sensitive* to energy imbalance. Hence, we can investigate not only how energy affects STPD, but also how energy imbalance affects STDP given a certain level of *energy imbalance sensitivity* in that synapse's plasticity. Using the aforementioned logic we extend $f_+(w)$ to $f_+(w, A)$ as follows:

$$f_+(w, A) = f_+(w)\mathrm{e}^{-\eta\frac{A_H - A}{A_H}}, \tag{4.11}$$

[2]STDP effects can be thought as a change in postsynaptic receptors density, and because the postsynaptic neuron has to modify receptors density, then their energy level is the one affecting receptors density modifications, and we do not need to take care about presynaptic energy level.

where η is the sensitivity of the synapse's plasticity to energy imbalances, A_H is the homeostatic energy level, and A is the postsynaptic energy level. Please note that if the synapse is not sensitive to energy imbalances (*i.e.* $\eta = 0$), then we recover the original STDP rule. The postsynaptic energy level can be interpreted as a plasticity modulator. Thus, our energy-dependent STDP rule is a special case of a three-factor learning rule, with postsynaptic available energy A as modulator (see Eqn. (2.28) and Fig. 4.1).

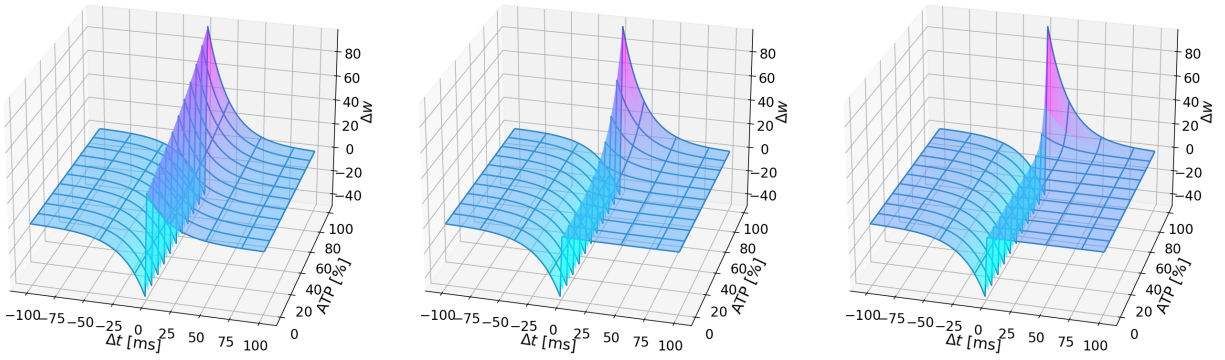

(a) $\eta = 1$ (b) $\eta = 5$ (c) $\eta = 20$

Figure 4.1: **Energy-dependent STDP.**
Weight potentiation depends on postsynaptic available energy A. If energy $A = A_H$, the original STDP rule is recovered (see Figure 2.5), while for $\eta = 0$ the synapse's plasticity is insensitive to energy imbalance, thus weight update only depends on spike-timing differences (Δt). If the postsynaptic available energy decreases, potentiations is suppressed and potentiation suppression depends on the sensitivity parameter η. a) sensitivity $\eta = 1$, b) sensitivity $\eta = 5$, c) sensitivity $\eta = 20$.

For the depression updating function $f_-(w)$ we keep the original formulation ($f_-(w) = \alpha w^{\mu-}$, see Eqn. (2.26)) because we do not have conclusive evidence justifying the depression dependence on postsynaptic available energy. However, energy may be also affecting depression. The inclusion of energy dependence on STDP depression, as well as other ways in which energy affects plasticity is subject of future research.

Plugging Eqn. (4.11) into Eqn. (2.25), it is possible to describe weight's update accounting for pre- and postsynaptic spike-time and postsynaptic energy level:

$$\Delta w = \begin{cases} \lambda f_+(w, A) \mathrm{e}^{-\Delta t/\tau_+}, & \text{if } \Delta t > 0. \\ -\lambda f_-(w) \mathrm{e}^{\Delta t/\tau_-}, & \text{if } \Delta t \leq 0. \end{cases} \tag{4.12}$$

In principle, Eqn. (4.12) allows to include weight w dependencies in the updating rule if $\mu_\pm > 0$[3]. In those cases, the updating rule is called a multiplicative rule, while if $\mu_\pm = 0$ the updating rule is additive, because weight update is independent of the current weight value. Multiplicative rules generate uni-modal weights distributions while additive rules generates bi-modal weights distributions [54]. As bi-modal weights distributions are observed in biology and because mathematical tractability of STDP additive rules is easier than multiplicative

[3]Please remember that $f_+(w) = (1-w)^{\mu_+}$ and $f_-(w) = \alpha w^{\mu-}$, as described in Chapter 2.

ones, in what follows we decided to use an additive update rule for weights update ($\mu_{\pm} = 0$), however, there is also significant biological evidence supporting multiplicative STDP. For this reason we define Eqn. (4.12) in a general form, allowing the exploration of multiplicative energy-dependent STDP in future work.

4.2.1 Energy-dependent plasticity and equilibrium

As we previously explained, our energy-dependent STDP rule uses postsynaptic available energy as a neuromodulator. Therefore, for low postsynaptic energy levels, potentiation is suppressed and the suppression depends on the sensitivity parameter η. For the following explanation let us assume equal synaptic time constants (*i.e.* $\tau_+ = \tau_-$). Intuitively, given Eqn. (4.12) and $A(t = 0) = A_H$ initial postsynaptic available energy, if peak potentiation is stronger than peak depression (*i.e.* $\alpha \in [0, 1)$) then, for uniformly random pre- and postsynaptic spike times, in a short-time window simulation, weights tend to increase in average (see Figure 4.2a). Higher weights induce more energy consumption in the postsynaptic neuron (because of the increased energy expenditure related to postsynaptic potentials and, also, because postsynaptic neurons will integrate more current potentially increasing firing rate, which also contributes to energy consumption). Therefore, postsynaptic available energy decreases, suppressing potentiation. If potentiation is strongly suppressed then, for uniformly random pre- and postsynaptic spike times, in a short-time window simulation, depression will have a greater effect on weights, generating a net depression effect on weights (see Figure 4.2b). This net depression force weights to decrease on average, thus decreasing the postsynaptic firing rate and also diminishing postsynaptic energy consumption. Consequently, postsynaptic available energy increases, allowing stronger potentiation than depression, which put us back in the loop (see Figure 4.2). However, it is also possible that the postsynaptic available energy reaches an equilibrium level where potentiation and depression balance each other. Before proceeding with further experiments, let us formally explain this intuition.

Let us assume random uniformly distributed inter-spike intervals $\Delta t = t_{post} - t_{pre}$:

$$\Delta t \sim U[-\Delta t', \Delta t']. \tag{4.13}$$

Given the postsynaptic available energy A, the net effect, also called drift, experienced by weights is the integral of Δw from Eqn. (4.12) over all possible Δt:

$$\int_{-\Delta t'}^{\Delta t'} \Delta w \mathrm{d}t = \int_{-\Delta t'}^{0} -\lambda\alpha \mathrm{e}^{t/\tau_-}\mathrm{d}t + \int_{0}^{\Delta t'} \lambda \mathrm{e}^{-\eta(A_H - A)/A_H}\mathrm{e}^{-t/\tau_+}\mathrm{d}t \tag{4.14}$$

$$= \lambda\Big[-\alpha\tau_- \mathrm{e}^{t/\tau_-}\Big|_{-\Delta t'}^{0} - \tau_+ \mathrm{e}^{\eta(A_H - A)/A_H}\mathrm{e}^{-t/\tau_+}\Big|_{0}^{\Delta t'}\Big] \tag{4.15}$$

$$= \lambda[-\alpha\tau_-(1 - \mathrm{e}^{-\Delta t'/\tau_-}) - \tau_+ \mathrm{e}^{-\eta(A_H - A)/A_H}(1 - \mathrm{e}^{-\Delta t'/\tau_+})] \tag{4.16}$$

If $\tau_+ = \tau_- = \tau_{syn}$, Eqn. (4.16) reads:

$$\int_{-\Delta t'}^{\Delta t'} \Delta w \mathrm{d}t = \underbrace{\lambda\tau_{syn}(1 - \mathrm{e}^{-\Delta t'/\tau_{syn}})}_{\geq 0}[-\alpha + \mathrm{e}^{-\eta(A_H - A)/A_H}]. \tag{4.17}$$

Consequently, if $e^{-\eta(A_H-A)/A_H} > \alpha$, then potentiation is favored (*i.e.* $\int_{-\Delta t'}^{\Delta t'} \Delta w dt \geq 0$). Whereas if $e^{-\eta(A_H-A)/A_H} < \alpha$ depression is favored. Similarly, if $e^{-\eta(A_H-A)/A_H} \stackrel{!}{=} \alpha$ we can find the update weight fixed point (*i.e.* $\Delta w = 0$), which gives the energy level $\breve{A}$ value for which potentiation and depression mutually balance each other:

$$\breve{A} = A_H\Big(1 + \frac{\ln(\alpha)}{\eta}\Big). \tag{4.18}$$

Eqn. (4.18) predicts the available energy level on the postsynaptic neuron for which, on average, potentiation and depression are compensated[4]. Moreover, the equilibrium level for postsynaptic available energy $\breve{A}$ is inversely proportional to the sensitivity parameter η. As a consequence, if the plasticity rule is highly sensitive to energy imbalances, then Eqn. (4.18) guarantees that the postsynaptic energy level stay close to A_H (see Figure 4.3). As we will explain in chapter 5, this fixed point is crucial for the network dynamics, because for $A = \breve{A}$ the weights are static (on average), thus average incoming current to the neuron should stay approximately constant if average is calculated over a time period T_w greater than membrane and synaptic time constant (*i.e.* $T_w \gg \tau_m, \tau_{syn}$). Thus, we should expect a fixed point for the firing rate also. In chapter 5 we will formalize this intuition.

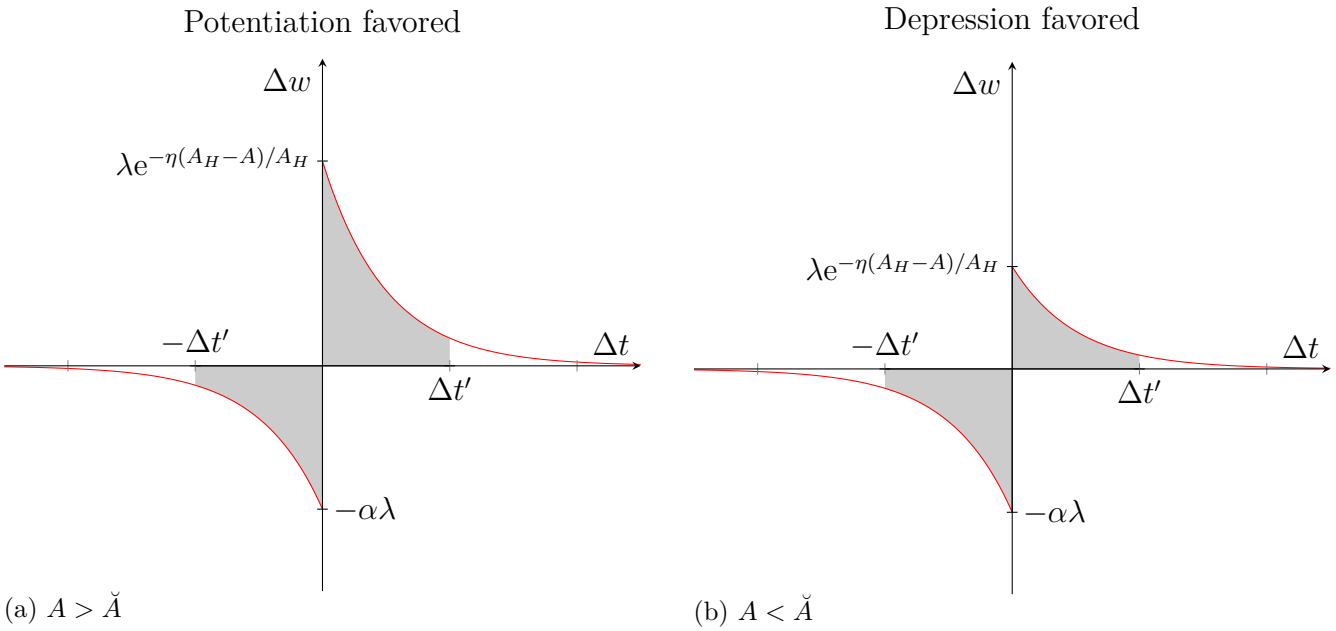

(a) $A > \breve{A}$ (b) $A < \breve{A}$

Figure 4.2: **Energy-dependent plasticity and postsynaptic available energy.** Potentiation suppression depends on postsynaptic energy level A. If $A > \breve{A}$ potentiation is favored a), while for $A < \breve{A}$ depression is favored b)

[4]Given that in our setup A represents the energy level with respect to $A_H = 100\%$, the energy level found using Eqn. (4.18) should be in the $[0, 100]$ range. Therefore, in case $\breve{A}$ escapes from $[0, 100]$ it should be clipped to respect biologically plausible energy levels.

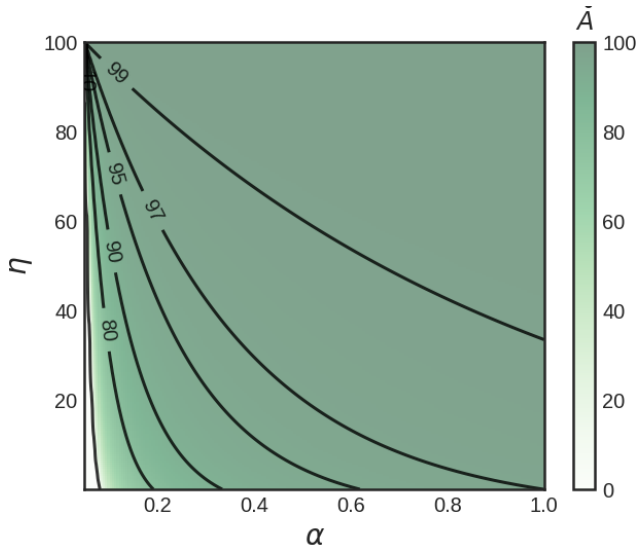

Figure 4.3: **Available postsynaptic energy equilibrium level $\breve{A}$.**
Postsynaptic energy equilibrium level $\breve{A}$ as a function of the sensitivity parameter η and depression scaling factor α. $A_H = 100\%$.

4.3 Results

To numerically test our theoretical predictions, the experiments are simulated utilizing the NEural Simulation Tool program (NEST) [74] and the EDLIF neuronal model as well as the ED-STDP synaptic model are specified using NESTML [75]. The domain specific language tailored for the spiking neural network simulator NEST.

4.3.1 Two-neurons experiment

To validate that our energy-dependent STDP rule defined in Eqn. (4.12) is in agreement with numerical simulations, we first test the ED-STDP rule under the simplest experimental setup: a single pre- and postsynaptic excitatory neuron, as ilustated in Fig. 4.4. In this setup, the pre- and postsynaptic neurons were assigned arbitrary spike times, allowing the measurement of specific spiking-time delays, calculated as the difference between the postsynaptic and presynaptic spike times. This experiment is an *in silico* analogous to the *in vitro* experiment carried out in [50].

By comparing the expected weight updates, computed using Eqn. (4.12), with the weight updates obtained through simulations using one presynaptic and one postsynaptic EDLIF neuron model, it is possible to evaluate the agreement between the theoretical and simulated

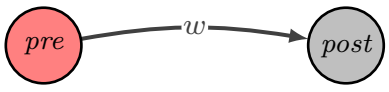

Figure 4.4: **Two-neurons experiment setup.**
A single excitatory presynaptic neuron connected by synapse w to a single excitatory postsynaptic.

results. To properly compare the weight updates given by Eqn. (4.12) against simulation, we set the ATP energy level of the EDLIF neuron to $100\%, 80\%$ and 60% values, each of those corresponding to a different weight update curve as shown in Fig. 4.5 (the weight update curve associated to an specific ATP level ATP^* is the intersection between the Eqn. (4.12) and the plane satisfying $ATP = ATP^*$ in Fig. 4.1). In this manner, it is possible to compare the expected weight updates from Eqn. (4.12) against numerical simulations. If the ATP energy level of the EDLIF neuron is not set to a constant value, then each spike and post-synaptic potential in the simulation generates an energy consumption thus making it harder to compare experimental results against what is expected from theory.

Fig. 4.5 shows the contrast between the weight updated expected using Eqn. (4.12) (referred to as the "Theory" curve) with respect to the one obtained when the plasticity rule is computed through simulations using the EDLIF neuron model, thus having spiking neurons (referred to as the "Experiment"curve). In this manner, Fig. 4.5 demonstrate that

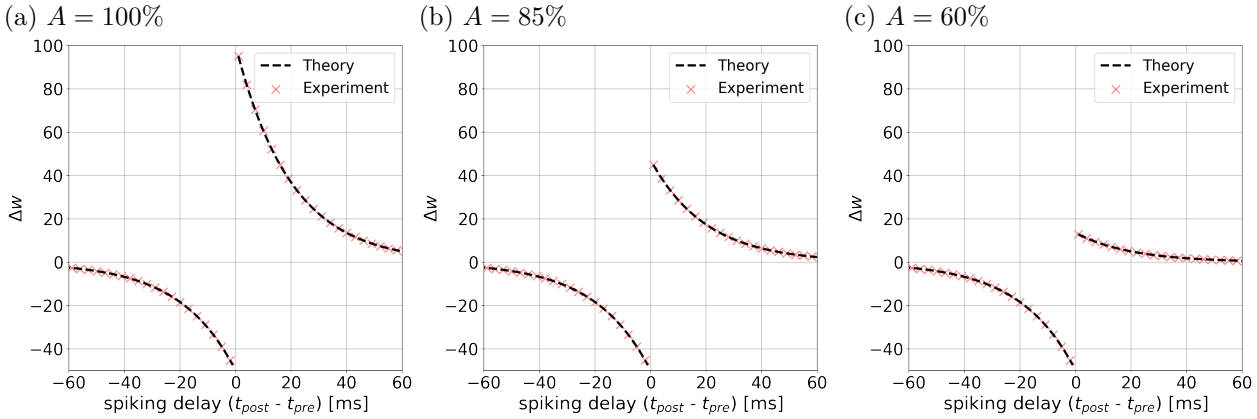

Figure 4.5: **Energy-dependent STDP theory versus *in-silico* experiment.** The contrast between theoretically expected weight updates using Eqn. (4.12) versus measured weight updates obtained through simulations using *in silico* EDLIF neurons (one presynaptic and one postsynaptic neuron, in accordance with the experiments carried out in [50]. See Fig. 4.4). For contrasting the theory and observations, in the simulated experiment the postsynaptic energy level (A) is fixed to a constant value. a) fixed postsynaptic energy level $A = 100\%$, b) fixed postsynaptic energy level $A = 85\%$, c) fixed postsynaptic energy level $A = 60\%$. All simulations use $\eta = 5$.

the weight updates under different ATP levels obtained through simulations using EDLIF spiking neurons align well with the expected theoretical weight updates values derived from Eqn. (4.12).

4.3.2 Bombarding postynaptic neuron

So far we have developed an energy-dependent STDP rule which allows the suppression of synaptic potentiation when the available energy level drops. We found a closed-form expression that allows us to predict the available energy equilibrium level under uniformly distributed spikes times (Eqn. (4.18)). Now we proceed to verify if the theory corresponds with experimental results. To evaluate the theoretical prediction given by Eqn. (4.18) we test

our predictions connecting m presynaptic neurons to one postsynaptic unit as it is shown in Figure 4.6. An excitatory current (I_{ex}^{post}) is injected into the postsynaptic neuron generating a basal firing rate for this unit and, similarly, each presynaptic neuron has an excitatory current I_{ex}^{pre} sampled from a random normal distribution, thus every presynaptic neuron has its own firing rate. For the experiment, we use the EDLIF model (see Chapter 3) but with no sensitivity to energy imbalance (*i.e.* $\gamma = 0$), hence recovering the classical LIF model dynamics (section 2.1.2.1), but enabling the measurement of energy level on each neuron, which is necessary in order to use ED-STDP. Figure 4.7 shows the results of applying ED-

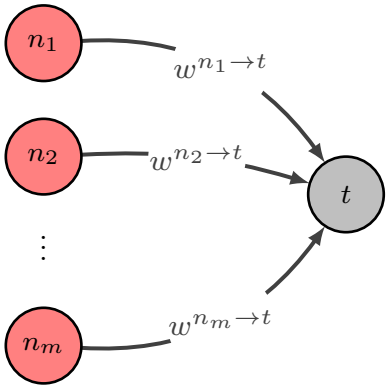

Figure 4.6: **Weight equilibrium experiment setup.**
Multiple excitatory presynaptic neurons stimulating one postsynaptic neuron.

STDP on the all-to-one architecture ilustrated in Figure 4.6, with 1000 presynaptic units for 12 seconds. Each row in Figure 4.7 corresponds to the simulation of the same experiment with equal initial conditions but with different η sensitivity.

The first column of Figure 4.7 shows available ATP on the postsynaptic neuron through time, as well as the postsynaptic firing rate. The second column shows the weights strength evolution, and the third column shows the histogram associated with the value of the weights at the end of the simulation. In agreement with Eqn. (4.18), while increasing η the postsynaptic equilibrium available energy ($\breve{A}$) increases. Moreover, the available energy in the postsynaptic neuron converges towards the predicted equilibrium value coherently with our theoretical predictions. Although the weights are always varying because of the specific inter-spike intervals, the postsynaptic energy level oscillates around $\breve{A}$ and, coherently with our previous explanations, this oscillation occurs because when $A < \breve{A}$ depression is favored allowing the postsynaptic neuron to recover from the energy deficit. If the neuron energy recovers in such a way that the condition $A > \breve{A}$ is fulfilled, then potentiation is favored which in turn will push the postsynaptic neuron's energy to lower energy levels. This explains why the neurons energy oscillates around $\breve{A}$, which is the energy level that enables counterbalance between potentiation and depression. Consequently, $\breve{A}$ is an attractor for the system described by Eqn. (4.10).

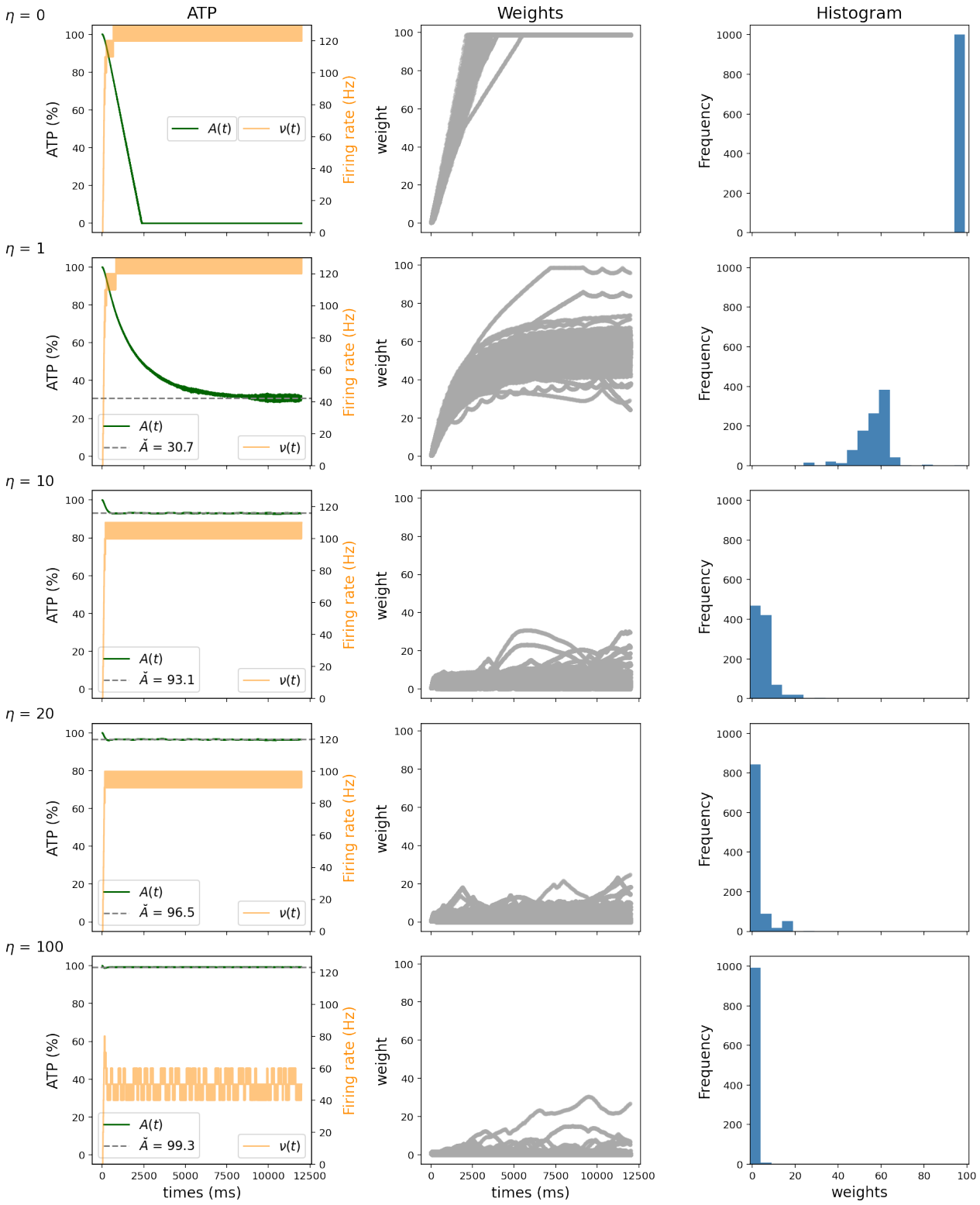

Figure 4.7: **Weight sensitivity to energy imbalance and equilibrium.** Multiple excitatory presynaptic neurons ($m = 1000$) stimulating one postsynaptic neuron for different sensitivity η values. As η increases, $\breve{A}$ is closer to A_H, consequently with Eqn. (4.18). Only excitatory synapses are present in the experiment, and the initial value for all weights is zero. Specific parameter values for the experiment are shown in Table 4.1.

Table 4.1: **Parameters used in the experiment.**
Parameter values associated with the experiment described in Figure 4.6 and the results shown in Figure 4.7.

Parameter	Value	Unit
Δt_{sim}	0.1	ms
α	0.5	-
μ_-	0	-
μ_+	0	-
λ	0.01	-
τ_m	20	ms
τ_{ref}	8	ms
C_m	200	pF
v_{reset}	-70	mV
v_{rest}	-70	mV
v_{th}	-50	mV
τ_{syn}	6	ms
τ_{ap}	100	ms
I_{ex}^{pre}	210 $\pm$ 10	pA
I_{ex}^{post}	175	pA
τ_{syn}^{A}	100	ms
E_{AP}	8	%
E_{syn}	4	%
E_{RP}	5	%
E_{HK}	5	%

4.4 Discussion

In this chapter, inspired by spike-timing-dependent plasticity models, we develop an energy-dependent plasticity model which allows replicating wet-biology experimental results, namely, the suppression of long-term potentiation when the available energy level on the postsynaptic neuron drops. Additionally, we derived a general mathematical expression for the available energy on every neuron in a network with arbitrary architecture.

The energy-dependent STDP model can be interpreted as a neo-Hebbian plasticity rule, where the postsynaptic available energy is the neuromodulator. The newly introduced model has a general structure that allows the implementation of both multiplicative and additive learning rules. However, we focus on the additive learning rules (*i.e.* $\mu_\pm = 0$) and found closed-form expression predicting the available energy level equilibrium point $\breve{A}$ on the post-synaptic neuron. The theoretical predictions are confirmed using our previously developed EDLIF model in a two-neuron experiment (Figure 4.4), which proves that numerical simulations with spiking neurons are in good agreement with the theoretically expected weight update value given by Eqn. (4.12).

Regarding the theoretical developments predicting the equilibrium postsynaptic available energy, we tested the theory in an all-to-one architecture experiment (Figure 4.6), where a

single postsynaptic neuron is stimulated by multiple presynaptic neurons. Consistent with our proposal, the available energy on the postsynaptic neuron reaches the predicted equilibrium point $\breve{A}$ and oscillates around it, following the previously mentioned rationale and graphically explained through Figure 4.2, where postsynaptic energy levels above $\breve{A}$ favored potentiation, while $A < \breve{A}$ favored depression. These results highlight how including local energy constraints restrict network structure by imposing limitations in the weight distribution and, also, pushing postsynaptic energy level towards the system's attractor $\breve{A}$. These results are essential to understand the structure and dynamic emergence in a more complex network, where excitatory and inhibitory neurons coexist and recurrent connections are present, as we will show in chapter 5.

Finally, it is worth mentioning that our model focuses on the effect of postsynaptic available energy on the excitatory-excitatory synaptic potentiation, however, available energy is possibly also affecting depression. The mathematical formulation of ED-STDP (see Eqn. (4.12)) allows extending of the proposed model for accounting energy dependencies on depression plasticity, and it is part of the future work related to the energy homeostatic principle.

Chapter 5

Energy-dependent Spiking Neuronal Networks

The brain is one of the most complex systems that we know. Therefore, to study it and try to understand the mechanism driving dynamics and structure, it is practical to divide the problem into simpler ones. That is the approach that we followed throughout this thesis. Firstly, by defining and studying a single-neuron model, then we modeled the interaction between neurons by introducing an energy-dependent plasticity rule, which dictates the synaptic strength modifications between neurons. Now all the required ingredients to study and simulate a spiking neural network under energy dependencies are available. In this regard, there is biological evidence suggesting the existence of excitatory-inhibitory (E-I) balanced networks in different parts of the brain, such as the CA3 region of the hippocampus, basal ganglia, and the primary visual cortex [76]. Thus, E-I balanced networks appear as a suitable model to explore neural networks' dynamics and structure. However, in general, when simulating and studying E-I balanced networks, energy or metabolic constraints are not considered.

In this chapter, built on the energy-dependent single-neuron model (Chapter 3) and the energy-dependent synaptic plasticity model (Chapter 4), we formalize, simulate, and investigate the dynamic and structure of E-I balanced networks including energy constraints in both, the single-neuron model as well as the synaptic plasticity. The developed models allow investigating how different sensitivities to energy imbalances at single neuron and synaptic level affects the network's dynamics and structure.

In this chapter, we find the conditions under which the network converges toward a fixed-point. Then, we contrast the predictions made by theory against numerical simulations, observing a good agreement between both. Regarding different simulation cases, we divide the experiments into three main scenarios. Firstly, we study the dynamics and structure of the E-I balanced networks when there is only synaptic sensitivity to energy imbalances. Next, the neuronal sensitivity to energy imbalances is included in the simulations. Finally, motivated by the evidence suggesting the relation between neurodegenerative diseases and metabolic impairments, we study the effect of neuronal impaired metabolic productions in the network's dynamics and structure.

5.1 Network dynamics under the Energy Homeostasis Principle

To mathematically describe an E-I balanced network (Figure 5.1) with n_{ex} excitatory and n_{in} inhibitory neurons, we introduce the network's weight matrix $\mathbf{w}$ of $(n_{ex}+n_{in})\times(n_{ex}+n_{in})$ dimension:

$$\mathbf{w} = \left(\begin{array}{c|c} \mathbf{w^{ex\to ex}} & \mathbf{w^{ex\to in}} \\ \hline \mathbf{w^{in\to ex}} & \mathbf{w^{in\to in}} \end{array}\right),$$

where the i,j element of $\mathbf{w}$ correspond to the synapse from the ith presynaptic neuron to the jth postsynaptic neuron. $\mathbf{w^{ex\to ex}}$ is the $n_{ex}\times n_{ex}$ matrix containing all the excitatory-excitatory connections, $\mathbf{w^{ex\to in}}$ is the $n_{ex}\times n_{in}$ matrix containing all the excitatory-inhibitory connections, $\mathbf{w^{in\to ex}}$ is the $n_{in}\times n_{ex}$ matrix containing all the inhibitory-excitatory connections, and $\mathbf{w^{in\to in}}$ is the $n_{in}\times n_{in}$ matrix containing all the inhibitory-inhibitory connections. The mean firing rate of each neuron in the $[t,t+T]$ interval, is described by the $(n_{ex}+n_{in})\times 1$ vector $\bar{\nu}_{\mathbf{t}}$:

$$\bar{\nu}_{\mathbf{t}} = \left(\begin{array}{c} \bar{\nu}^{\mathbf{ex}}_{\mathbf{t}} \\ \hline \bar{\nu}^{\mathbf{in}}_{\mathbf{t}} \end{array}\right),$$

where $\bar{\nu}^{\mathbf{ex}}_{\mathbf{t}}$ is the $n_{ex}\times 1$ dimension vector containing the excitatory mean firing rate, whereas $\bar{\nu}^{\mathbf{in}}_{\mathbf{t}}$ contains the inhibitory mean firing rates in a $n_{in}\times 1$ dimension vector.

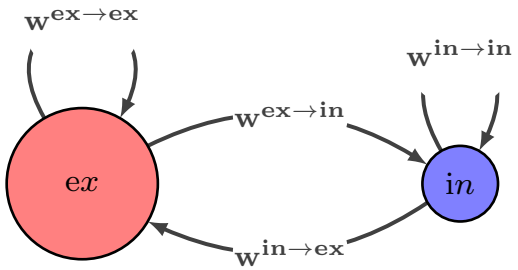

Figure 5.1: **Excitatory-inhibitory balanced network.**
The network is composed of excitatory and inhibitory neuronal populations, with excitatory-excitatory $\mathbf{w^{ex\to ex}}$, excitatory-inhibitory $\mathbf{w^{ex\to in}}$, inhibitory-excitatory $\mathbf{w^{in\to ex}}$ and inhibitory-inhibitory $\mathbf{w^{in\to in}}$ connections. All connections are static, except the excitatory-excitatory connections, which evolve following the Energy-Dependent STDP plasticity rule (see Chapter 4).

5.1.1 Network's firing-rate

To continue with the analytical treatment of the E-I balanced network, it is practical to have an approximation of the network's firing rate ν, quantifying each neuron firing rate. As previously explained in Chapter 3, the firing rate of a neuron excited by a constant current can be calculated utilizing Eqn. (3.8). In a more general way, the firing rate of a neuron can be calculated by defining a function $\phi:\mathbb{R}\to\mathbb{R}$, mapping stimulation current to firing rate. If the neuron is insensitive to energy imbalance (*i.e.* $\gamma=0$), the function $\phi(\cdot)$ can be found

utilizing Eqn. (2.12), such as $\nu = T_n^{-1} = \phi(I)$, where I is the constant incoming current to the neuron. Thus, the firing rate of each neuron under a constant current stimulation can be calculated knowing the neuron's parameters as well as the incoming constant current and the $\phi(\cdot)$ function, which is monotonically increasing in I[1]. Therefore, if we can approximate the mean incoming current $\bar{I}_t$ to a neuron in a small time-window, it is possible to approximate the neuron's firing rate $\bar{\nu}_t \approx \phi(\bar{I}_t)$, where $\bar{x}_t = T^{-1}\int_t^{t+T} x(t')\mathrm{d}t'$. Hence, to approximate each neuron's firing rate, let us approximate the mean incoming current $\bar{I}_t$ to each neuron:

$$\begin{aligned}\bar{I}_t =& \frac{1}{T}\int_t^{t+T} I(t')\mathrm{d}t' \\ =& \frac{1}{T}\int_t^{t+T} I_{stim} + \underbrace{\sum_{synapses\ k}\sum_{spike\ s} w_k \varepsilon_k(t'-t_s)}_{Eqn.(2.13)}\,\mathrm{d}t'.\end{aligned} \tag{5.1}$$

Therefore, the mean incoming current to a neuron is the mean incoming synaptic current, plus the constant external incoming stimulation current I_{stim} injected into the neuron. Eqn. (5.1) describes the mean incoming current to a neuron utilizing an $\varepsilon_k(\cdot)$ interaction kernel. If we use a delta Dirac interaction kernel (*i.e.* $\varepsilon_k(\cdot) = \delta(\cdot)$), Eqn. (5.1) reads:

$$\begin{aligned}\bar{I}_t =& I_{stim} + \sum_{synapse\ k} w_k \underbrace{\frac{1}{T}\int_t^{t+T}\sum_{spike\ s}\delta(t'-t_s)\mathrm{d}t'}_{\bar{\nu}_t^k} \\ =& I_{stim} + \sum_{synapse\ k} w_k \bar{\nu}_t^k.\end{aligned} \tag{5.2}$$

If we define the constant incoming stimulation current to each neuron as the $(n_{ex}+n_{in})\times 1$ dimension vector $\mathbf{I_{stim}^\top} = [(\mathbf{I_{stim}^{ex}})^\top, (\mathbf{I_{stim}^{in}})^\top]^\top$, and the mean incoming synaptic current as the $(n_{ex}+n_{in})\times 1$ dimension vector $\bar{\mathbf{I}}_\mathbf{t}^\top = [(\bar{\mathbf{I}}_\mathbf{t}^\mathbf{ex})^\top, (\bar{\mathbf{I}}_\mathbf{t}^\mathbf{in})^\top]^\top$, Eqn. (5.2) can be expressed in matrix form as follows:

$$\bar{\mathbf{I}}_\mathbf{t}^\top = \mathbf{I_{stim}^\top} + \bar{\nu}_\mathbf{t}^\top \bar{\mathbf{w}}_\mathbf{t}. \tag{5.3}$$

It is possible to apply $\phi(\cdot)$ point-wise to obtain the approximated network's firing rate:

$$\begin{aligned}\bar{\nu}_\mathbf{t}^\top \approx& \phi(\bar{\mathbf{I}}_\mathbf{t}^\top) \\ =& \phi(\mathbf{I_{stim}^\top} + \bar{\nu}_\mathbf{t}^\top \bar{\mathbf{w}}_\mathbf{t}).\end{aligned} \tag{5.4}$$

Eqn. (5.4) imposes a current-frequency constraint on the network. In general, $\phi(\cdot)$ defines a nonlinear relationship between incoming current and the neuron's firing rate. However, we can Taylor expand Eqn. (5.4) around $\mathbf{I_{stim}^\top}$:

$$\begin{aligned}\bar{\nu}_\mathbf{t}^\top \approx& \phi(\mathbf{I_{stim}^\top}) + \phi'(\mathbf{I_{stim}^\top})\bar{\nu}_\mathbf{t}^\top \bar{\mathbf{w}}_\mathbf{t} \\ \Rightarrow \bar{\nu}_\mathbf{t}^\top \approx& \phi(\mathbf{I_{stim}^\top})[\mathbb{I} - \phi'(\mathbf{I_{stim}^\top})\bar{\mathbf{w}}_\mathbf{t}]^{-1},\end{aligned} \tag{5.5}$$

[1] if $I \leq I' \Rightarrow \phi(I) \leq \phi(I')$. Thus, if the incoming current I increase, the firing rate of the neuron increases or stays constant.

where $\mathbb{I}$ is the identity matrix. Moreover, if $\phi(\cdot)$ is a linear transformation such as $\phi(x) = \xi x$, the following relationship holds:

$$\begin{aligned} \bar{\nu}_{\mathbf{t}}^{\top} \approx & \xi(\mathbf{I}_{\mathbf{stim}}^{\top} + \bar{\nu}_{\mathbf{t}}^{\top} \bar{\mathbf{w}}_{\mathbf{t}}) \\ \Rightarrow \bar{\nu}_{\mathbf{t}}^{\top} \approx & \xi \mathbf{I}_{\mathbf{stim}}^{\top} [\mathbb{I} - \xi \bar{\mathbf{w}}_{\mathbf{t}}]^{-1}. \end{aligned} \tag{5.6}$$

Eqns. (5.5) and (5.6) shows that, if the weights are static ($\Delta \bar{\mathbf{w}}_{\mathbf{t}} = 0$), then the firing rate of the network converge towards an equilibrium. This observation is important because it highlights the fact that, in general, constant weights are needed to achieve a constant firing rate.

Eqn. (5.4) defines a relation determining plausible weight-frequency values, which, in principle, is independent of the network's energy dynamics. However, given that our network has energy constraints that must be fulfilled, let us include energy dynamics in the analytical study of the network dynamics.

5.1.2 Energy dynamics

When studying the network's dynamics, we are particularly interested in knowing if the network converges or oscillates toward a specific state. If the network evolves toward an specific state independently of the initial conditions[2], those states are attractors of the network. Therefore, to find fixed points in the network dynamics, we start by trying to find if there are energy attractors in the network dynamics. Accordingly, we analyze stable fixed points for energy states of an arbitrary neuron in the network.

The total energy change $\Delta A(t) = A(t+T) - A(t)$ of any neuron in the network in a time interval T is calculated by summing the contributions of energy production and consumption occurring in the time interval $[t, t+T]$. From Eqn. 4.1 we obtain:

$$\Delta A(t) = \int_{t}^{t+T} A_s(t') - A_c(t') \mathrm{d}t'. \tag{5.7}$$

In section 4.1 we formalized synaptic energy consumption A_{syn} (see Eqn. 4.5) as well as the neuron's own action potential energy consumption A_{ap} (see Eqn. 4.7), for arbitrary ε_{syn} and ε_{ap} kernels. To simplify the mathematical tractability, now we will choose the delta

[2]When analyzing the fixed points of the network independently of the initial constraints, we mean that the network's state converges towards an attractor when considering a certain range of initial conditions. However, it is not completely independent of the initial conditions. For instance, if the inhibitory-excitatory weight values in the network are such that there is no excitatory activity (excitatory population has zero firing rate), then there are no weight updates in the networks and, consequently, the network is already in a fixed point. Therefore, in what follows, we are assuming that the initial conditions allow significant excitatory and inhibitory activity, thus avoiding the study of *trivial solutions* as the one previously explained.

kernel $\varepsilon(t-t_s)=\delta(t-t_s)$ for ε_{syn} and ε_{ap}. Thus, Eqn. 5.7 reads:

$$\frac{1}{T}\Delta A(t) = \frac{1}{T}\int_t^{t+T} K(A_H - A(t'))\mathrm{d}t' - E_{ap}\frac{1}{T}\int_t^{t+T}\sum_{spike\ s}\delta(t'-t_s)\mathrm{d}t' - \tag{5.8}$$

$$E_{syn}\frac{1}{T}\int_t^{t+T}\sum_{synapse\ k}\sum_{spike\ s}\bar{w}^k(t')\delta(t'-t_s)\mathrm{d}t'. \tag{5.9}$$

Because weights change slowly (*i.e.* $\lambda \ll 1$ in Eqn. (4.12)), for small T we can assume they are constant in the $[t, t+T]$ interval[3] (*i.e.* $\bar{w}^k(t) = \bar{w}^k_t$). In addition, because of the linearity of the integral operator ($\int\sum = \sum\int$):

$$\begin{aligned}\frac{1}{T}\Delta A(t) =& K(A_H - \bar{A}_t) - E_{ap}\frac{1}{T}\sum_{spike\ s}\delta(t-t_s) - E_{syn}\frac{1}{T}\sum_{synapse\ k}\sum_{spike\ s}\bar{w}^k_t\delta(t-t_s)\\ =& K(A_H - \bar{A}_t) - E_{ap}\bar{\nu}_t - E_{syn}\sum_{synapse\ k}\bar{w}^k_t\bar{\nu}^k_t,\end{aligned} \tag{5.10}$$

where $\bar{A}_t = T^{-1}\int_t^{t+T}A(t')\mathrm{d}t'$ is the mean energy level of the neuron in the $[t, t+T]$ interval, and in the second and third terms we obtain the neuron self and connected neighbor's firing rates, respectively ($T^{-1}\int_t^{t+T}\sum_{spikes\ s}\delta(t'-t_s)\mathrm{d}t'$). Now, if we force $\Delta A \overset{!}{=} 0$ in Eqn. (5.10), it is possible to find neuron's firing rates, incoming weight, and energy expenditure values that satisfies the energy fixed point constraints:

$$\bar{A}_t = A_H - \frac{1}{K}\Big[E_{ap}\bar{\nu}_t + E_{syn}\sum_{synapse\ k}\bar{w}^k_t\bar{\nu}^k_t\Big], \tag{5.11}$$

which in matrix form reads:

$$\bar{\mathbf{A}}_\mathbf{t}{}^\top = \mathbf{A}_\mathbf{H}{}^\top - \frac{1}{K}\bar{\nu}_\mathbf{t}{}^\top\Big[E_{ap}\mathbb{I} + E_{syn}\bar{\mathbf{w}}_\mathbf{t}\Big], \tag{5.12}$$

where $\bar{\mathbf{A}}_\mathbf{t} = [\bar{\mathbf{A}}^\mathbf{ex}_\mathbf{t}{}^\top, \bar{\mathbf{A}}^\mathbf{in}_\mathbf{t}{}^\top]^\top$. Eqn. (5.11) holds if the neuron is in an energy fixed-point and, to achieve the energy fixed point, the excitatory-excitatory connections to the neuron under study also need to achieve a fixed point (the other connections are static). Otherwise, the synaptic energy consumption (A_{syn}) will stay varying, impeding to achieve an energy fixed point in the postsynaptic excitatory neuron. Please realize that, if the excitatory-excitatory connections achieve a fixed point as well as the presynaptic neuron's firing rate, then the firing rate of the postsynaptic neuron also achieves a fixed point (*i.e.* $\Delta\bar{\nu}_t = 0$). The excitatory-excitatory connections achieve a fixed point if the postsynaptic excitatory neuron has an energy level equal to $\breve{A}$[4] (see Chapter 4 and, in particular, Eqn. (4.18)). Thus, in the fixed

[3]Formally, we are assuming that time scales of learning and neuronal spike dynamics can be separated [77]

[4]Here we are again neglecting the *trivial solutions* where the neuron's own firing rate $\bar{\nu}_t$ is zero. If $\bar{\nu}_t = 0$ ($\Delta\bar{\nu}_t = 0$) there are no spikes to update the incoming weights to the neurons, so incoming weights are constant and the total energy change in the neuron is also constant ($\Delta A = 0$), even if $\bar{A}_t \not\approx \breve{A}$. Thus, silent neurons satisfies Eqn. (5.11), and if there is no increment in their incoming current, they will remain in the $\Delta A = \Delta w = \Delta\nu = 0$ fixed point, but without the neet to satisfy the $\bar{A}_t \approx \breve{A}$ condition.

point, we can approximate $\bar{A}_t \approx \breve{A}$, obtaining:

$$\begin{aligned}\breve{A} \approx & A_H - \frac{1}{K}\Big[E_{ap}\bar{\nu}_t + E_{syn}\sum_{synapse\ k}\bar{w}_t^k\bar{\nu}_t^k\Big] \\ A_H\Big(1+\frac{\ln(\alpha)}{\eta}\Big) \approx & A_H - \frac{1}{K}\Big[E_{ap}\bar{\nu}_t + E_{syn}\sum_{synapse\ k}\bar{w}_t^k\bar{\nu}_t^k\Big].\end{aligned} \tag{5.13}$$

By rearranging (5.13), we arrive to the following relationship constraining weights and firing rates of each neuron in the network:

$$-\frac{A_H K\ln(\alpha)}{\eta} \approx E_{ap}\bar{\nu}_t + E_{syn}\sum_{synapse\ k}\bar{w}_t^k\bar{\nu}_t^k. \tag{5.14}$$

If all the neurons in the network converge towards a fixed point, they must satisfy Eqn. (5.11) and, in particular, non-silent excitatory neurons must satisfy Eqn. (5.14). In consequence, in this state, all the excitatory-excitatory connections in the network remain constant (*i.e.* $\Delta\bar{w}_t = 0$) in average as well as the firing rates (*i.e.* $\Delta\bar{\nu}_t = 0$). As a result, Eqn. (5.14) predicts the energy level for each non-silent excitatory neuron in the network after converging towards a fixed point.

However, under certain conditions, such as the neuron under study has $n \gg 1$ synapses, high E_{syn} values or strong incoming w weights, it is possible to neglect the neuron's own action potentials energy consumption (*i.e.* $E_{ap}\bar{\nu}_t \ll E_{syn}\sum_k \bar{w}_t^k\bar{\nu}_t^k$), thus we approximate (5.14) by:

$$\begin{aligned}-\frac{A_H K\ln(\alpha)}{\eta E_{syn}} &\approx \sum_{synapse\ k}\bar{w}_t^k\bar{\nu}_t^k \\ &= \sum_{ex\to ex\ synapse\ k}\bar{w}_t^{ex\to ex,\ k}\bar{\nu}_t^{ex,\ k} + \sum_{in\to ex\ synapse\ k}\bar{w}_t^{in\to ex,\ k}\bar{\nu}_t^{in,\ k}.\end{aligned} \tag{5.15}$$

Consequently,

$$\underbrace{-\frac{A_H K\ln(\alpha)}{\eta E_{syn}} - \sum_{in\to ex\ synapse\ k}\bar{w}_t^{in\to ex,\ k}\bar{\nu}_t^{in,\ k}}_{\Lambda} \approx \sum_{ex\to ex\ synapse\ k}\bar{w}_t^{ex\to ex,\ k}\bar{\nu}_t^{ex,\ k}. \tag{5.16}$$

Eqn. (5.11) reveals a metabolic constraint over incoming synapse strengths and their respective presynaptic neuronal firing rates, affecting non-silent excitatory neurons in the energy fixed point. In particular, Eqn. (5.14) shows that, in order to achieve a metabolic fixed point in the excitatory postsynaptic neurons, there is a trade-off between synaptic strength and the corresponding presynaptic neuronal firing rate. Interestingly, the metabolic constraint in Eqn. (5.14) dictates an inverse relationship between weights and firing rates, which is a completely new constraint in the system, given that in general, previous models do not account for metabolic activity. Moreover, the aforementioned constraint enables the

emergence of an attractor state to the network, as a consequence of the interception between the metabolic and the physically plausible states of the network given by the previously introduced metabolic (see Eqn. (5.14)) and weight-frequency relations (see Eqn. (5.4)).

On the one hand, Eqn. (5.4) gives a weight-rate relationship where increasing excitatory-excitatory weights $\mathbf{w}^{\mathbf{ex}\to\mathbf{ex}}$ generates higher excitatory firing rates $\nu^{\mathbf{ex}}$, due to higher mean incoming synaptic currents to postsynaptic neurons. On the other hand, if either excitatory-excitatory weights or excitatory firing rates increase, the postsynaptic energy levels drop (see Eqn. (5.12)). In addition, at the metabolic fixed point, non-silent excitatory neurons fulfill Eqn. (5.16). As a consequence, if excitatory firing rates (excitatory-excitatory weight) increase, then excitatory-excitatory weights (excitatory firing rates) must decrease. Thus, Eqn. (5.16) imposes an inverse relationship between excitatory-excitatory weights and excitatory firing rates, contrary to Eqn. (5.4), where the relationship between the two variables is direct. Figure 5.2 shows a conceptualization of the previous reasoning. As a consequence of Eqns. (5.4) and (5.16) restricting the network's dynamics and structure, it is possible to predict the effect of modifying some parameters on the metabolic fixed point achieved by the network. For instance, if the synapses are less sensitive to energy imbalance (by imposing a smaller η), then the energy level fixed point $\breve{A}$ decreases. As a consequence of having a lower energy level fixed point, allowed energy consumption per neuron increases. Thus, if η decreases, higher synaptic strengths and firing rates state are allowed (see dashed red line in Figure 5.2). Likewise, it is possible to anticipate the effect of increasing the neuronal sensitivity to energy imbalances γ. Greater γ values decreases the interspike intervals (see Eqn. 3.7), meaning that neurons become more excitable under metabolic challenging situations. For example, the same constant current produces a higher firing rate in a neuron with high γ with respect to a neuron without energy imbalance sensitivity (see Figure 5.3). Thus, for the same incoming synaptic strengths and presynaptic firing rates, the postsynaptic neuron with higher γ has a higher or equal firing rate than the postsynaptic neuron with lower γ. Consequently, for higher γ, if the network achieves a fixed point, the synaptic strengths should be weaker and the firing rates higher with respect to a network composed of neurons with no energy imbalance sensitivity (*i.e.* $\gamma = 0$).

5.2 Results

To numerically test our theoretical predictions, the network is simulated utilizing the NEural Simulation Tool program (NEST) [74] and the EDLIF neuronal model as well as the ED-STDP synaptic model are specified using NESTML [75], the domain specific language tailored for the spiking neural network simulator NEST.

The simulated network has $n = 500$ neurons and the excitatory-inhibitory ratio is $n_{ex} : n_{in} = 4 : 1$ following biologically realistic excitatory-inhibitory ratio values [78]. Figure 5.4 shows the excitatory and inhibitory neurons randomly distributed in a $1\,mm^2$ surface area. The network architecture is defined by an all-to-all connectivity. In addition, following *in vitro* measured weights strength in neuronal cell assemblies [79], initial synaptic strength values for the simulated network are drawn from an exponential distribution (see Figure 5.5

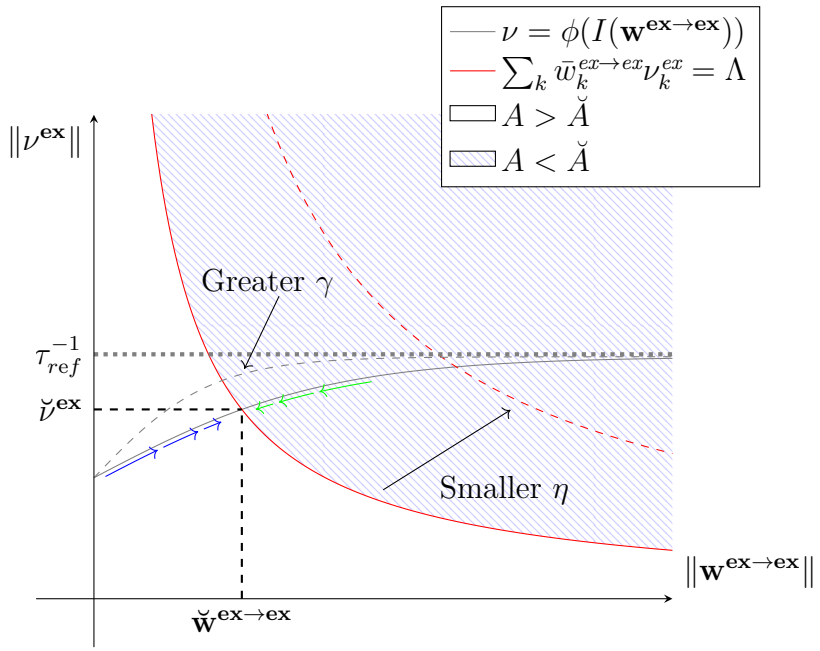

Figure 5.2: **Energy-dependent E-I balanced network and constraints intersection.** The gray curve describes excitatory firing rate magnitude as a function of excitatory-excitatory weights magnitude (see Eqn. (5.4)), whereas the red curve conceptualizes the inverse relation between excitatory firing rates and excitatory-excitatory weights magnitudes given by metabolic constraints (see Eqn. (5.16)) afecting non-silent excitatory neurons in the energy fixed-point. On the blue region, the postsynaptic energy level drops below the energy level fixed-point $\breve{A}$. Thus, in the blue region, $\mathbf{w}^{\mathbf{ex}\to\mathbf{ex}}$ experience a net depression drift (see Eqn. (4.16)), whereas in the white region, the postsynaptic energy level is above $\breve{A}$. Consequently, in the white region, there is a net potentiation drift. Therefore, if the network state is in the blue region, energy-dependent plasticity rules push the network state toward the intersection between the two curves (following the green arrows). Likewise, if the network is in the white region, energy-dependent plasticity push the network state toward the intersection point between the two curves (following the blue arrows). Finally, in the intersection between the two curves (the system's metabolic fixed point) the postsynaptic energy level is $\breve{A}$ and, as a consequence, $\Delta\mathbf{w}^{\mathbf{ex}\to\mathbf{ex}} = 0$ on average.

and Eqn. (5.17))

$$f(w;\beta) = \begin{cases} \frac{1}{\beta}\mathrm{e}^{-w/\beta}, & \text{if } w \geq 0, \\ 0, & \text{otherwise,} \end{cases} \tag{5.17}$$

where $f(w;\beta)$ is the probability density function of the exponential distribution[5]. To emulate the incoming activity to each neuron from other brain areas, we inject into each neuron a constant current I_{stim} drawn from a Gaussian distribution with mean $\mu = 166\,pA$ and standard deviation $\sigma = 15\,pA$. By assuming that all neurons share the same parameters values we study the homogeneous parameter scenario (neuronal parameters are presented in Table 4.1, but in this chapter the simulations use $E_{syn} = 0.5\%$, $E_{AP} = 2\%$, and the previously described stimulation current to each neuron). However, formalizing and simulating the

[5]This means that the distribution of the weights w is described by an exponential distribution with scale parameter β. Therefore, the expected value of the weights is $\mathrm{E}[w] = \beta$ and the variance $\mathrm{Var}[w] = \beta$.

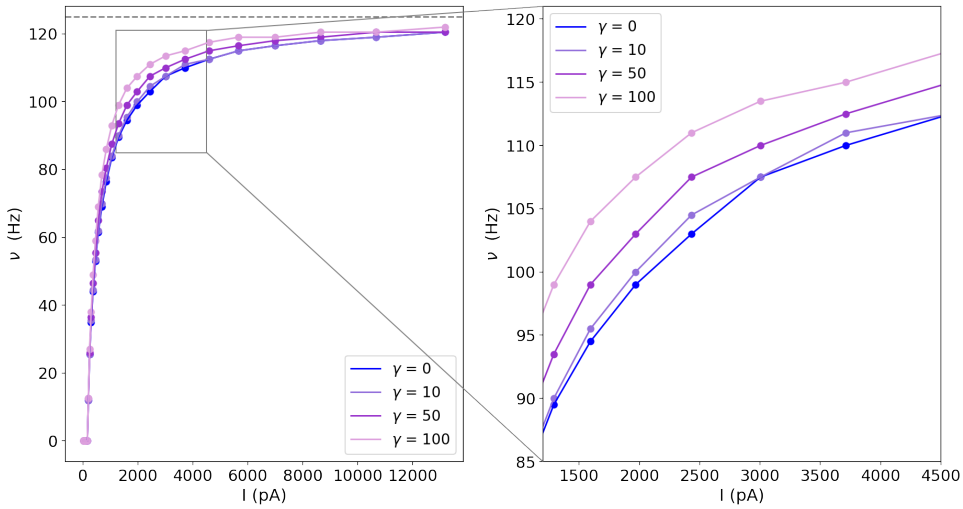

Figure 5.3: **Current-frequency mapping for neurons with different γ sensitivity.** The current-frequency mapping $\phi(\cdot)$ depends on the neuronal sensitivity to energy imbalances. If γ is higher the neuron's firing rate saturates before (with a smaller current) in contrast to a neuron with lower neuronal sensitivity to energy imbalances.

heterogeneous parameter case is left to future work.

Before studying the network's structure and dynamics under energy constraints, we first simulate the network without energy constraints (*i.e.* $\gamma = \eta = 0$). Thus, the current-rate relation from Eqn. (5.4) as well as the available energy in the neuron dictated by Eqn. (5.12) holds, but Eqn. (5.14) does not hold, because Eqn. (5.14) holds for the excitatory population only if energy constraints are affecting $\mathbf{w}^{\mathbf{ex}\to\mathbf{ex}}$ plasticity (*i.e.* $\eta > 0$).

Simulating the network without metabolic constraints is useful as a base case for comparison before including metabolic constraints[6]. Figure 5.6 shows the network's dynamics and structure when no metabolic constraints are included. As expected, firing rates increase until saturation due to favored synaptic potentiation ($\alpha = 0.5$). In this regard, the refractory period for each neuron in the network is $\tau_{ref} = 8\,ms$. Thus, the maximum theoretical firing rate for an infinite stimulation current is $\tau_{ref}^{-1}\,kHz \Rightarrow \nu_{max} = 125Hz$ (see Eqn. (2.12)). Therefore, the network's firing rate is close to the saturation state. Moreover, the mean energy level of the excitatory population (Figure 5.6a) decreases until stabilizing at $A(t) \approx 75\%$. The energy stabilization point occurs at the firing rate and excitatory-excitatory strength satu-

[6]All the simulations presented in this chapter have the same initial conditions

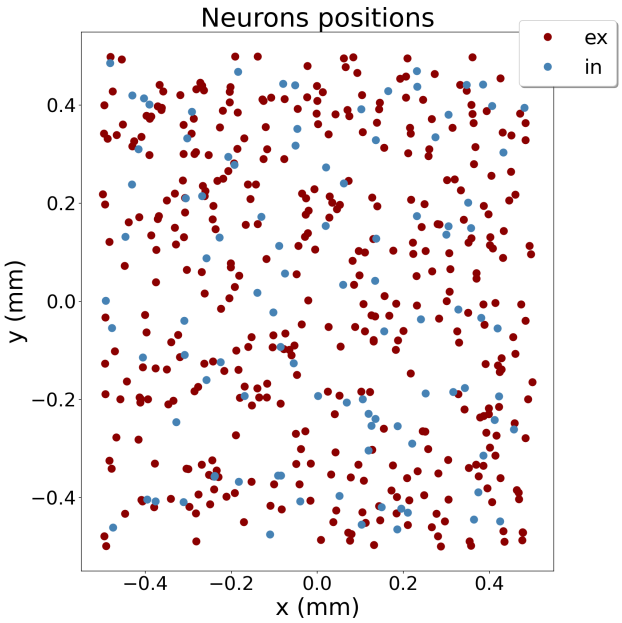

Figure 5.4: **Excitatory-inhibitory balanced network.**
Excitatory and inhibitory neuronal positions in a $1\,mm^2$ surface area. Each neuron x and y position is drawn from a random uniform distribution $U[-0.5, 0.5]$.

ration[7]. However, in principle, without energy constraints, each neuron's energy level can decrease until achieving $A(t) = 0$. This is the case if we, for instance, sufficiently increase the number of neurons in the network, or increase the energy consumption related to post-synaptic potentials E_{syn}. Eqn. (5.11) describes which variables affect energy consumption and, consequently, the available energy in the neuron. Now it is possible to include metabolic constraints and study their impact on the network's dynamic and structure. We start only including synaptic sensitivity to energy imbalances ($\eta > 0$), but no neuronal sensitivity to energy imbalances ($\gamma = 0$). Later, we also include neuronal sensitivity to energy imbalances in the simulation ($\eta, \gamma > 0$), thus energy constraints directly affects neuronal dynamics as well as plasticity. Finally, we maintain neuronal and synaptic energy imbalance sensitivity ($\eta, \gamma > 0$), but emulate a metabolic impairment by decreasing K neuronal parameter. Thus decreasing the rate at which ATP is produced.

[7]If firing rates and excitatory-excitatory weights are saturated, the energy consumption in each neuron can be approximated by:

$$\begin{aligned} A_c \approx & E_{syn} \sum_k \bar{w}_k \bar{\nu}_k \\ \approx & E_{syn} \times n_{ex} \times \bar{w}_{max} \times \nu_{max} \\ = & 0.5 \times 400 \times 1 \times 0.125 \\ = & 25\%, \end{aligned}$$

in agreement with what is observed in Figure 5.6a

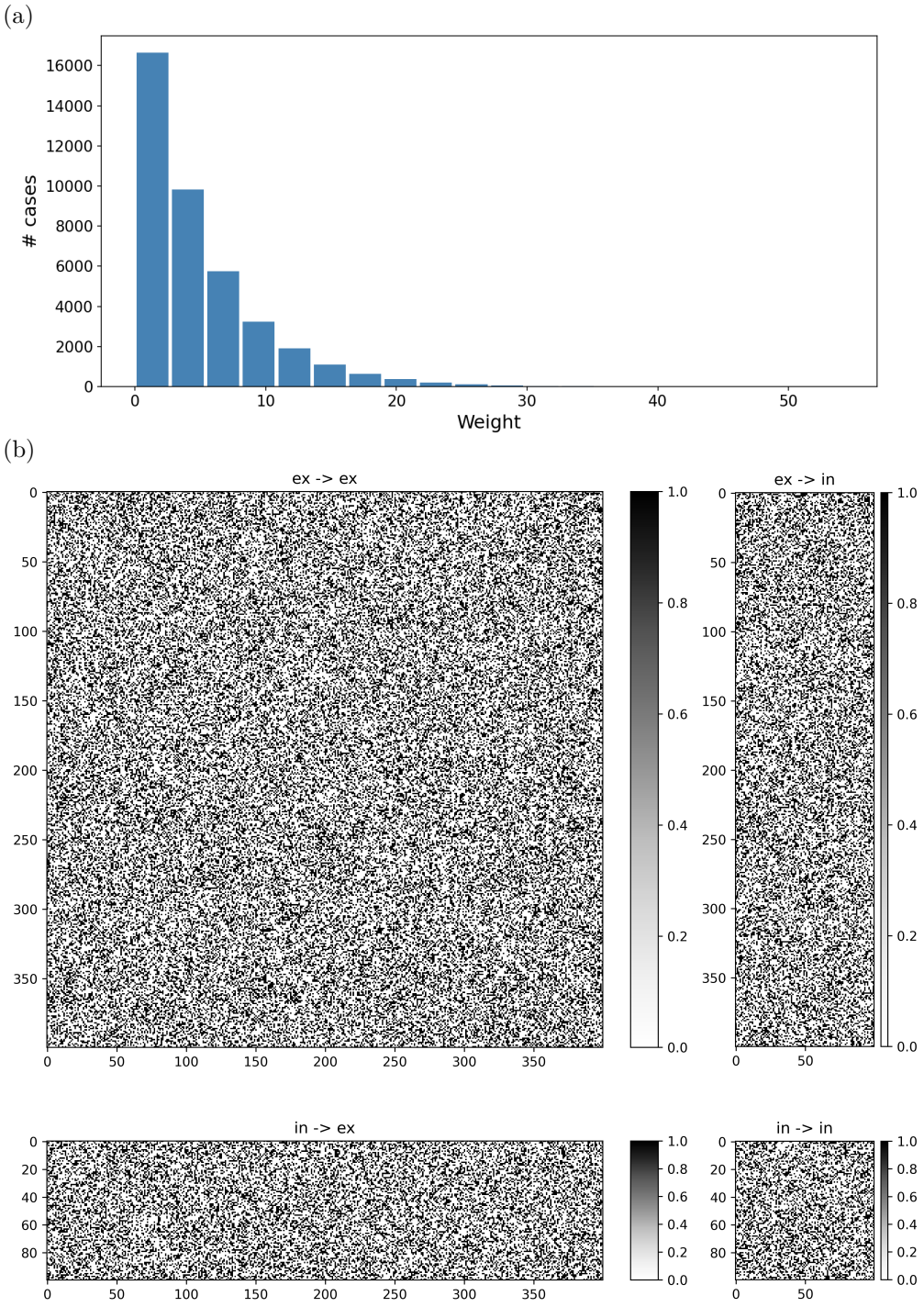

Figure 5.5: **Initial weight distribution and adjacency matrix.**
Weights distribution in a) follows an exponential distribution with scale parameter $\beta = 5$. $\mathbf{w}^{\mathbf{ex}\to\mathbf{ex}}$, $\mathbf{w}^{\mathbf{ex}\to\mathbf{in}}$, $\mathbf{w}^{\mathbf{in}\to\mathbf{ex}}$, and $\mathbf{w}^{\mathbf{in}\to\mathbf{in}}$ synaptic strengths follow the same exponential distribution with scale parameter $\beta = 5$, but $\mathbf{w}^{\mathbf{in}\to\mathbf{ex}}$ and $\mathbf{w}^{\mathbf{in}\to\mathbf{in}}$ synapses are inhibitory, thus their strengths are negative. Figure b) shows the respective adjacency matrices A obtained from the weight matrices, where if $w_{i,j} \geq 5 \Rightarrow A_{i,j} = 1$ and $A_{i,j} = 0$ otherwise.

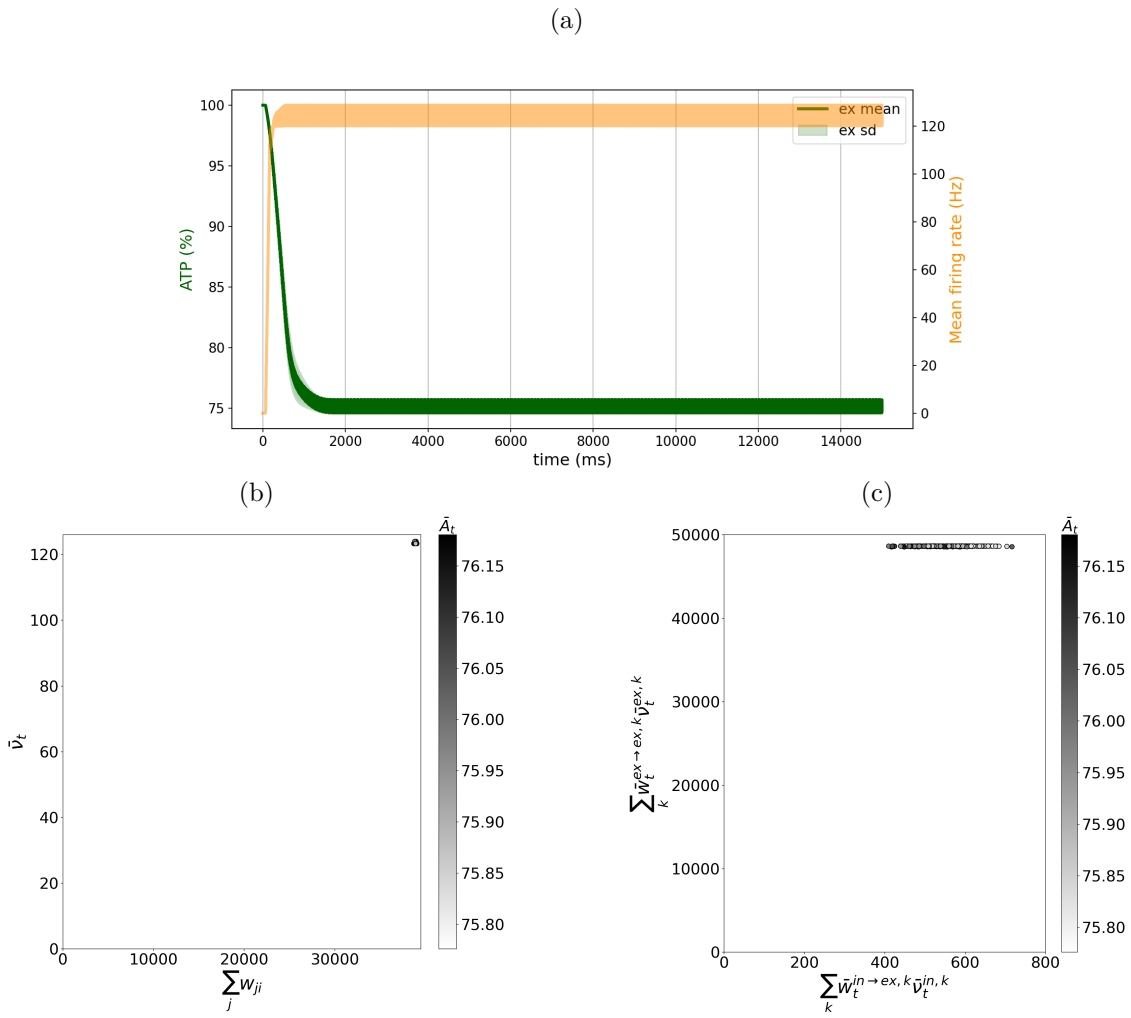

Figure 5.6: **Network dynamic and structure without energy constraints.** Network simulation when there are no metabolic constraints in the network. Mean available energy in the excitatory population keeps dropping until neuronal firing rates are saturated. Figure a) shows mean energy level and mean firing rate for the excitatory population, while Figure b) shows final incoming synaptic strength per neuron ($\sum_j w_{j,\mathrm{i}}$) and mean firing rate per neuron. The mean firing rates in Figures b) and c) are calculated considering the last 10% of the simulation.

5.2.1 Exploring synaptic energy imbalance sensitivities η

From our previous theoretical developments, for higher synaptic energy imbalance sensitivities η we expect higher energy level equilibrium values $\breve{A}$ (Eqn. (4.18)). In this regard, to achieve $\breve{A}$ closer to A_H, energy consumption needs to decrease, and postsynaptic energy consumption decreases if presynaptic rate decreases, or if incoming synaptic strengths decrease (Eqn. (5.15)). Consequently, as we increase η, lower firing rates as well as weaker excitatory-excitatory synaptic strengths are expected as Figure 5.2 conceptually represents. In addition, to satisfy Eqn. (5.15) an inverse relation between $\sum_k \bar{w}_t^{in\to ex,\ k}\bar{\nu}_t^{in,\ k}$ and $\sum_k \bar{w}_t^{ex\to ex,\ k}\bar{\nu}_t^{ex,\ k}$ should be observable in the simulations.

Figure 5.7 shows the mean available energy and neuronal firing rate through the simulation, for the excitatory population. Consistently with Eqn. (4.18), while synaptic energy imbalance sensitivity η increases, the energy level equilibrium point increases and stays close to our analytical prediction (dashed gray line). Also, while the energy fixed-point $\breve{A}$ increases, the mean neuronal firing rate decreases, which aligns with the theoretical description represented in Figure 5.2.

The first column of Figure 5.8 shows neuronal firing rate as a function of incoming synaptic strength, for different synaptic sensitivities η values. In agreement with Eqn. (5.4), as the incoming synaptic strengths increases, the firing rate increases. Also, when η increases, neuronal rates and excitatory-excitatory weights decrease, as it can be observed from Figure 5.8a with $\eta = 30$ having higher firing rates and stronger excitatory-excitatory synapses than the ones observed in Figure 5.8c where $\eta = 50$. The previous observation is also valid when contrasting Figure 5.8c where $\eta = 50$ against Figure 5.8e where $\eta = 100$; when synaptic sensitivity η increases, excitatory firing rates tend to decrease.

Regarding the inverse relation between $\sum_k \bar{w}_t^{in\to ex,\ k}\bar{\nu}_t^{in,\ k}$ and $\sum_k \bar{w}_t^{ex\to ex,\ k}\bar{\nu}_t^{ex,\ k}$ dictated by Eqn. (5.15), the second column of Figure 5.8 shows the relationship between these two variables for simulations with increasing η. For a low synaptic sensitivity to energy imbalance, there seems to be an inverse relation present in Figure 5.8b, although not very clear. However, if synaptic sensitivity η increases, the inverse relationship between the two variables becomes more evident, as shown in Figure 5.8d. Interestingly, when the synapses are highly sensitive to energy imbalance (Figures 5.8e and 5.8f), it is not possible for all the neurons to achieve the metabolic fixed point, and some neurons achieve the silent fixed point described in the footnote 4.

When there is an extreme synaptic sensitivity to energy imbalances (Figures 5.8e and 5.8f), a subpopulation of excitatory neurons remains silent (neurons with zero firing rate in Fig. 5.8e). It is not surprising that silent neurons have higher inhibitory weights (black dots in Fig. 5.8f). This happens because just before the separation of the network into two subpopulations ($t \approx 7000ms$), there is a slight decrease (increase) in available energy (firing rate), followed by an increase (decrease) in available energy (firing rate). This last increase in available energy must be accompanied by a general decrease in excitatory-excitatory weights ($A < \breve{A}$ implies a net negative drift in excitatory-excitatory weights), and if there is a general decrement in excitatory-excitatory weights, then the first neurons to be silent are the ones with higher inhibitory incoming weights. After entering the silent state, their excitatory-excitatory weights remain constant, so the only possibility for them to stop being silent, is

(a)

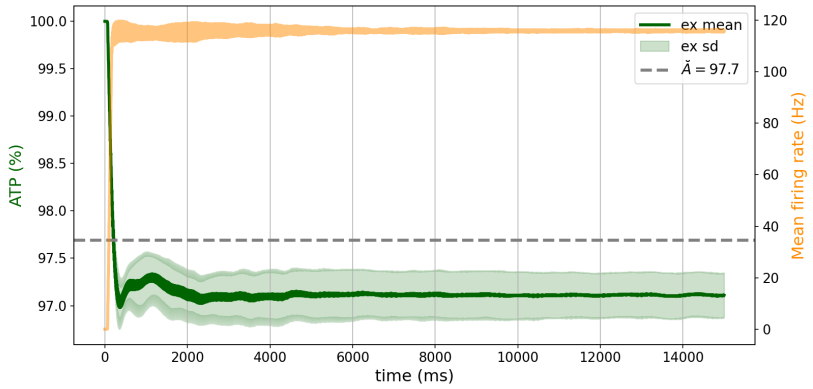

(b)

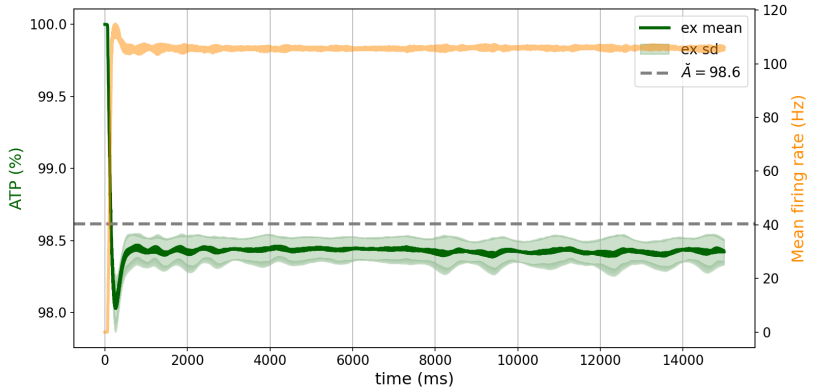

(c)

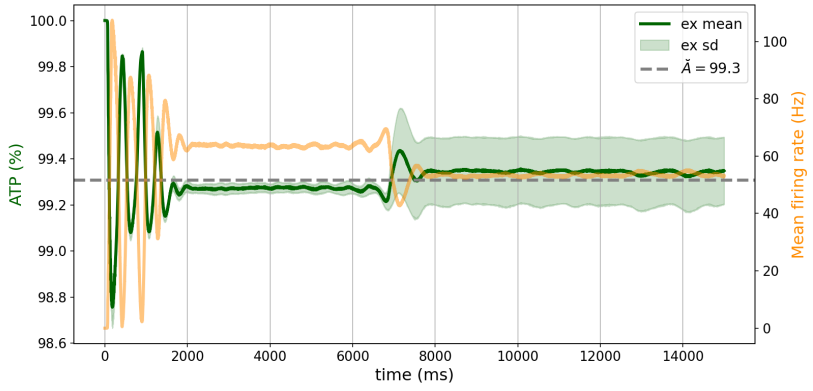

Figure 5.7: **Mean available energy and firing rate for different synaptic sensitivities to energy imbalances.**
Figure a) is obtained with $\eta = 30$ parameter, while for Figure b) $\eta = 50$, and $\eta = 100$ in Figure c). Figures show the mean energy level and firing rate for the excitatory population, and there is no neuronal sensitivity to energy imbalances (*i.e.* $\gamma = 0$).

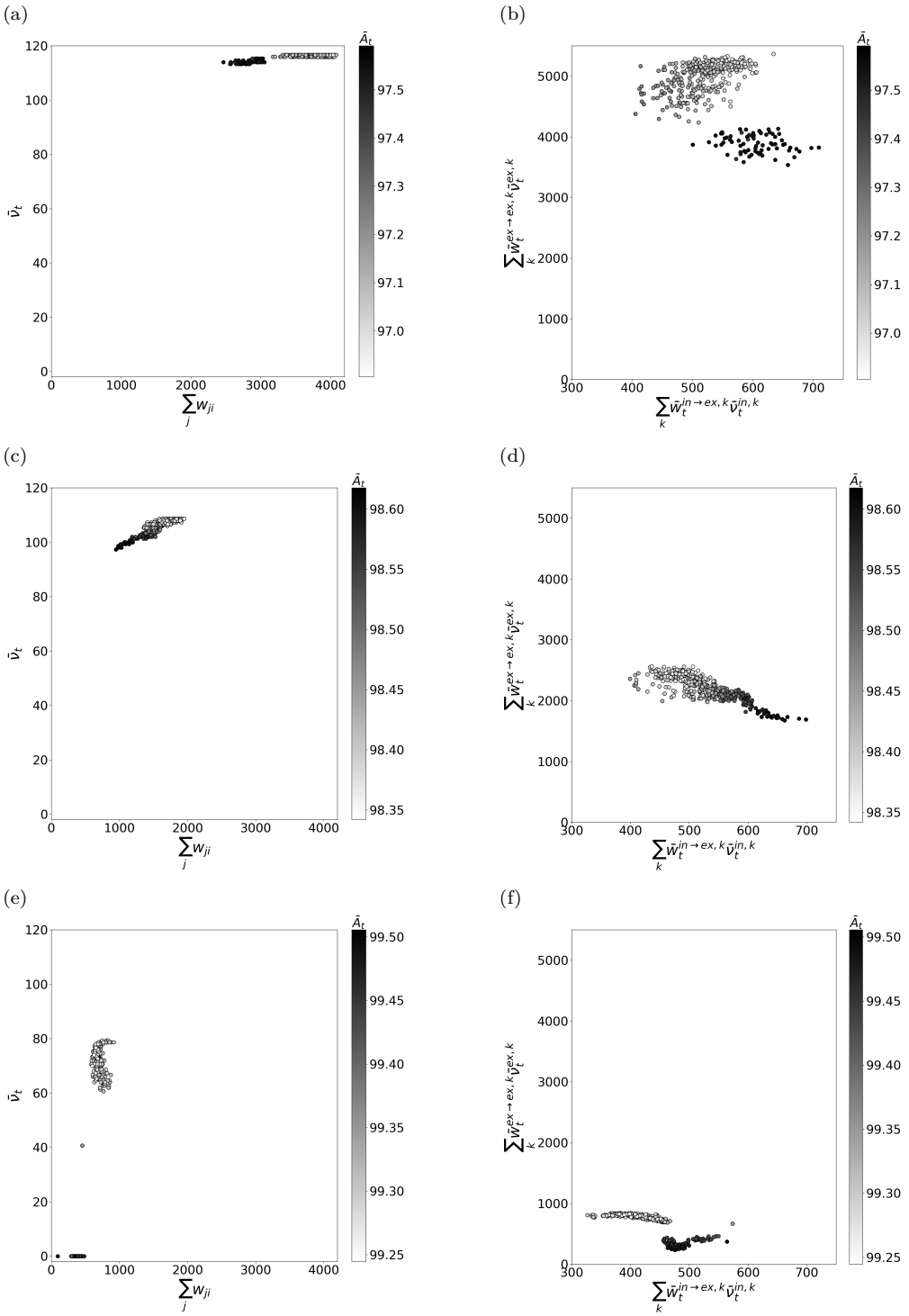

Figure 5.8: **Weight-rate and synaptic energy consumptions when the synaptic sensitivity to energy imbalances varies.**
The Figures in the first column show the mean firing rates versus incoming synaptic strengths, thus the numerically equivalent to the current-rate mapping defined by $\phi(\cdot)$. The Figures in the second column show the energy consumption in each neuron due to presynaptic excitatory neurons and presynaptic inhibitory neurons. Figures a) and b) are obtained with $\eta = 30, \gamma = 0$ parameter values, while for Figures c) and d) $\eta = 50, \gamma = 0$. finally, figures e) and f) show the simulations results when $\eta = 100, \gamma = 0$. The mean firing rates $\bar{\nu}_t$ in all cases were calculated considering the last 10% of the simulation.

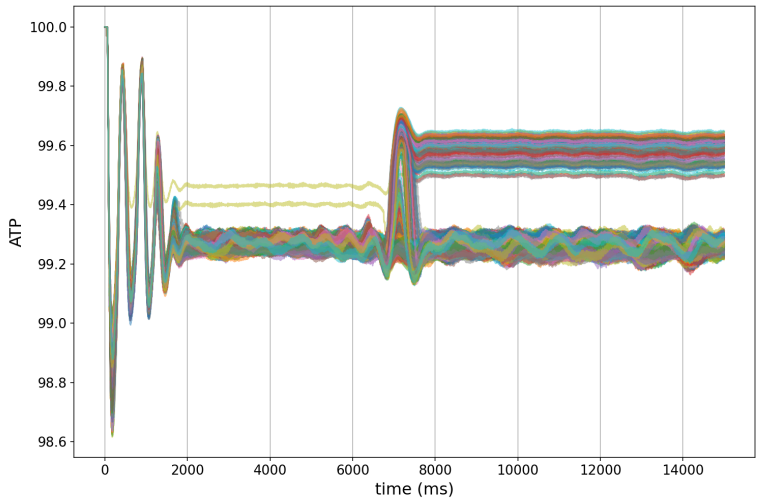

Figure 5.9: **Excitatory population separations.**
The excitatory population divides into two subpopulations due to high synaptic sensitivity to energy imbalances η. The silent subpopulation is the one with higher available energy ($ATP \sim 99.6\%$).

to receive higher incoming current, but this is not possible, because the silent neurons allow decreasing the energy consumption in the non-silent neurons such as the non-silent neurons can satisfy the metabolic fixed-point where $A \approx \breve{A}$. As a consequence, the silence of those neurons enables the network to converge toward a stable fixed point,with one subpopulation staying in the metabolic fixed point, while another subpopulation stays in the silent fixed point (see footnote 4). In this scenario, one group of neurons still tries to satisfy the $\bar{A}_t \approx \breve{A}$ energy constraints, and their energy equilibrium point is close to the one predicted by Eqn. (5.14), as shown in Figure 5.9. The second group of silent neurons has a higher available energy, but their energy consumption is different than zero. This is not the only case in which there must be silent neurons to achieve a global fixed point. For instance, if the neuronal population is huge, then this phenomenon also occurs (although there is no need for extreme synaptic sensitivity to energy imbalances in this case), or if a metabolic impairment is simulated, as we will show later. The separation of excitatory populations in two subpopulations can be interpreted as a specialization. Surprisingly, under the developed framework, silent neurons emerge as a consequence of local energy constraints in the network and, if this silent neurons are not present, then it is not possible to achieve a global fixed point in the network. This is interesting because silent neurons are present in our brains and it is not clear why would we have them. In fact, silent neurons have been referred to as 'dark neurons' in analogy to the astrophysical observation that much of the matter in the universe is undetectable, or dark [80]. In our framework, silent neurons are playing an important role from a metabolic point of view. One hypothesis is that given local energy constraints in biological neural networks, the price to pay due to having redundant neurons in the brain is to silence some of them to achieve a network energy equilibrium.

5.2.2 Including neuronal sensitivities to energy imbalances γ

So far, the developed theoretical analysis of the energy-dependent network does not account explicitly for neuronal energy imbalance sensitivity γ. However, in Chapter 3, we showed that neuronal sensitivity to energy imbalances γ affects neuronal firing rate. Thus, we can include the neuronal sensitivity parameter in the current-rate mapping $\phi(\cdot) := \phi_\gamma(\cdot)$. In particular, if the energy level in a neuron is below the homeostatic energy level (*i.e.* $A \leq A_H$), for the same incoming input current, the neuron's firing rate is higher for higher γ, as demonstrated by Eqn. (3.8) and shown in Figure 5.3. Consequently, if two networks (A and B) are equal (in particular, have the same initial excitatory-excitatory weights), but the neurons in network A have higher γ sensitivity than neurons in network B, then network A must have higher or equal excitatory firing rates than network B. As a consequence, to achieve an energy equilibrium point, network A needs to decrease excitatory-excitatory synaptic strengths. This idea is conceptualized in Figure 5.2 with the gray dashed line representing the current-rate mapping when γ is increased. Following the previous explanation, for higher γ we expect the network to have weaker excitatory-excitatory synaptic strengths as well as higher firing rates.

To numerically explore the effect of modifying γ, we maintain synaptic sensitivity $\eta = 50$ fixed and vary the neuronal sensitivity to energy imbalances γ. Because the synaptic sensitivity η is constant for all cases in Fig 5.10 and the energy level fixed point is independent of the neuronal sensitivity parameter γ, the theory predicts that networks with different neuronal sensitivity γ should converges towards the same energy level. The previous prediction is confirmed by observing Figure 5.10, where for different γ values, the energy fixed points are almost the same. However, as already anticipated by the theory, in the metabolic fixed point, higher γ value are associated with higher mean excitatory firing rates $\bar{\nu}_t^{ex}$. This prediction is confirm by calculating the mean excitatory firing rate $\bar{\nu}_t^{ex}$ considering the last 10% of the simulation for each case. Particularly, when $\gamma = 10$ we obtain $\bar{\nu}_t^{ex} = 106.5$, while for $\gamma = 20$ the mean excitatory firing rate ($\bar{\nu}_t^{ex}$) is 107.6, finally for $\gamma = 50$ we obtain $\bar{\nu}_t^{ex} = 111.1$. Although not easily recognizable, this pattern is also observable by comparing the weight-rate relationship in Fig. 5.11 for each case. When $\gamma = 10$ (Figure 5.10a) the firing rate is slightly lower compared with the $\gamma = 20$ case (Figure 5.10b). Moreover, this relation also holds when comparing the $\gamma = 20$ case against the $\gamma = 50$ case (Figure 5.10c). The first column in Figure 5.11 shows the experimental current-rate relationship for excitatory neurons in the network. In agreement with the previous explanation and with Figure 5.2, as neuronal sensitivity γ increases from Figure 5.11a to 5.11c and 5.11e, numerical experiments show that neurons become more easily excitable. Thus, generating higher firing rates when γ is higher. Further, if we observe the second column in Figure 5.11, it is clear that the relationship defined by Eqn. (5.15) is satisfied, thus respecting the relationship between $\sum_k \bar{w}_t^{in\to ex,\,k}\bar{\nu}_t^{in,\,k}$ and $\sum_k \bar{w}_t^{ex\to ex,\,k}\bar{\nu}_t^{ex,\,k}$.

Regarding excitatory-excitatory synaptic strength, simulations shows that excitatory-excitatory weight slightly decreases as neuronal sensitivity γ increases This observation is supported by realizing that when γ increases, the energy fixed point does not change, but the firing rates increases (Figure 5.10). This is only possible because the excitatory-excitatory weights decrease, compensating the increased firing rates and thus allowing to keep the same energy consumption. Thus, the theoretical predictions regarding the effect of increasing γ

(a)

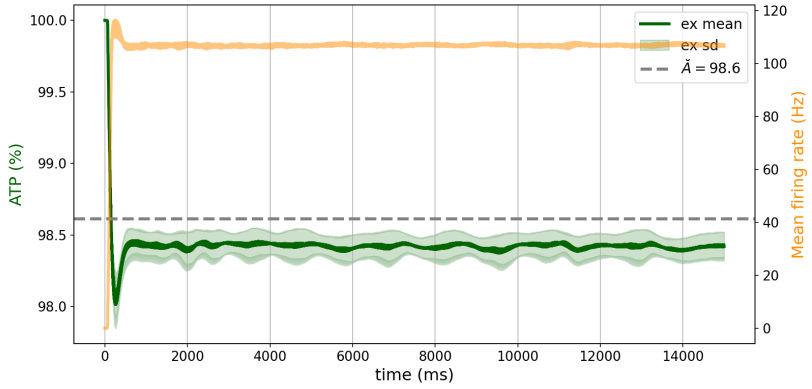

(b)

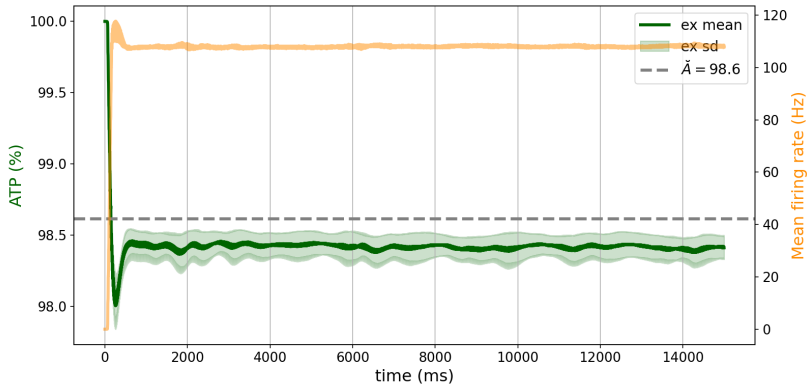

(c)

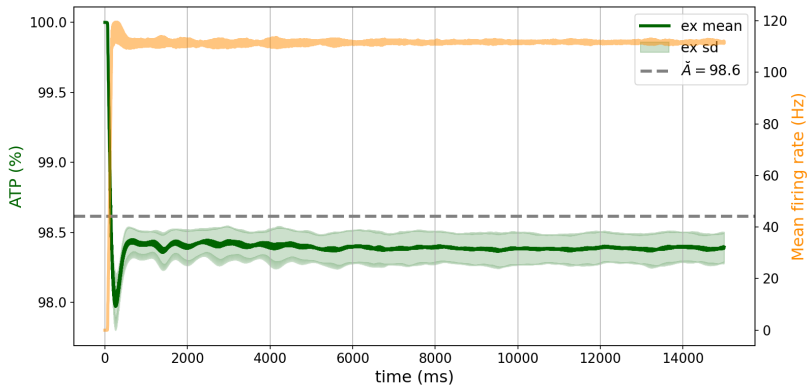

Figure 5.10: **Mean available energy and firing rate for different neuronal sensitivities to energy imbalances.**
Figure a) is obtained with $\eta = 50, \gamma = 10$ parameter values, while for Figure b) $\eta = 50, \gamma = 20$, and $\eta = 50, \gamma = 50$ in Figure c). Figures show the mean energy level and firing rate for the excitatory population.

while keeping η fixed is proved and in well agreement with numerical experiments.

5.2.3 Impaired metabolic production

Regarding biology, our theoretical and simulation framework allows us to study what happens when there is impaired metabolic production affecting neurons. This question is relevant because there is evidence suggesting that metabolic impairments are a common cause for various neurodegenerative diseases [12, 13, 14, 15, 16, 17]. Therefore, improving the understanding of how metabolic impairments affect network dynamics and structure is potentially valuable from a treatment point of view.

From our theoretical developments, if the ATP rate production controlled by parameter K decreases, we expect:

1) Given that the energy level equilibrium point for non-silent neurons $\breve{A}$ guaranteeing $\Delta w^{ex\to ex} = 0$ on average is independent of K (see Eqn. (4.18)), if there is a mean energy level fixed-point for non-silent neurons, it should stay constant as K varies.
2) By analyzing Eqn. (5.15), for non-silent neurons, if K decrease, $\sum_k \bar{w}_t^{in\to ex,\ k}\bar{\nu}_t^{in,\ k}$ or $\sum_k \bar{w}_t^{ex\to ex,\ k}\bar{\nu}_t^{ex,\ k}$ needs to decrease to satisfy the aforementioned metabolic relation. The only plastic synapses in the network are $\mathbf{w^{ex\to ex}}$. Therefore, if the metabolic production is impaired, we expect lower firing rates as well as weaker excitatory-excitatory synaptic strengths.
3) By analyzing Eqn. (4.3) and the fact that the time constant of the energy production in the neuron is $\tau_A = 1/K$, we know that lower production rate K values are associated with slower production responses. As a consequence, if a neuron with impaired metabolic production is subjected to an abrupt constant energy consumption, the energy production response to that consumption will be slower than the energy production response of a *healthy* neuron. In addition, this abrupt energy consumption will pull the neuron's available energy to a lower level compared to a *healthy* neuron subjected to the same energy consumption[8]. Given the slower response to energy consumption in the impaired case, producing higher delays between energy production and consumption, we expect to observe more oscillations in the ATP dynamics when simulating the network.

For the metabolically impaired simulation we vary K, but keep the synaptic sensitivity to energy imbalances $\eta = 50$ and the neuronal sensitivity $\gamma = 20$ (Figs. 5.10b, 5.11c and 5.11d).

Figure 5.12 shows the mean available energy level and firing rate of the network through the simulations. In particular, Figure 5.12a is obtained when $K = 0.7$. Please note that the numerical energy level fixed point when $K = 0.7$ is very close to the one obtained with $K = 1$ simulation (Fig. 5.10b), confirming that if there is an energy fixed point for non-silent neurons, it is independent of the ATP rate production K, in agreement with our first theoretical prediction. Moreover, if we compare Figures 5.11d and 5.13b, it is clear that

[8]Formally, we can describe an abrupt and constant consumption as a step energy consumption $A_c(t) = \Theta(t')A_c$ starting at time $t = t'$. Given enough time, the available energy of a neuron subjected to such energy consumption is $A = A_H - \frac{A_c}{K}$.

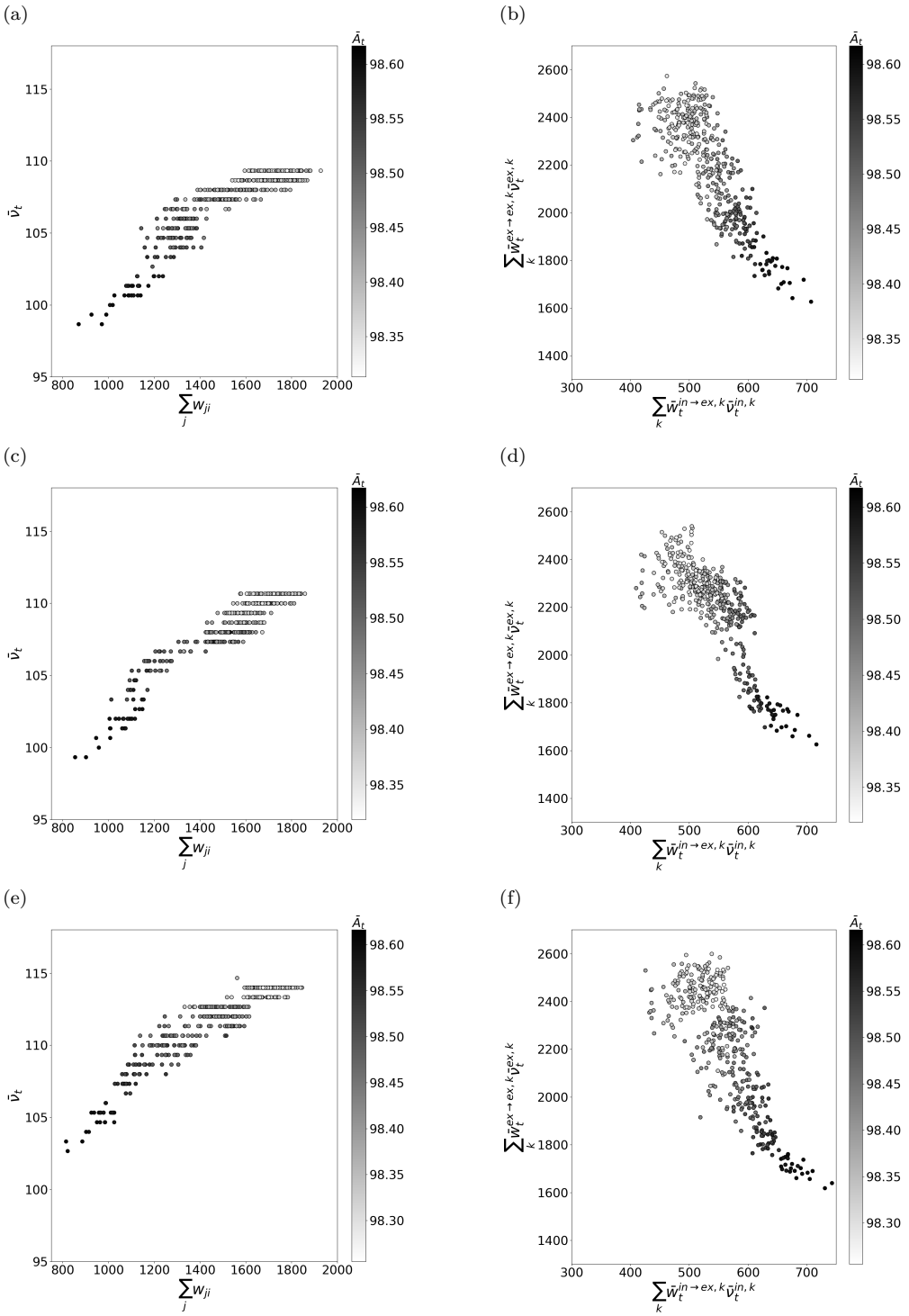

Figure 5.11: **Weight-rate and energy consumptions when neuronal sensitivity to energy imbalances varies.**
The Figures in the first column show mean firing rates versus incoming synaptic strengths, thus the numerically equivalent to the current-rate mapping defined by $\phi(\cdot)$. The Figures in the second columns show the energy consumption in each neuron due to presynaptic excitatory neurons and presynaptic inhibitory neurons. Figures a) and b) are obtained with $\eta = 50, \gamma = 10$ parameter values, while for Figures c) and d) $\eta = 50, \gamma = 20$. Finally, Figures e) and f) show the simulations results when $\eta = 50, \gamma = 50$. The mean firing rates $\bar{\nu}_t$ in all cases were calculated considering the last 10% of the simulation.

both simulations satisfy the energy relationship defined by Eqn. (5.15). However, in Figure 5.11d ($K = 1$) the mean $\sum_k \bar{w}_t^{ex \to ex,\, k} \bar{\nu}_t^{ex,\, k}$ energy consumption is much higher than the one consumed in Figure 5.13b when $K = 0.7$, in agreement with the second theory prediction. Besides, contrasting Figures 5.10b and 5.12a, a decrease in mean firing rate (orange curve) for the excitatory populations is observed when ATP rate production K decreases, also in agreement with the second prediction from theory. The decrease in excitatory population firing rate when K decreases can also be observed by contrasting Figure 5.11c ($K = 1$) and Figure 5.13a ($K = 0.7$). Therefore, if energy production is impaired in any neuron, then the energy consumption of that neuron needs to decrease to achieve a fixed point.

Hence, if we keep decreasing K (higher production impairment), energy consumption needs to drop to be consistent with the theory. In Figures 5.12b, 5.13c and 5.13d the ATP rate production is $K = 0.5$. Although the mean average rate and excitatory-excitatory weights decrease (Figs. 5.12b and 5.13d, respectively) with respect to the $K = 0.7$ case, when $K = 0.5$ the convergence towards a global fixed point is possible when a subpopulation of the network becomes silent. This behavior is in agreement with the energy constraints imposed on the network. In particular, as previously explained, if the ATP rate production parameter K decreases, then the energy consumption needs to drop. To decrease energy consumption, excitatory-excitatory weights decrease and, consequently, mean excitatory firing rates decrease. Then, silencing a subpopulation of neurons is a consequence of a strict policy toward diminishing energy consumption. Even though this is a similar phenomenon to the one observed when there is a high synaptic sensitivity to energy imbalances (Figs. 5.7c, 5.8f, 5.8e and 5.9), it is not the same, because the cause of the phenomenon is different. When there is a high synaptic energy imbalance sensitivity η, the energy level fixed point is close to the homeostatic energy level A_H (Eqn. (4.18)), thus decreasing energy consumption is necessary to converge towards a global fixed point. In contrast, in the metabolic production impairment case, the energy level fixed point is not necessarily close to the homeostatic energy level A_H. However, because energy production is impaired, energy consumption needs to drop to achieve an energy fixed point. Therefore, in the high synaptic sensitivity case, the energy consumption drops because the energy level fixed point needs to be close to A_H in order to achieve $\Delta w \approx 0$, which is a constraint imposed by the synapses, while in the metabolically impaired case, the energy consumption needs to drop because neuronal on-demand energy production does not match energy consumption (a constraint imposed by neurons, not by the synaptic energy sensitivity), thus decreasing energy consumption is necessary to achieve the energy fixed point. However, despite both phenomena being different, in the metabolic impaired case again the silent neurons are the ones with higher inhibitory synapses, and the reason is the same as in the case where high synaptic sensitivity to energy imbalances is present: before the network separates into two subpopulations there is an increase in available energy accompanied by a global excitatory-excitatory weights strength's decrease. If all the excitatory neurons receive a decreasing incoming current, the first in becoming silent are the ones that have higher inhibitory weights.

If we continue aggravating the metabolic production impairment and the network is able to achieve a fixed point, theoretically, we expect even weaker excitatory-excitatory synaptic strengths as well as lower firing rates in the equilibrium state. Accordingly, we simulate the network with $K = 0.1$, emulating the case where neurons can produce energy at a 10% rate with respect to the healthy case (*i.e.* $K = 1$). Figure 5.12c shows that the energy

(a)

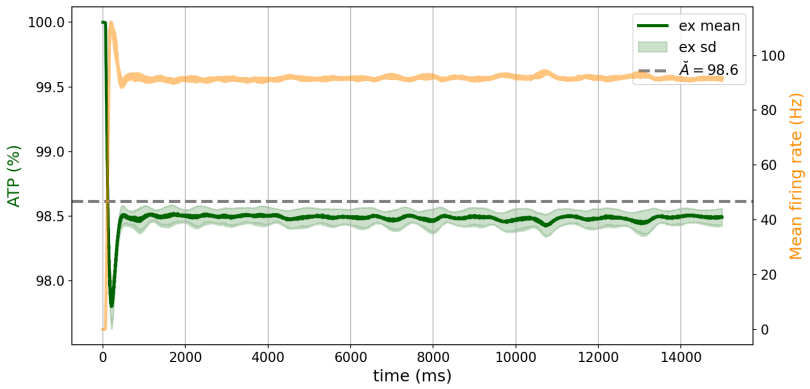

(b)

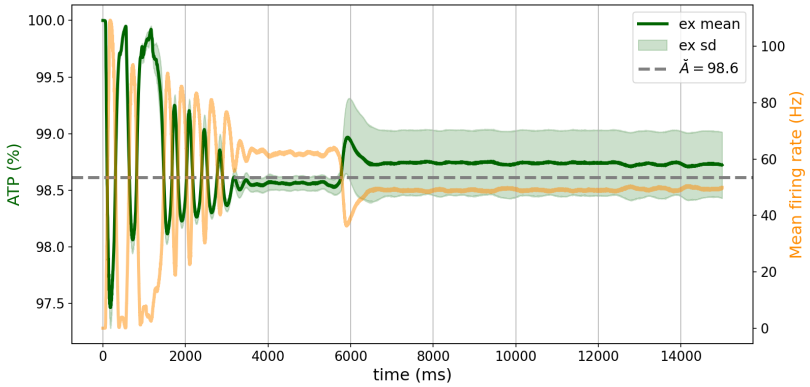

(c)

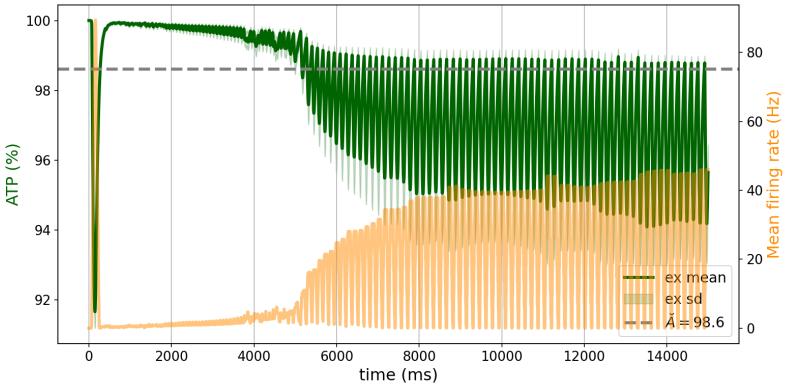

Figure 5.12: **Mean energy and firing rate for different ATP production impairment.** Figure a) is obtained with $\eta = 50, \gamma = 20, K = 0.7$ parameters, while for Figure b) $\eta = 50, \gamma = 20, K = 0.5$, and $\eta = 50, \gamma = 20, K = 0.1$ in Figure c). Figures show the mean energy level and firing rate for the excitatory population.

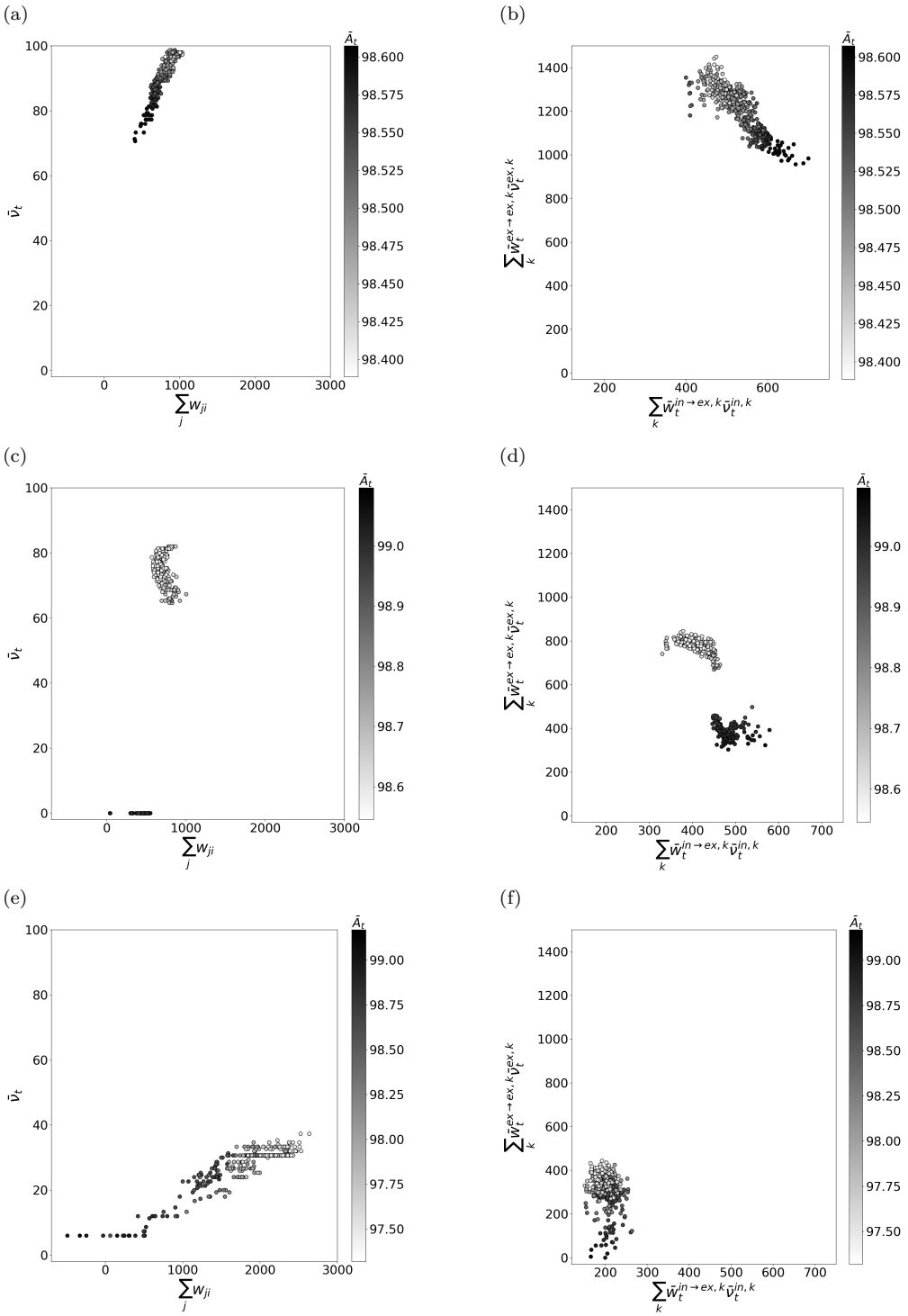

Figure 5.13: **Weight-rate and energy consumptions when neuronal ATP production is impaired.**
The Figures in the first column show mean firing rates versus incoming synaptic strengths, thus the numerically equivalent to the current-rate mapping defined by $\phi(\cdot)$, while the Figures in the second column show the energy consumption in each neuron due to presynaptic excitatory neurons and presynaptic inhibitory neurons. Figures a) and b) are obtained with $\eta = 50, \gamma = 20, K = 0.7$ parameter values, while for Figures c) and d) $\eta = 50, \gamma = 20, K = 0.5$. Finally, Figures e) and f) show the simulations results when $\eta = 50, \gamma = 20, K = 0.1$. The mean firing rates $\bar{\nu}_t$ in all cases were calculated considering the last 10% of the simulation.

production is so impaired that the network is not able to achieve an equilibrium point and stays oscillating, exploring excitatory-excitatory weights strengths which allow for achieving an equilibrium state. The problem appears to be that there are no excitatory-excitatory weights values that allow a firing rate and energy consumption which can be compensated by the impaired energy production. Specifically, an abrupt change in firing rate as a consequence of a small variation in excitatory-excitatory strengths seems to be part of the problem. Thus, small excitatory-excitatory weight variations generate energy consumptions that cannot be compensated by on-demand energy production. This is coherent with the third prediction and shows and extreme case where energy production is so impaired that it is not possible to converge towards a homeostatic balance where energy production and consumption match each other. To understand more intuitively what is happening, besides considering that neurons with impaired metabolism (small K) have slower responses to energy consumptions, thus a higher delay between consumption and production, it is relevant to remember that the excitatory-excitatory weight net drift depends on the available energy in the neurons (see Eqn. (4.17) and Fig. 4.2). Thus, if we start the simulation with all the neurons with the homeostatic energy level (*i.e.* $A(t=0) = A_H$), given that the energy fixed point value is smaller than the initially available energy (*i.e.* $\breve{A} < A_H$), then at the begging of the simulation and while the condition $\breve{A} < A(t)$ is fulfilled, weights will increase and, because of the current-rate relationship, firing rates also. Consequently, energy consumption in the neurons increases, but energy production is severely delayed, so the available energy in the neurons will tend to decrease on average (*i.e.* $\Delta A(t) < 0$). If the available energy continues to decrease, at some point, on average the available energy in the excitatory neurons will be lower than the energy fixed point value (*i.e.* $A(t) < \breve{A}$). When this condition is fulfilled, the excitatory-excitatory weights will tend to decrease on average, generating a decrease in the excitatory firing rates. This decrease in excitatory-excitatory weights and the accompanied decrease in firing rates will continue while the available energy is lower than the energy fixed point value (*i.e.* $A(t) < \breve{A}$). This decrease in energy consumption enables the possibility of energy production surpassing the energy consumption (while $\Delta A(t) < 0$ and $A(t) < \breve{A}$ energy consumption is decreasing but energy production is increasing). If energy production surpasses energy consumption, the available energy in the neurons is increasing (*i.e.* $\Delta A(t) > 0$). This increase in the available energy $A(t)$ should continue at least until the available energy match the energy equilibrium point (*i.e.* $A(t) = \breve{A}$), because when the available energy $A(t)$ is below the energy fixed point $\breve{A}$, energy consumption is always decreasing, but energy production is always active (because $A_s(t) = K(A_H - A(t))$). This behavior of energy production and consumption allows that available energy increases above the energy fixed point value $\breve{A}$ in the $\Delta A(t) > 0$ regimen. When the available energy is above the energy $\breve{A}$ equilibrium value, then the loop starts again, and excitatory-excitatory weights as well as excitatory firing rates increase, thus increasing energy consumption faster than the capacity of the neuron to compensate for those consumptions, thus entering the decreasing available energy regimen (*i.e.* $\Delta A(t) < 0$). This behavior stop when it is possible to match energy production and consumption, while having, on average, available energy near to the energy fixed point (*i.e.* $A(t) \approx \breve{A}$). When on-demand energy production can compensate energy consumption in the neurons it is easier to find that equilibrium.

Accordingly to our understanding of how energy constraint affects the networks, one possible solution to solve the non-converging system due to a dramatic ATP production impairment ($K = 0.1$), is decreasing the synaptic sensitivity to energy imbalances η. In this manner,

synapses experience softer strengths updates transitions when they are close to the analytical fixed-point $\breve{A}$. Thus, diminishing the oscillations due to changes in the peak energy-dependent potentiation described in Eqn. (4.12). To test this hypothesis, we simulate the network (Fig. 5.14) with the same initial conditions and parameters as the one shown in Figure 5.12c, but decreasing the synaptic sensitivity to energy imbalances to $\eta = 10$. The proposed solution allows for alleviating the oscillations in the system. However, the equilibrium is achieved by silencing a subpopulation of excitatory neurons. The logic behind this phenomenon is the same as the one explained for the $\eta = 50, \gamma = 20, K = 0.5$ case (Figs. 5.12b, 5.13e and 5.13f). Figure 5.14 shows that non-converging networks due to a dramatic metabolic impairment can be alleviated by modifying other parameters in the network. However, there are other solutions to this problem that might alleviate the oscillations. For instance, a simple solution is to decrease the energy expenditure due to postsynaptic potentials E_{syn}, thus forcing a decrease in energy consumption. Other possible solution could be modifying the neuron's time-constant τ_m. In particular, if τ_m decreases, each neuron has an *slower* dynamic. Thus, decreasing the slope of the current-rate relation. As a consequence, new weights and rates combinations allows to satisfy the required energy constraints, but with lower rates, thus with slower weights updates (weights update when pre- and postsynaptic spikes are present. Thus, lower rates implies less spikes and, therefore, slower weight updates). In addition, if the slope of the current-rate mapping decreases, weights modifications should produce softer transitions in rates, thus helping to decrease the oscillations due to the sensitivity of the firing rates to weights modifications.

5.3 Discussion

Based on the developments described in Chapters 3 and 4, in this chapter we mathematically formalize and simulate spiking neuronal networks under metabolic constraints. The work focuses on the emergence of dynamics, structure, and the study of attractors under energy constraints for homogeneous neuronal populations in E-I balanced networks. In general terms, the developed theory allows us to predict behaviors observed in numerical experiments. Moreover, the introduced neuronal and synaptic energy constraints generate a new attractor in E-I balanced networks due to the intersection of classic physical constraints (neuronal current-rate relations (5.4)) and the new constraints emerged from the local energy constraint imposed to each neuron in the network. We mathematically describe this phenomenon and conceptualize it in Figure 5.2.

Regarding the network's fixed points, synaptic sensitivity to energy imbalances is the main parameter affecting the available energy fixed-point for each neuron. As a consequence, through energy-dependent plasticity, synaptic strengths change until non-silent neurons achieve the energy equilibrium point $\breve{A}$. When the weights change, the neuron's firing rates change accordingly. We mathematically describe the required constraints on the postsynaptic neuron between inhibitory and excitatory presynaptic energy consumptions (Eqn. (5.15)), in order to achieve the energy equilibrium point. Surprisingly, if synaptic sensitivity to energy imbalances η is too high, in order to achieve a global fixed point in the network, the neuronal excitatory population divides into two subpopulations, with one of them composed of silent neurons. The occurrence of this phenomenon shed light on why silencing excita-

(a)

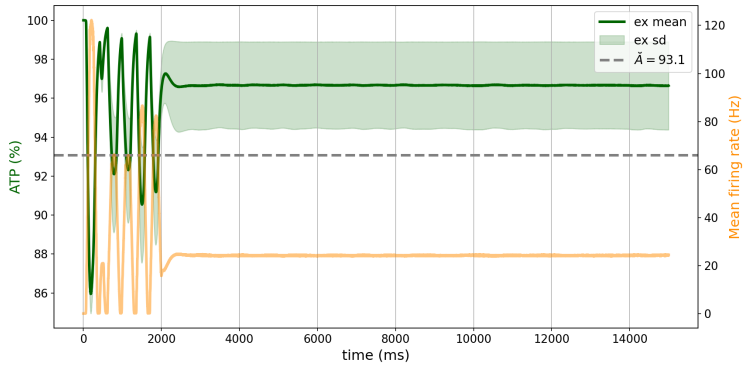

(b)

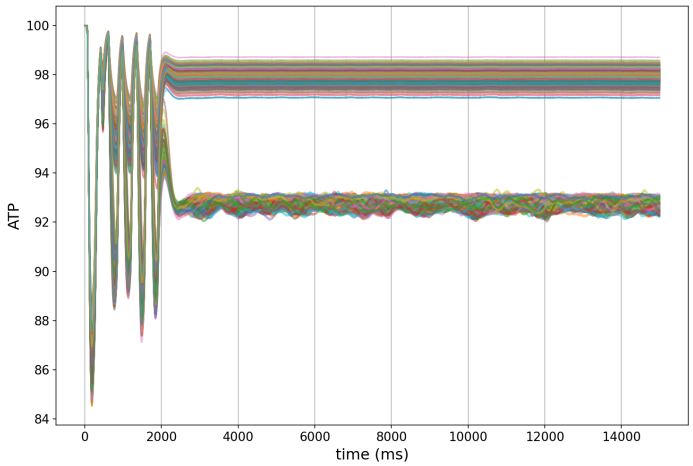

Figure 5.14: **Energy and firing rates for a dramatic metabolic impairment with low synaptic sensitivity to energy imbalances.**
Simulations are obtained with $\eta = 10, \gamma = 20, K = 0.1$ parameters. Figures show results for the excitatory population. In particular, b shows the mean energy and firing rate dynamics of the entire network, while in b the energy dynamic for each neuron in the populations is shown.

tory neurons could be practical to diminish energy consumption in neuronal networks, thus allowing the network's convergence towards a fixed point. Moreover, this phenomenon can be interpreted as a specialization in the excitatory population. Is surprising that this sort of behavior emerges given the simplicity of the developed rules constraining the network's energy, dynamics and, structure.

The effect of neuronal sensitivity to energy imbalances γ in the network's dynamics and structure is also analyzed. Theoretically, the available energy fixed point is independent of the neuronal sensitivity γ. Also, to achieve an energy fixed point when neuronal sensitivity γ is higher, excitatory-excitatory synaptic strengths need to decrease due to higher neuronal excitability produced by increased neuronal sensitivity γ. Numerical experiments confirm the predictions made by theory (Figures 5.10 and 5.11).

Regarding neurodegenerative diseases and given the biological evidence suggesting their relation with metabolic impairment, we study how neurons with impaired energy production affect the network dynamics and structure. Our theoretical developments predict that in impaired energy production cases, energy consumption needs to drop. Consequently, lower firing rates and excitatory-excitatory synapses are expected. These predictions are confirmed by numerical experiments (Figure 5.13). However, there are other important details in the metabolic impaired scenario. For instance, if the metabolic impairment is high enough, it is also possible that the excitatory population divides into two subpopulations, with one of them composed of silent neurons, although the source of this phenomenon (neuronal incapacity to produce enough energy on demand) is different from the one explained previously when too high synaptic energy sensitivity is present in the network (the energy fixed point $\breve{A}$ must be close to A_H, forcing low energy consumption). Even more dramatic energy production impairments may produce constant oscillations in the network, preventing the convergence towards an attractor (Fig. 5.12c). We show how these oscillations can be alleviated by modifying other parameters of the simulations. Trying to alleviate the oscillations present in dramatic metabolic impairment scenarios is important because it could help in developing new treatments for neurodegenerative diseases. A detailed study of how to alleviate pathological behaviors due to metabolic impairments is out of the scope of this thesis. However, the proposed theory as well as the simulation framework could be valuable to deepen the knowledge about the relationship between neurodegenerative diseases and metabolic impairments at the neuronal, synaptic, and network levels.

It is important to mention some of the limitations of this work. Firstly, we use a simple single-neuron model that neglects the neuron's morphology and the effect of some relevant ions, such as calcium kinetics, on the neuron's activity. Also, the model includes one type of plasticity, which only modifies excitatory-excitatory connections. Thus, we are neglecting other types of plasticity acting at different time scales, such as short-term plasticity or synaptic scaling. In addition, all the connections in the model, except excitatory-excitatory connections, are static. This is also an important limitation because different types of plasticity acting on other connections could have a significant impact on the network's activity and structure.

Finally, it is worth mentioning that -in general- previous neuronal and synaptic models do not account for energy dependencies. Thus, the developed framework and analysis of

dynamics and structure in spiking neural networks under metabolic impairment as well as the analysis of the effect of energy constraints in E-I balanced networks are the main contributions of this thesis.

Chapter 6

Conclusion and future work

The objective of this thesis is to formalize, simulate and study spiking neural networks under metabolic constraints. To achieve that goal, we proceed by studying and developing neuronal and synaptic energy-dependent models. The first contribution of this thesis is the development of a computationally simple but biologically meaningful energy-dependent single-neuron model. The model allows us to adapt the neural sensitivity to energy imbalances, thus allowing the representation of neurons with different sensitivities to energy imbalances. Despite its simplicity, the model allows for the replication of pathological behavior that was previously simulated by much more complex and computationally demanding models.

The second contribution of this thesis is the creation of an energy-dependent spike-timing-dependent model, where synaptic modifications depend on the postsynaptic ATP level. In particular, this model allows for the replication of biological evidence supporting the suppression of long-term potentiation when there is a deficit in the postsynaptic energy level. Furthermore, we formulated an analytical expression that allows us to predict the postsynaptic energy level when a single neuron is bombarded by several presynaptic neurons. The introduced plasticity model allows for the modification of synaptic sensitivity to postsynaptic energy levels, thus enabling the representation of plastic synapses with different energy sensitivities.

In addition, taking advantage of the energy-dependent single-neuron and plasticity model, we mathematically analyze the behavior of an Excitatory-Inhibitory balanced network affected by metabolic constraints. Through the proposed theory, analytical expressions predicting the network's activity and structure were derived. Then, the E-I balanced network is simulated for different scenarios, and the theoretical predictions are compared against experimental observations, giving reasonable agreement between the observations and the qualitative predictions given by the theory. In this regard, the developed mathematical framework as well as the understanding of the impact of metabolic constraints at different scales in neural networks through computational simulations are novel contributions of this thesis.

Unfortunately, and despite current technology, the majority of the predictions made by the developed theory are not easy to measure *in vitro* or *in vivo*. However, from a computational

neuroscience point of view, the hypotheses on which this work is based have been validated *in silico*, and the committed goals of this thesis have been accomplished, namely, the development of an energy-dependent single-neuron model, the development of an energy-dependent synaptic plasticity model, and the study of neural networks under metabolic constraints.

An interesting observation related to artificial intelligence emerges inspired by the work developed in this thesis. Studying how energy dynamics affect neurons, it can be observed that the energy dynamic is much slower than the other dynamics involved in the system (at least the ones considered in this study). As such, energy level can be thought of as a state giving long term *memory* to the cell. In particular, because it changes slower than, for instance, membrane voltage or synaptic currents, the current energy level of the neuron can be connected to a much previous activity affecting it. Built on that observation, it might be possible to create a simple neuronal model where the energy level gives the neuron a recurrent internal dynamic. Following this idea, we are working on the simplest computational neuronal model accounting for the role of energy in the neural dynamic for solving AI challenges. Thus allowing us to explore what could be the role of a biologically-inspired energy dynamic variable in the training and performance of conventional ANN when solving a specific task. This is far beyond the scope of this thesis, however, we would like to finish this manuscript by giving to the reader an example of how studying the brain from a biological point of view can inspire the creation of new AI algorithms, thus opening new avenues for the virtuous circle between neuroscience and engineering collaborations, from which both can benefit.

Interestingly, despite the new knowledge that we have developed and gained through this doctoral thesis, understanding how metabolic constraints affect dynamics and structure at the network level is still a very difficult task and, regardless of the efforts made here, there are still many unanswered questions (known unknowns) and unformulated questions (unknown unknowns). We hope that this observation does not produce frustration in the reader but, on the contrary, stimulates curiosity and passion for discovering new knowledge and keeps expanding the sphere of what is known. In this regard, there are a few avenues, along which to continue and extend the work presented in this thesis. We will outline four such possible directions:

- ➢ **Include long-term plasticity in other connection types** In this thesis, we only included energy-dependent long-term plasticity in the excitatory-excitatory connections. Presumably, there are other types of connections experiencing long-term energy-dependent plasticity. Those plasticities affecting other connection types may have a significant impact on the network structure and activity. Therefore, one possible extension of the work presented here is the creation of an energy-dependent long-term plasticity for other connection types.
- ➢ **Include plasticity occurring at different time scales** In this thesis, regarding synaptic modification phenomena, we focused on long-term plasticity. However, as explained in Chapter 3, synaptic plasticity occurs at different time scales. Therefore, a possible extension is to include synaptic plasticity mechanisms affecting synaptic strength at different time scales. A candidate is the inclusion of short-term plasticity rules. In particular, following the formalization of short-term plasticity introduced in [49] and the arguments presented in [16, 17], it is possible to extend known models of short-term plasticity to account for energy dependence by making the recuperation

rate of neurotransmitters ATP dependent. Thus, including energy dependencies in the synaptic vesicle recycling process.

- ➢ **Extend theory to the heterogeneous scenario** For mathematical treatment and simplifying the study and analysis of neural networks under metabolic constraints, in this thesis we focused on the homogeneous case, meaning that all neurons have the same parameters (consequently, they have the same current-rate mapping). However, noise represents an inherent property of biological substrates. Therefore, to get closer to biology, a generalization by relaxing the homogeneous assumption and extending the theory for studying heterogeneous neural networks under metabolic constraints could be developed.
- ➢ **Extend theory to the frequency domain** This work does not include a detailed study or mathematical analysis of how coupling phenomena between neurons or populations of them could affect the structure and activity of a network. However, given the long-term plasticity mechanism used here where synaptic strengths are modified by pre- and postsynaptic spike times, specific neurons' coupling may have a relevant effect on the networks' structure. Therefore, the work presented in this thesis could be extended by carrying out analytical studies as well as computational simulations measuring the effect of coupling effects and oscillation on the network structure and activity.

Bibliography

[1] N. R. Council. *Opportunities in Biology*. The National Academies Press, Washington, DC, 1989.

[2] S. Herculano-Houzel. The human brain in numbers: a linearly scaled-up primate brain. *Frontiers in human neuroscience*, 3:31–31, Nov 2009.

[3] H. Markram, E. Muller, S. Ramaswamy, M. W. Reimann, and et al. Reconstruction and simulation of neocortical microcircuitry. *Cell*, 163(2):456 – 492, 2015.

[4] J. W. Mink, R. J. Blumenschine, and D. B. Adams. Ratio of central nervous system to body metabolism in vertebrates: its constancy and functional basis. *American Journal of Physiology-Regulatory, Integrative and Comparative Physiology*, 241(3):R203–R212, 1981.

[5] R. G. Shulman, D. L. Rothman, K. L. Behar, and F. Hyder. Energetic basis of brain activity: implications for neuroimaging. *Trends in Neurosciences*, 27(8):489–495, Aug 2004.

[6] D. Attwell and S. B. Laughlin. An energy budget for signaling in the grey matter of the brain. *Journal of Cerebral Blood Flow & Metabolism*, 21(10):1133–1145, 2001.

[7] M. E. Watts, R. Pocock, and C. Claudianos. Brain energy and oxygen metabolism: Emerging role in normal function and disease. *Frontiers in Molecular Neuroscience*, 11:216, 2018.

[8] J. J. Harris, R. Jolivet, and D. Attwell. Synaptic energy use and supply. *Neuron*, 75(5):762 – 777, 2012.

[9] E. Elisabeth and A. David. Nonsignalling energy use in the brain. *The Journal of Physiology*, 593(16):3417–3429, 2015.

[10] E. Bullmore and O. Sporns. The economy of brain network organization. *Nature Reviews*

Neuroscience, 13(5):336–349, 2012.

[11] K. Friston. The free-energy principle: a unified brain theory? *Nature Reviews Neuroscience*, 11(2):127–138, 2010.

[12] M. T. Lin and M. F. Beal. Mitochondrial dysfunction and oxidative stress in neurodegenerative diseases. *Nature*, 443(7113):787–795, 2006.

[13] H. Kawamata and G. Manfredi. Mitochondrial dysfunction and intracellular calcium dysregulation in als. *Mechanisms of Ageing and Development*, 131(7):517 – 526, 2010.

[14] A. Maruszak and C. Żekanowski. Mitochondrial dysfunction and alzheimer's disease. *Progress in Neuro-Psychopharmacology and Biological Psychiatry*, 35(2):320 – 330, 2011.

[15] J.-S. Park, R. L. Davis, and C. M. Sue. Mitochondrial dysfunction in parkinson's disease: New mechanistic insights and therapeutic perspectives. *Current neurology and neuroscience reports*, 18(5):21–21, Apr 2018.

[16] D. Pathak, L. Y. Shields, B. A. Mendelsohn, D. Haddad, W. Lin, A. A. Gerencser, H. Kim, M. D. Brand, R. H. Edwards, and K. Nakamura. The role of mitochondrially derived atp in synaptic vesicle recycling. *Journal of Biological Chemistry*, 290(37):22325–22336, 2015.

[17] V. Rangaraju, N. Calloway, and T. A. Ryan. Activity-driven local atp synthesis is required for synaptic function. *Cell*, 156(4):825–835, Feb 2014.

[18] Y. Yu, P. Herman, D. L. Rothman, D. Agarwal, and F. Hyder. Evaluating the gray and white matter energy budgets of human brain function. *Journal of Cerebral Blood Flow & Metabolism*, 38(8):1339–1353, 2018.

[19] J. J. Harris and D. Attwell. The energetics of cns white matter. *Journal of Neuroscience*, 32(1):356–371, 2012.

[20] A. Ames. Cns energy metabolism as related to function. *Brain Research Reviews*, 34(1):42 – 68, 2000.

[21] D. Attwell and A. Gibb. Neuroenergetics and the kinetic design of excitatory synapses. *Nature Reviews Neuroscience*, 6:841 EP –, Nov 2005.

[22] B. S. Chander and V. S. Chakravarthy. A computational model of neuro-glio-vascular loop interactions. *PLOS ONE*, 7(11):1–11, 11 2012.

[23] G. LeMasson, S. Przedborski, and L. F. Abbott. A computational model of motor

neuron degeneration. *Neuron*, 83(4):990, Aug 2014.

[24] S. Ching, P. L. Purdon, S. Vijayan, N. J. Kopell, and E. N. Brown. A neurophysiological metabolic model for burst suppression. *Proceedings of the National Academy of Sciences*, 109(8):3095–3100, 2012.

[25] R. Jolivet, J. S. Coggan, I. Allaman, and P. J. Magistretti. Multi-timescale modeling of activity-dependent metabolic coupling in the neuron-glia-vasculature ensemble. *PLOS Computational Biology*, 11(2):1–23, 02 2015.

[26] D. E. Feldman. Synaptic mechanisms for plasticity in neocortex. *Annual review of neuroscience*, 32:33–55, 2009.

[27] D. O. Hebb. *The organization of behavior; a neuropsychological theory*. Oxford, England: Wiley, 1949.

[28] C. J. Shatz. The developing brain. *Scientific American*, 267(3):60–67, 1992.

[29] H. Markram, W. Gerstner, and P. J. Sjöström. Spike-timing-dependent plasticity: a comprehensive overview. *Frontiers in synaptic neuroscience*, 4:2–2, Jul 2012.

[30] M. P. Mattson and D. Liu. Mitochondrial potassium channels and uncoupling proteins in synaptic plasticity and neuronal cell death. *Biochemical and Biophysical Research Communications*, 304(3):539 – 549, 2003.

[31] V. Todorova and A. Blokland. Mitochondria and synaptic plasticity in the mature and aging nervous system. *Current neuropharmacology*, 15(1):166–173, 2017.

[32] T. Sun, H. Qiao, P.-Y. Pan, Y. Chen, and Z.-H. Sheng. Motile axonal mitochondria contribute to the variability of presynaptic strength. *Cell Reports*, 4(3):413 – 419, 2013.

[33] A. Cheng, Y. Hou, and M. P. Mattson. Mitochondria and neuroplasticity. *ASN neuro*, 2(5):e00045–e00045, Oct 2010.

[34] F. Jeanneteau and M. Arango-Lievano. Linking Mitochondria to Synapses: New Insights for Stress-Related Neuropsychiatric Disorders. *Neural Plast*, 2016:3985063, 2016.

[35] C. I. Thomas, C. Keine, S. Okayama, R. Satterfield, M. Musgrove, D. Guerrero-Given, N. Kamasawa, and S. M. Young. Presynaptic mitochondria volume and abundance increase during development of a high-fidelity synapse. *Journal of Neuroscience*, 39(41):7994–8012, 2019.

[36] R. C. Vergara, S. Jaramillo-Riveri, A. Luarte, C. Moënne-Loccoz, R. Fuentes, A. Couve,

and P. E. Maldonado. The energy homeostasis principle: Neuronal energy regulation drives local network dynamics generating behavior. *Frontiers in Computational Neuroscience*, 13:49, 2019.

[37] M. Pfeiffer and T. Pfeil. Deep learning with spiking neurons: Opportunities and challenges. *Frontiers in Neuroscience*, 12:774, 2018.

[38] I. Jaras, T. Harada, M. E. Orchard, P. E. Maldonado, and R. C. Vergara. Extending the integrate-and-fire model to account for metabolic dependencies. *European Journal of Neuroscience*, 54(4):5249–5260, 2021.

[39] E. R. Kandel, J. H. Schwartz, and T. M. Jessell, editors. *Principles of Neural Science*. Elsevier, New York, third edition, 1991.

[40] A. L. Hodgkin and A. F. Huxley. A quantitative description of membrane current and its application to conduction and excitation in nerve. *The Journal of Physiology*, 117(4):500–544, 1952.

[41] E. M. Izhikevich. Which model to use for cortical spiking neurons? *IEEE Transactions on Neural Networks*, 15(5):1063–1070, Sep. 2004.

[42] L. Lapicque. Recherches quantitatives sur l'excitation électrique des nerfs traitée comme une polarisation. *J. Physiol. Pathol. Gen.*, 9:620–635, 1907.

[43] W. Gerstner, W. M. Kistler, R. Naud, and L. Paninski. *Neuronal dynamics: From single neurons to networks and models of cognition*. Cambridge University Press, 2014.

[44] W. Gerstner and R. Brette. Adaptive exponential integrate-and-fire model. *Scholarpedia*, 4(6):8427, 2009.

[45] A. N. Burkitt. A review of the integrate-and-fire neuron model: I. homogeneous synaptic input. *Biological Cybernetics*, 95(1):1–19, Jul 2006.

[46] M. A. Petrovici. *Introduction: From Biological Experiments to Mathematical Models*, pages 7–58. Springer International Publishing, Cham, 2016.

[47] M. A. Petrovici. *Dynamics and Statistics of Poisson-Driven LIF Neurons*, pages 83–142. Springer International Publishing, Cham, 2016.

[48] A. Morrison, M. Diesmann, and W. Gerstner. Phenomenological models of synaptic plasticity based on spike timing. *Biological cybernetics*, 98(6):459–478, Jun 2008.

[49] M. V. Tsodyks and H. Markram. The neural code between neocortical pyramidal neurons

depends on neurotransmitter release probability. *Proceedings of the National Academy of Sciences*, 94(2):719–723, 1997.

[50] G.-q. Bi and M.-m. Poo. Synaptic modifications in cultured hippocampal neurons: Dependence on spike timing, synaptic strength, and postsynaptic cell type. *Journal of Neuroscience*, 18(24):10464–10472, 1998.

[51] H. Markram, J. Lübke, M. Frotscher, and B. Sakmann. Regulation of synaptic efficacy by coincidence of postsynaptic aps and epsps. *Science*, 275(5297):213–215, 1997.

[52] D. Chowdhury and J. Hell. Homeostatic synaptic scaling: molecular regulators of synaptic ampa-type glutamate receptors [version 1; peer review: 4 approved]. *F1000Research*, 7(234), 2018.

[53] J. Sjöström and W. Gerstner. Spike-timing dependent plasticity. *Scholarpedia*, 5(2):1362, 2010.

[54] R. Gütig, R. Aharonov, S. Rotter, and H. Sompolinsky. Learning input correlations through nonlinear temporally asymmetric hebbian plasticity. *Journal of Neuroscience*, 23(9):3697–3714, 2003.

[55] J. Rubin, D. D. Lee, and H. Sompolinsky. Equilibrium properties of temporally asymmetric hebbian plasticity. *Phys. Rev. Lett.*, 86:364–367, Jan 2001.

[56] M. C. W. van Rossum, G. Q. Bi, and G. G. Turrigiano. Stable hebbian learning from spike timing-dependent plasticity. *Journal of Neuroscience*, 20(23):8812–8821, 2000.

[57] S. Song, K. D. Miller, and L. F. Abbott. Competitive hebbian learning through spike-timing-dependent synaptic plasticity. *Nature Neuroscience*, 3(9):919–926, Sep 2000.

[58] N. Frémaux and W. Gerstner. Neuromodulated spike-timing-dependent plasticity, and theory of three-factor learning rules. *Frontiers in Neural Circuits*, 9:85, 2016.

[59] G. Bugmann, C. Christodoulou, and J. G. Taylor. Role of temporal integration and fluctuation detection in the highly irregular firing of a leaky integrator neuron model with partial reset. *Neural Computation*, 9:985–1000, 1997.

[60] M. DiNuzzo and F. Giove. Activity-dependent energy budget for neocortical signaling: Effect of short-term synaptic plasticity on the energy expended by spiking and synaptic activity. *Journal of Neuroscience Research*, 90(11):2094–2102, 2012.

[61] Y. Yuan, H. Huo, P. Zhao, J. Liu, J. Liu, F. Xing, and T. Fang. Constraints of metabolic energy on the number of synaptic connections of neurons and the density of neuronal

networks. *Frontiers in Computational Neuroscience*, 12:91, 2018.

[62] R. Naud, T. Berger, B. Batheliar, M. Caradini, and W. Gestern. Quantitative single-neuron modeling: Competition 2009. *Front. Neuroinform. Conference Abstract: Neuroinformatics 2009*, May 2019.

[63] R. Eberhart and Y. Shi. Particle swarm optimization: developments, applications and resources. In *Proceedings of the 2001 Congress on Evolutionary Computation (IEEE Cat. No.01TH8546)*, volume 1, pages 81–86 vol. 1, May 2001.

[64] R. Jolivet, R. Kobayashi, A. Rauch, R. Naud, S. Shinomoto, and W. Gerstner. A benchmark test for a quantitative assessment of simple neuron models. *Journal of Neuroscience Methods*, 169(2):417 – 424, 2008.

[65] R. Jolivet, F. Schürmann, T. K. Berger, R. Naud, W. Gerstner, and A. Roth. The quantitative single-neuron modeling competition. *Biological Cybernetics*, 99(4):417, Nov 2008.

[66] J. Lin. Divergence measures based on the shannon entropy. *IEEE Transactions on Information Theory*, 37(1):145–151, 1991.

[67] F. Baeza-Lehnert, A. S. Saab, R. Gutiérrez, V. Larenas, E. Díaz, M. Horn, M. Vargas, L. Hösli, J. Stobart, J. Hirrlinger, B. Weber, and L. F. Barros. Non-canonical control of neuronal energy status by the na^+ pump. *Cell Metabolism*, 29(3):668–680.e4, Mar 2019.

[68] G. Yi and W. M. Grill. Average firing rate rather than temporal pattern determines metabolic cost of activity in thalamocortical relay neurons. *Scientific Reports*, 9(1):6940, May 2019.

[69] Y.-C. Wang and R.-C. Huang. Effects of sodium pump activity on spontaneous firing in neurons of the rat suprachiasmatic nucleus. *Journal of Neurophysiology*, 96(1):109–118, 2006.

[70] K. M. Raley-Susman, I. S. Kass, J. E. Cottrell, R. B. Newman, G. Chambers, and J. Wang. Sodium influx blockade and hypoxic damage to ca1 pyramidal neurons in rat hippocampal slices. *Journal of Neurophysiology*, 86(6):2715–2726, 2001.

[71] R. Fremont, D. P. Calderon, S. Maleki, and K. Khodakhah. Abnormal high-frequency burst firing of cerebellar neurons in rapid-onset dystonia-parkinsonism. *Journal of Neuroscience*, 34(35):11723–11732, 2014.

[72] Y. Zilberter and M. Zilberter. The vicious circle of hypometabolism in neurodegenera-

tive diseases: Ways and mechanisms of metabolic correction. *Journal of Neuroscience Research*, 95(11):2217–2235, 2017.

[73] W. B. Potter, K. J. O'Riordan, D. Barnett, S. M. K. Osting, M. Wagoner, C. Burger, and A. Roopra. Metabolic regulation of neuronal plasticity by the energy sensor ampk. *PLOS ONE*, 5(2):1–9, 02 2010.

[74] M.-O. Gewaltig and M. Diesmann. Nest (neural simulation tool). *Scholarpedia*, 2(4):1430, 2007.

[75] C. A. Linssen, P. N. Babu, A. Benelhedi, R. De Schepper, T. Fardet, J. M. Eppler, B. Rumpe, and A. Morrison. Nestml 5.0.0, May 2022.

[76] Y. Wang, X. Shi, B. Si, B. Cheng, and J. Chen. Synchronization and oscillation behaviors of excitatory and inhibitory populations with spike-timing-dependent plasticity. *Cognitive Neurodynamics*, Aug 2022.

[77] R. Kempter, W. Gerstner, and J. L. van Hemmen. Hebbian learning and spiking neurons. *Phys. Rev. E*, 59:4498–4514, Apr 1999.

[78] S. Sahara, Y. Yanagawa, D. D. M. O'Leary, and C. F. Stevens. The fraction of cortical gabaergic neurons is constant from near the start of cortical neurogenesis to adulthood. *Journal of Neuroscience*, 32(14):4755–4761, 2012.

[79] L. M. A. Bettencourt, G. J. Stephens, M. I. Ham, and G. W. Gross. Functional structure of cortical neuronal networks grown in vitro. *Phys. Rev. E*, 75:021915, Feb 2007.

[80] S. Shoham, D. H. O'Connor, and R. Segev. How silent is the brain: is there a "dark matter" problem in neuroscience? *Journal of Comparative Physiology A*, 192(8):777–784, Aug 2006.